BRNO UNIVERSITY OF TECHNOLOGY
VYSOKÉ UČENÍ TECHNICKÉ V BRNĚ

FACULTY OF MECHANICAL ENGINEERING
FAKULTA STROJNÍHO INŽENÝRSTVÍ

INSTITUTE OF PRODUCTION MACHINES, SYSTEMS AND ROBOTICS
ÚSTAV VÝROBNÍCH STROJŮ, SYSTÉMŮ A ROBOTIKY

COMPUTATIONAL MODELLING OF SELF-EXCITED OSCILLATION DURING METAL CUTTING

VÝPOČTOVÉ MODELOVÁNÍ SAMOBUZENÉHO KMITÁNÍ PŘI OBRÁBĚNÍ

MASTER'S THESIS
DIPLOMOVÁ PRÁCE

AUTHOR — Bc. Pavel Malý
AUTOR

SUPERVISOR — Ing. Pavel Švancara, Ph.D.
VEDOUCÍ PRÁCE

BRNO 2017

BRNO FACULTY OF MECHANICAL ENGINEERING
UNIVERSITY OF TECHNOLOGY

Master's Thesis Assignment

Institut:	Institute of Production Machines, Systems and Robotics
Student:	**Bc. Pavel Malý**
Degree programm:	Mechanical Engineering
Branch:	Design of Product Machines and Equipment
Supervisor:	**Ing. Pavel Švancara, Ph.D.**
Academic year:	2016/17

As provided for by the Act No. 111/98 Coll. on higher education institutions and the BUT Study and Examination Regulations, the director of the Institute hereby assigns the following topic of Master's Thesis:

Computational modelling of self-excited oscillation during metal cutting

Brief description:

One of the limiting factors of reducing machining time and increasing productivity of modern machine tools is the emergence of self-excited oscillation. The aim of the thesis is to create a computational model of the self-excited vibrations of the milling machine with simplified geometry using finite element method and multi-body systems. On this model, analyze the stability of the cutting process for selected operations and further analyze the effect of selected parameters on the occurrence of self-excited oscillation and the possibility of its suppression.

Master's Thesis goals:

1) Based on the literature describe the principles and mechanisms of the self-excited oscillation during machining.
2) Provide a brief overview of current computational methods for the analysis of the self-excited oscillation.
3) Editing a simplified geometric model of the milling machine and creating a finite element mesh.
4) Analysis of the stability of the cutting process for the selected operations and create stability diagrams.
5) Analysis of selected model parameters in relation to self-excited oscillation.

Recommended bibliography:

TLUSTÝ, G. Manufacturing Processes and Equipment. Prentice Hall, 1999. ISBN 0-201-49865-0.

BRECHER, C., M. ESSER a S. WIT. Interaction of manufacturing process and machine tool. CIRP Annals – Manufcturing Technology. 2009, roč. 58, s. 588-607. ISSN 00078506.

ALTINTAS, Y. a M. WECK. Chatter Stability of Metal Cutting and Grinding CIRP Annals – Manufcturing Technology. 2004, roč. 53, č. 2, s. 619-642. ISSN 00078506.

Students are required to submit the thesis within the deadlines stated in the schedule of the academic year 2016/17.

In Brno, 4. 11. 2016

VYSOKÉ UČENÍ TECHNICKÉ V BRNĚ FAKULTA STROJNÍHO INŽENÝRSTVÍ DĚKANÁT L. S.

doc. Ing. Petr Blecha, Ph.D.
Director of the Institute

doc. Ing. Jaroslav Katolický, Ph.D.
FME dean

SUMMARY

This master thesis deals with analysing of productivity and effectivity of cutting process in milling. Real milling machine is used to find out the critical chip width. Geometric model of the milling machine is created in Autodesk Inventor software. Ansys Workbench software is used for corresponding analysis of cutting process. Results of analysis are used for creating stability lobe diagrams. Due to results evaluated there are two different approaches proposed in order to get more effective milling process. Effects of these two approaches are verified by comparison with previous analysis.

Key words: milling, chatter, Loby diagram

ABSTRAKT

Diplomová práce se zabývá analýzou produktivity a efektivity řezného procesu frézování. Pro zjištění kritické hloubky třísky byla analyzována reálná frézka. Model frézky byl vytvořen v programu Autodesk Inventor. Analýza řezného procesu probíhala v programu Ansys Workbench. Výsledky byly použity pro sestavení stabilitních diagramů. Po vyhodnocení výsledků byly navrženy dva přístupy pro zefektivnění procesu frézování. Vliv těchto změn na produktivitu řezného procesu byl ověřen porovnáním výsledků s předchozí analýzou.

Klíčová slova: frézování, samobuzené kmitání v obrábění, diagram stability

BIBLIOGRAPHIC CITATION

MALÝ, P. *Výpočtové modelování samobuzeného kmitání u obrábění.* Brno: Vysoké učení technické v Brně, Fakulta strojního inženýrství, 2016. 77 s. Vedoucí diplomové práce Ing. Pavel Švancara, Ph.D..

DECLARATION

I declare that I have written the master's thesis **Computational modelling of self-excited oscillations during metal cutting** on my own according to advice of my master's thesis supervisor Ing. Pavel Švancara Ph.D., and using the sources listed in references.

Date

Pavel Malý

ACKNOWELEDGMENT

I would like to express my gratitude to my thesis supervisor Ing. Pavel Švancara, Ph.D. for his professional and valuable guidance. My thanks also goes to my family, girlfriend and friends for all their support during my studies.

CONTENT

PROBLEM INTRODUCTION

At the beggining of this master thesis I present general information from chosen field of study. First of all, fundamentals of the milling are shown. Natural, forced and self-excited vibrations are presented with all the necessary equations and behaviour of mentoined vibrations is shown in corresponding graphs. Two general principals how the chatter can occur in machining, are explained and for easier imagination corresponing pictures are used. All major conditions, which can influence the stability of machining, are discussed. In following, critical chip width is derived and three different approaches for analysing of the stability in chatter are defined. Fundamentals of stability lobe diagram are explained and computing methods about harmonic analysis are presented.

Actual problems, researches and approaches about chatter are discussed in second chapter. Chatter in milling has big significance in machining, in order to perform brief summary of this topic, some samples are shown in this work.

Whether the chatter occurs during machining process is analyzed using 3-axis “hobby” milling machine, which was the topic of another bachelor thesis. The model of this milling machine is introduced. This model is created in Autodesk Inventor Professional 2015 software. Following analyses are performed in ANSYS Workbench 2016 software. In chapter three there are also discussions on the meshing method and all the general conditions which are needed for the most precise results.

Chapter four is divided into two parts. The first one is about modal analysis of milling machine. First hundred natural frequencies are investigated and evaluated. The second part is about harmonic response of the milling machine. Harmonic response is solved in X, Y and Z directions. Evaluated results are used to create corresponding stability lobe diagrams. ANSYS Workbench is used for analyzing and stability diagrams are created in Microsoft Excel.

Two approaches to improve cutting process are performed. Material change is one of them. The second change is editing construction. New results are evaluated for both changes.

MOTOVATION

High-speed milling processes are widely employed in the aerospace, automotive, ship building and also in all kind of industry, because they offer a high precision, high surface quality and high material removal rate. However, in recent years, with the rapid development of modern industry and the ever increasing pressure of market competition, mechanical products have shown a tendency to become more and more special. Yet, complex shapes, thin-walled structures, the use of materials that are difficult to process and high accuracy requirement all increase the probability of the occurrence of vibrations during product processing.

In the field of simulation of metal cutting the coupling of the cutting process and the dynamic behaviour of the machine tool and the cutting process e.g. lead to oscillations which influence the workpiece surface quality, tool wear and the stability of the cutting process. In order to ensure the coupling of cutting processes and machine tools it is necessary to identify the influences on both sides and to analyse their sensitivity.

When simulating a cutting process with the finite element method it is necessary to analyse not only the influence of the process parameters such as cutting speed, feed rate or material geometry but also the influence of modelling parameters such as mesh fineness, material failure modelling etc.

In my opinion, this topic has very big significance in machining and I would like to understand as much as possible in this field of study. From my point of view, it is nice, if there are some general theoretical information, which can be used for following process. The real machine is created in 3D software and this model is been subjected to necessary analysis. Its solutions are mathematically edited and final results can be practically verified. I hope that once my research on this theory will be morphed into practical use.

1 VIBRATION AND CHATTER IN MILLING PROCESSES

1.1 Milling

Milling is the cutting method, where the main cutting motion is the rotation of a cutter that machines a workpiece. The workpiece usually performs translational (mostly rectilinear) feed motions, where these motions are mostly perpendicular to the axis of cutter. Translational motions are fluently changeable and they should realize in each direction in modern milling machines (machining centres, multiaxis CNCs, multipurpose machining centres). Cutting process is discontinuous and each tooth of cutter cut very short chips in the various thicknesses.

From the technological point of view we distinguish different types of milling depends on applicable milling cutter. Slab milling is shown in the Figure 1 and face milling is shown in the Figure 2. We can derive the other types of milling from these two basic types.

Slab milling is applicable for end milling and edge profile milling processes. Teeth of cutter are created only circumferentially on the cutting tool. The depth of the layer *b* is removed from the workpiece and it is set perpendicular to the axis of cutter and in direction of workpiece feed motion. Machined surface is parallel with the rotation of spindle axis of the cutter. Depending on the relation between the direction of rotation of the cutter and the direction of feed, one distinguishes between up-milling and down-milling [1].

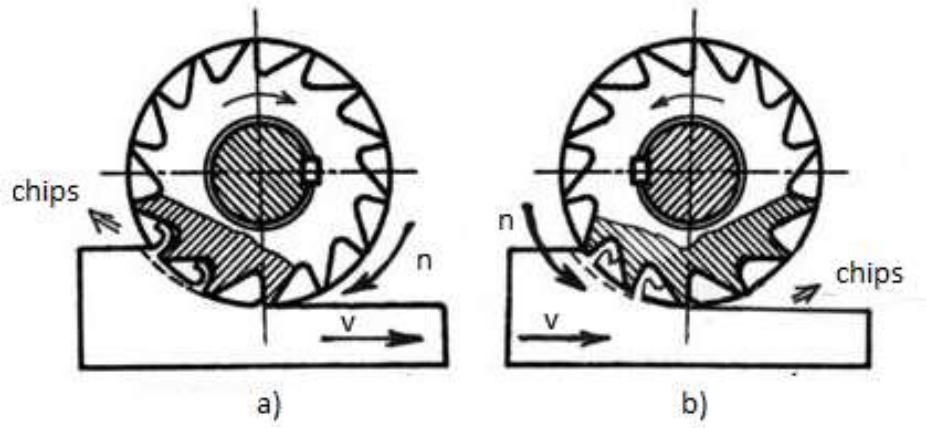

Figure 1: Kinematic of the slab milling [2]

The direction of the cutter rotation is in opposite direction as the workpiece motion in up-milling process (Figure 1 a)). Machined surface is created when the cutter start cutting the workpiece. The width of the chip is continuously changing from the zero value to the maximum value. The chip is not separated when the width of chip is zero but it is separated in specific motion on the edge of the surface created by the previous tooth. That causes bigger force effects and faster tool wear. Cutting force has the element, which pull up the workpiece from the working table in this type of milling.

The direction of the cutter rotation is in the same direction as the workpiece motion in down-milling process (Figure 1 b)). Machined surface is created when the tooth of cutter is leaving the workpiece. Maximum width of the chip is in the begging of the cutting process. Cutting forces pull down to the working table. There must be the initial slack in the milling machines and pre-tension between the sliding bolt and nut of milling machine's

table. Otherwise the initial slack causes uneven movement which can damage the cutter or the milling machine.

In face milling (Figure 2) the depth of the layer is removed from the workpiece which is the axial depth of cut and the width of workpiece is the radial depth of cut. The width of chip is *b*, and the chip thickness is *h*. There are symmetric and asymmetric types of face milling depending on the cutter axis position due to machining surface [2][3].

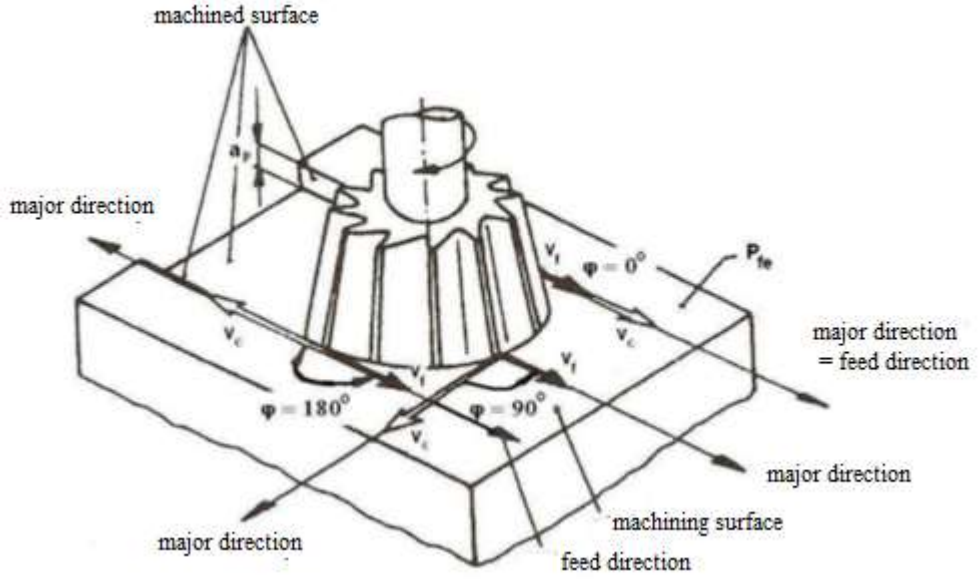

Figure 2: Kinematic of the face milling [3]

1.2 Fundamentals of mechanical vibrations

Machining centre, machine-tool and workpiece are machining system with dynamic characters. Vibration of each parts of the system present accompaniment to cutting process. There are four different types of vibration.

1.2.1 Natural vibrations

Free or natural vibrations occur if a vibratory system, represented in the diagram by a simple combination of a spring, a dashpot and a mass is firstly deflected from equilibrium position and then left free to move (Figure 3). The result is motion with an amplitude decaying, and frequency is equal to the natural frequency of the system $f = f_n$.

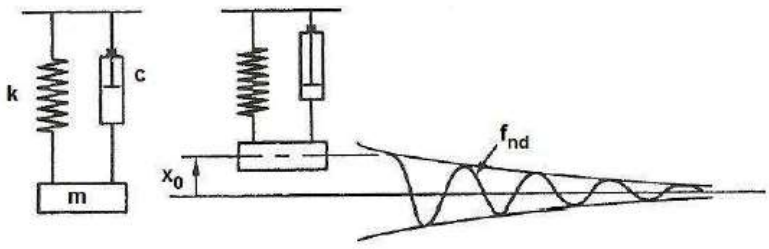

Figure 3: Natural vibrations, no external force, frequency natural, amplitude decays [1]

This motion is described by the differential equation:

$$m\ddot{x} + c\dot{x} + kx = 0 \tag{1.1}$$

where x is deflection, $\dot{x}$ is velocity a $\ddot{x}$ is acceleration of the system. Parameters of the system are mass m, the damping coefficient c, and the spring stiffness k. There is no external force acting on the system. For an initial displacement x_0 and no initial velocity, this motion is:

$$x = x_0 e^{-\lambda t} \cos(2\pi \cdot f_n \cdot t + \varphi) \tag{1.2}$$

This equation is solvable, if the parameters have these conditions:

- system is absolutely rigid and there is no damping,
- spring is absolutely rigid and intangible
- dashpot is stubborn and intangible [1].

By the Laplace operator for the equation (1.1) (damped vibrations) we obtain [22]:

$$m \cdot s^2 + c \cdot s + k = 0 \;\rightarrow\; s_{1,2} = \frac{-c \pm \sqrt{c^2 - 4 \cdot m \cdot k}}{2 \cdot m} \tag{1.3}$$

$$\frac{k}{m} = \Omega^2, \frac{c}{2 \cdot m} = \delta \rightarrow s_{1,2} = -\delta \pm \sqrt{\delta^2 - \Omega^2} \tag{1.4}$$

where

$$\delta = \frac{c}{2 \cdot m} \tag{1.5}$$

is damped factor and

$$\Omega = \sqrt{\frac{k}{m}} \tag{1.6}$$

is natural frequency.

If $\delta > \Omega$ in equation (1.4), the motion is oscilating but aperiodic. If $\delta = \Omega$ the system is damped by the critical damping c_c:

$$\delta = \frac{c_c}{2 \cdot m} \rightarrow c_c = 2 \cdot m \cdot \Omega = 2 \cdot \sqrt{k \cdot m} \tag{1.7}$$

If $\delta < \Omega$ in equation (1.4) we obtain the complex conjugate equation:

$$s = -\delta \pm i\sqrt{\Omega^2 - \delta^2} = -\delta \pm i \cdot \vartheta \tag{1.8}$$

it is vibration with circular frequency

$$\vartheta = \sqrt{\Omega^2 - \delta^2} \tag{1.9}$$

The general soltuion form is:

$$x = x_1 + x_2 = \bar{X}_1 \cdot e^{(-\delta + i\vartheta) \cdot t} + \bar{X}_2 \cdot e^{(-\delta + i\vartheta) \cdot t} = e^{-\delta t} \cdot (\bar{X}_1 \cdot e^{i \cdot \vartheta \cdot t} + \bar{X}_2 \cdot e^{i \cdot \vartheta \cdot t}) \tag{1.10}$$

where $\bar{X}_1, \bar{X}_2$ are the complex amplitudes and time period $T = \frac{2\pi}{\vartheta}$.

For damped vibration we also use damping ratio:

$$D = \frac{c}{c_c} = \frac{2 \cdot m \cdot \delta}{2 \cdot m \cdot \Omega} = \frac{\delta}{\Omega} \tag{1.11}$$

The motion of undamped vibrations is described by the differential equation:

$$m\ddot{x} + kx = 0 \tag{1.12}$$

By the Laplace operator we obtain the general solution form:

$$m \cdot s^2 + k = 0 \ \rightarrow s_{1,2} = \pm\sqrt{\frac{-k}{m}} = \pm i\sqrt{\frac{k}{m}} \tag{1.13}$$

$\frac{k}{m} = \Omega^2 \ \rightarrow s_{1,2} = \Omega^2; \Omega$ is natural frequency of undamped vibrations. The general solution is the sum of two particular solutions:

$$x = x_1 + x_2 = \bar{X}_1 \cdot e^{-i\Omega t} + \bar{X}_2 \cdot e^{-i\Omega t} \tag{1.14}$$

for the condition that $t = 0 \ \rightarrow x = a;\ \dot{x} = b$ we obtain $x_1 = \frac{1}{2} \cdot (a + i \cdot \frac{b}{\Omega})$, $x_2 = \frac{1}{2} \cdot (a - i \cdot \frac{b}{\Omega})$ and we get:

$$x = a \cdot \cos \Omega t + \frac{b}{\Omega} \cdot \sin \Omega t \tag{1.15}$$

the period time [22]: $T = \frac{2\pi}{\Omega}$ and the amplitude of undamped natural vibration is presented in Figure 4.

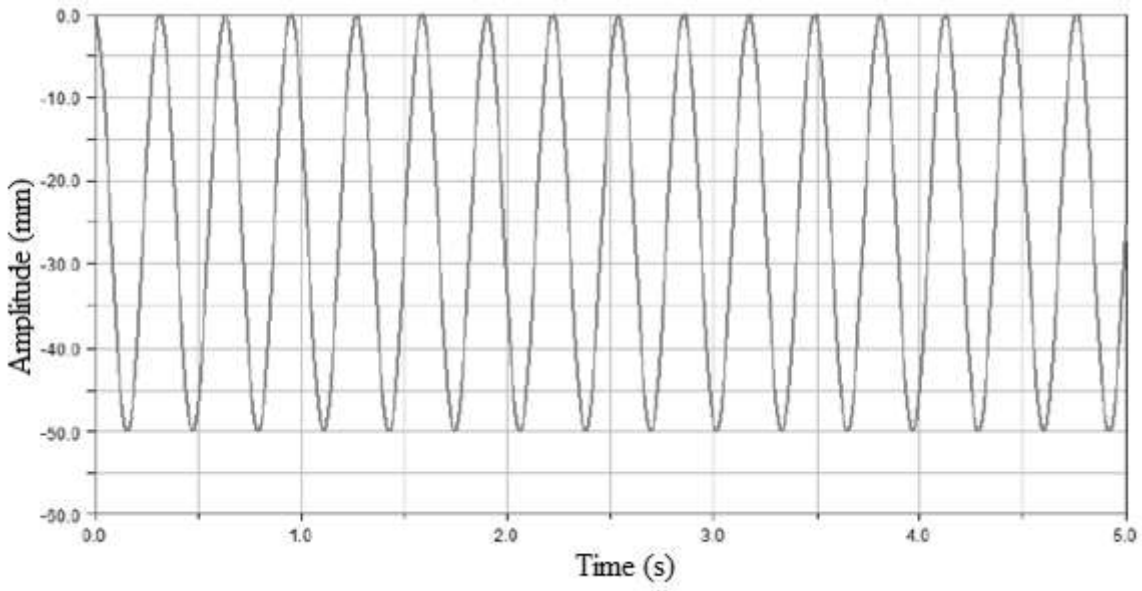

Figure 4: Amplitude of undamped natural vibration [22]

Natural vibrations have little practical significance. Theirs character are short and transient [1].

1.2.2 Forced vibrations

Forced vibrations are carried out if there is an external, periodic force F acting on the system:

$$F = F_0 \cos 2\pi f t \tag{1.16}$$

Factors cause forced vibrations:

a) Forced impulses appeared in milling system
   - imbalance of the rotating masses
   - reciprocating motion masses.

b) Periodically intermittent cutting process
   - periodic variation in sectional chip,
   - discontinues cutting process .

c) Forced pulses inside the machining system through the machine base [3].

After the subsequent period the resulting motion is in steady state. The amplitude A is constant there and the frequency of vibration is equal to the frequency of exciting force. There are also natural vibrations present [4].

The amplitude A of the vibration depends on the amplitude F_0 of the force, on the stiffness k and damping coefficient c of the system and on the ratio f/f_n of the exciting frequency over the natural frequency of the system. Amplitude is maximum for the $f = f_n$ and the resonance obtained (Figure 5).

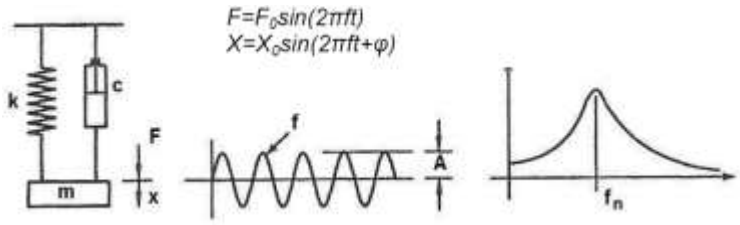

Figure 5: Forced vibrations [1]

All types of machinery present forced vibrations where periodic forces are generated. These are mostly due to unbalanced rotating shafts or the reciprocating motions. They are significant only it the case of resonance usually.

Equation of force undamped vibration is [1]:

$$m \cdot \ddot{x} + kx = F \text{ or } m \cdot \ddot{x} + kx = F \cdot e^{j\omega t} \tag{1.17}$$

General solution is sum of homogenous solution without the right side [22]:

$$x = \bar{X}_1 \cdot e^{j\Omega t} + \bar{X}_2 \cdot e^{-j\Omega t} = a \cdot \cos \Omega t + \frac{b}{\Omega} \cdot \sin \Omega t \tag{1.18}$$

and particular solution has form: $x = X \cdot e^{j\omega t}$.

The magnitude of the deflection is derived for the condition that equation motion (1.16) has the particular solution:

$$-m \cdot \omega^2 X e^{j\omega t} + k \cdot X \cdot e^{j\omega t} = F \cdot e^{j\omega t} \tag{1.19}$$

The amplitude of the deflection is:

$$X = \frac{F}{k - m \cdot \omega^2} = \frac{F}{k - \frac{k}{\Omega^2} \cdot \omega^2} = \frac{F}{k} \cdot \frac{1}{1 - \frac{\omega^2}{\Omega^2}} = \frac{F}{k} \cdot \frac{\Omega^2}{\Omega^2 - \omega^2} \tag{1.20}$$

The complex dynamic elasticity is derived by ratio of amplitude of the deflection and acting force $R_{dc} = \frac{X}{F} = \frac{1}{k} \cdot \frac{\Omega^2}{\Omega^2 - \omega^2}$

The equation of motion for the damped system:

$$m \cdot \ddot{x} + c\dot{x} + kx = F \text{ or } m \cdot \ddot{x} + c\dot{x} + kx = F \cdot e^{j\omega t} \tag{1.21}$$

General solution is sum of homogenous solution without the right side and particular solution with the right side:

$$x_h = e^{-\delta t} \cdot \left(X_1 \cdot e^{j\omega t} + X_2 \cdot e^{-j\omega t}\right) \tag{1.22}$$

$$x_p = X \cdot e^{j\omega t} \tag{1.23}$$

equation has form:

$$-m \cdot \omega^2 X \cdot e^{j\omega t} + c \cdot j \cdot \omega \cdot X \cdot e^{j\omega t} + k \cdot X \cdot e^{j\omega t} = F \cdot e^{j\omega t} \tag{1.24}$$

The complex amplitude *X* has magnitude:

$$X = \frac{F}{k - m \cdot \omega^2 + c \cdot j \cdot \omega} = \frac{F}{k - \frac{k}{\Omega^2}\omega^2 + 2 \cdot m \cdot \delta \cdot j \cdot \Omega} \tag{1.25}$$

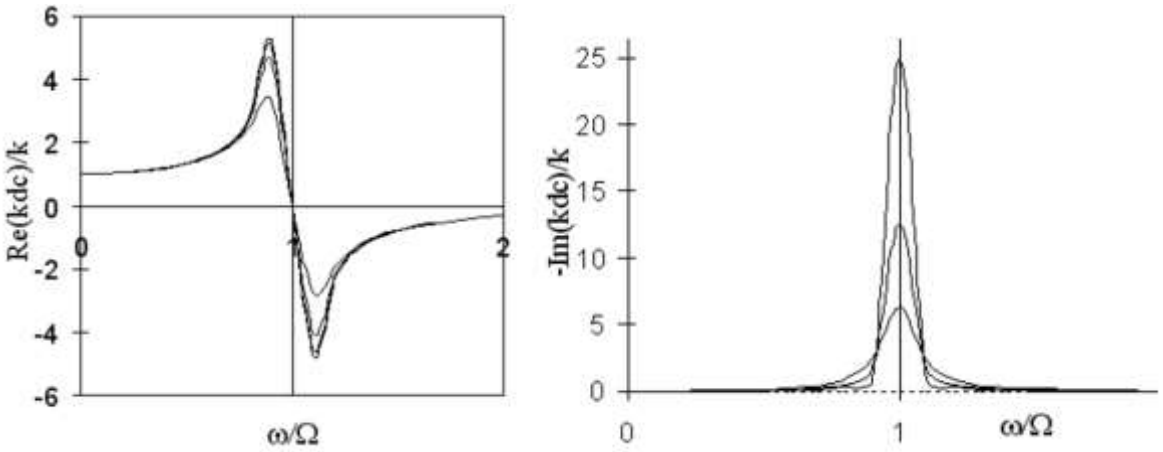

Figure 6: Real and imaginary parts of the transfer function [22]

from equation (1.6) and (1.11) we obtain:

$$X = \frac{F}{k} \cdot \frac{\Omega^2}{\Omega^2 - \omega^2 + 2 \cdot j \cdot \delta \cdot \omega} = \frac{F}{k} \cdot \frac{F}{1 - \frac{\omega^2}{\Omega^2} + 2 \cdot D \cdot j \cdot \frac{\omega}{\Omega}} \tag{1.26}$$

If we multiply equation (1.26) by the complex conjugate number we obtain:

$$X = \frac{F}{k} \cdot \frac{1 - \frac{\omega^2}{\Omega^2} - 2 \cdot D \cdot j \cdot \frac{\omega}{\Omega}}{\left(1 - \frac{\omega^2}{\Omega^2}\right)^2 + \left(2 \cdot D \cdot \frac{\omega}{\Omega}\right)^2} \tag{1.27}$$

The complex amplitude can be separate to real part Re(x) (see Figure 6) and imaginary part Im(x).

and

$$Re(x) = \frac{F}{k} \cdot \frac{1 - \frac{\omega^2}{\Omega^2}}{\left(1 - \frac{\omega^2}{\Omega^2}\right)^2 + \left(2 \cdot D \cdot \frac{\omega}{\Omega}\right)^2} \tag{1.28}$$

$$Im(x) = \frac{F}{k} \cdot \frac{2 \cdot D \cdot j \cdot \frac{\omega}{\Omega}}{\left(1 - \frac{\omega^2}{\Omega^2}\right)^2 + \left(2 \cdot D \cdot \frac{\omega}{\Omega}\right)^2} \tag{1.29}$$

$$|X| = \sqrt{Re(x)^2 + Im(x)^2} \tag{1.30}$$

$$|X| = \frac{F}{k} \cdot \frac{1}{\sqrt{\left(1 - \frac{\omega^2}{\Omega^2}\right)^2 + \left(2 \cdot D \cdot \frac{\omega}{\Omega}\right)^2}} \tag{1.31}$$

Complex dynamic elasticity [22]:

$$R_{dc} = \frac{X}{F} = \phi(\omega) = G(\omega) + j \cdot H(\omega) \tag{1.32}$$

$$G(\omega) = Re(R_{dc}) = \frac{Re(x)}{F}, jH(\omega) = Im(R_{dc}) = \frac{Im(x)}{F} \tag{1.33}$$

In machining, significant cases of the forced vibrations occur in final and fine machining like fine boring and grinding, where they produce waviness of the machined surface. In milling, forced vibrations are excited by the periodic component of the cutting force [1].

1.2.3 Self-excited vibrations

Basically, there is no external acting force in this type of vibrations but there is periodical acting force built-in mechanism. This periodical force is excited by the vibration of the system and it can occur in cases if the system oscillates. Amplitude of vibrations rising up till it attains stabile value, frequency is almost equal natural frequency and there is energy source for that system. An example of self-exciting vibration can be whistling, playing the violin or flute, and so on [1].

Literature [5] presents these types amplitude's of vibrations (see Figure 7):

a) parametric – excite due to the changes in one of the parameters of the elastic system, which is periodically varying

b) almost harmonic – harmonic course is similar as shape course

c) relax vibrations – time course has a saw-motion character

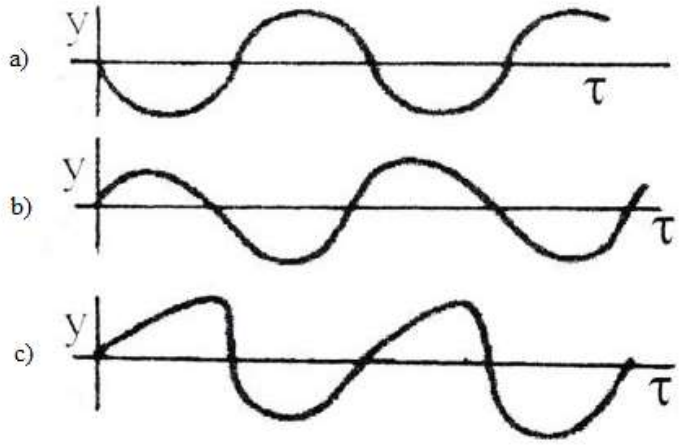

Figure 7: Types of amplitude vibration's: a) parametric (harmonic), b) almost harmonic, c) relax vibrations [5]

Van der Poll's model explain how the self-exciting vibrations arise, see Figure 8. There is friction force $F_t = \mu \cdot G$ when the belt is not moving. When the belt starts moving, there is force F_t. If the friction force F_t is equal to spring force F_p, the system get moving to each other (belt and body), by this situation the friction force immediately decrease and the system starts oscillating. There is an inner force which arises due to the difference in frictional force when the system is not moving and in a motion. This inner force is called excitation force [5].

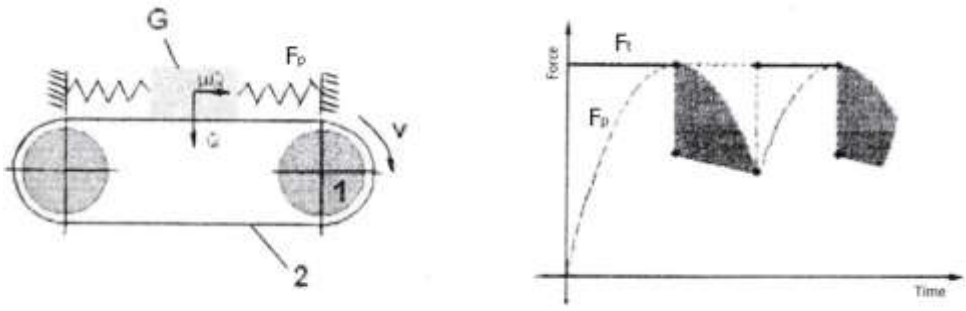

Figure 8: Van der Poll model [5]

1.3 Chatter in machining

The first basic researches about the chatter date to 50ies of 20 century. The theoretical basics were derivate for turning. This theoretical knowledge was applicate for milling with some improvements and in this field of study was shown big significance in machining. Stability lobes (stability diagrams) can be created by this theory and the power of the machine respectively spindle power can be set for maximal effectivity of the production.

Chatter can appear in all types of machining operations. The chatter arises by the interaction between cutting process and milling machine, this back loop system is shown in Figure 9. The whole system machine-cutter-workpiece can influence the variable depth of chip which is connected with variable position of the cutter due to workpiece. The cutting process is the origin of vibration inside the system [7].

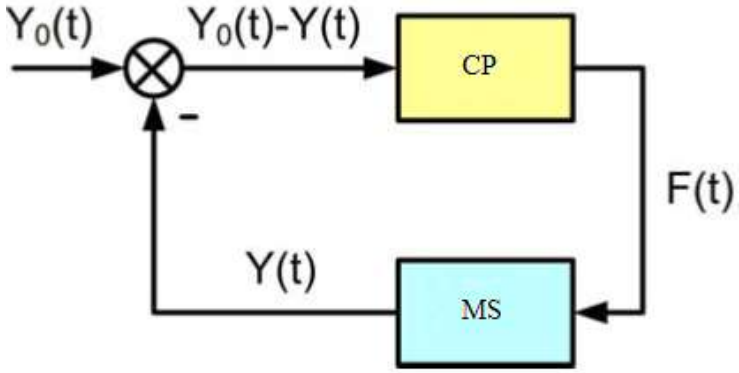

Figure 9: Back loop of the origin of chatter [7]

The most significant cutting parameter, which is decisive for the generation of chatter, is the width of cut *b*. For sufficiently small chip widths, cutting is stable and there is no chatter. By increasing *b* chatter starts to occur at a certain chip width b_{lim} and becomes more energetic for all values of $b>b_{lim}$. Parameters, which involve the value of b_{lim} are dynamic characteristics of the structure, material of the workpiece, geometry of the tool and cutting speed and feed. In milling, cumulative chip width b_{cum}, has to be considered, which is the sum of the chip widths of all the teeth cutting simultaneously (see Figure 10) [1].

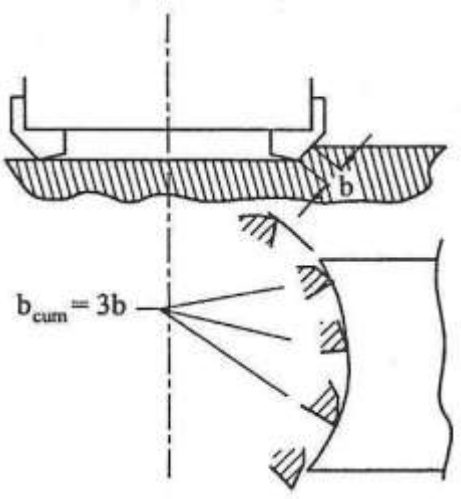

Figure 10: Cumulative chip width in milling [1]

We distinguish four different sources of self-excitation in metal cutting according to the different feedback modes:

1. mode-coupling chatter
2. regenerative chatter
3. frictional chatter

4. thermal chatter [15],

in following are discussed the first and the second sources.

1.3.1 Mode coupling

Mode coupling is a mechanism of self-excitation that can only be associated with situation where the relative vibration between the tool and the workpiece can exist simultaneously in at least two directions in the plane of the orthogonal cut and they have different natural frequencies. Periodic cutting force excites the system in the both directions with the same natural frequency and constant mutual phase, where the tool is moving on the elliptical path (see Figure 11).

Two orthogonal sets of the sprigs are connected to the tool which is connected to the body of the system. Simultaneous vibrations in the direction X1 and X2 with the same frequency and a phase shift between the two results in an elliptical motion. The workpiece is moving with the steady cutting speed v_f and the tool is moving on the elliptical path of the arrows. For the part of the periodic motion of the tool from A→B the force acts against the motion and takes energy away of the system. During the motion from B→A the force drives the tool and imparts energy to its motion. There is greater cutting force on the path BA and the tool cut in bigger depth, due to this the energy delivered is larger than energy taken away on the path AB. If the energy is not consumed by the damping, the amplitude of vibrations is raising and cutting process getting unstable. For various directional orientations of the system, its ability to derive the chatter in milling [1].

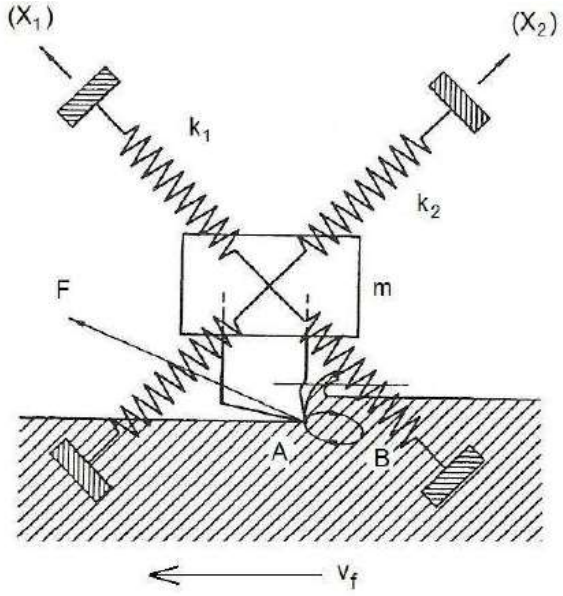

Figure 11: Mechanism of mode coupling in a system with two mutually perpendicular degrees of freedom [1]

1.3.2 Regeneration of waviness

In all machining operation the tool removes chip from a surface that was produced by the tool in the preceding pass, that is, the surface produced in milling by the preceding tooth of the cutter or, in turning, during preceding revolution (see Figure 12). If there is relative vibration between tool and workpiece, waviness is created on the surface. The tool in next tooth in milling encounters a wavy surface and removes a chip with periodically variable

thickness and the cutting force is periodically variable. This produces vibrations and due to the conditions derived further, these vibrations may be at least as large as in the previous cut. This is the reason why is the waviness continually regenerated.

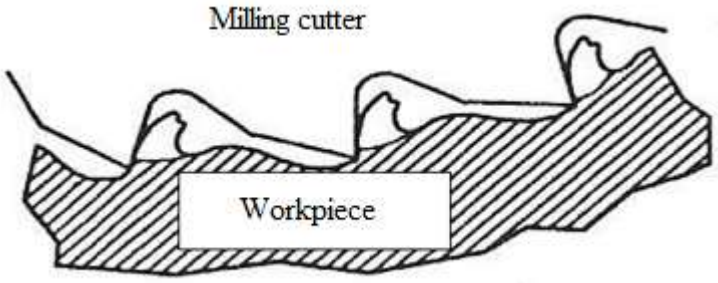

Figure 12: Regeneration of surface waviness in milling; the chip thickness variation [1]

Regeneration of waviness is influenced by the geometry of machining operation. It imposes constrain on the phasing between undulation produced in subsequent passes. The tool exists from the cut between the individual passes and its vibrations decay. At the beginning of following cut its vibration freely adjusts its phase for maximum regeneration.

Regeneration of waviness is described by equation:

$$p = N_l + \frac{\varepsilon}{2\pi} = \frac{f}{n} \tag{1.34}$$

where p is created by integer of full waves N_l (N_l is also called the lobe number) and a fraction $\varepsilon/2\pi$ of a wave on circumference of the workpiece.

If ε will be $\varepsilon = 2k\pi$, where k=1,2,3,…,n and the condition of the stability limit by equation (1.56), dynamic force by equation (1.39) leads to be equal 0 and machining will be stable.

Otherwise, if $\varepsilon = \frac{3}{2}k\pi$, the force leads to be the biggest, and the system is getting unstable. Due to this, rotation speed is regulated to achieve the condition $\varepsilon = 2k\pi$. Equation (1.34) can be changed to:

$$N + \frac{\varepsilon}{2\pi} = \frac{f}{n} \tag{1.35}$$

due to this, we derive the left side of equation (1.35) to determine the full waves and determine the rotation.

If the conditions are kept, the number of rotation exists:

$$n = \frac{f}{N} \tag{1.36}$$

where N=1,2,3,…,n which with selected cutter can guarantee machining without vibrations.

Maximum value of rotation without vibrations is [1]:

$$n = \frac{60f}{m \cdot N} \tag{1.37}$$

1.4 Cutting conditions influence the stability in machining

There are several conditions which include the stability of cutting process:

- material,
- feed rate,
- cutting speed,
- tool geometry.

Influence of the workpiece material is connected with cutting resistance *Ks*. This effect is described by the equation:

$$b_{lim} = \frac{-1}{2K_s Re(G)_{neg}} \tag{1.38}$$

If the cutting resistance Ks_A of material A is 1.5 Ks_B, due to this, material B will have 1.5 lower value of b_{lim}.

There is direct proportional between feed motion f and the middle width of chip h_m. Value of the cutting resistance K_s is connected with those parameters – influence of h due to b_{lim}. Value of K_s is decreasing if the value h is rising.

The stability of process is rising up due to raising the value of feed motion in turning and drilling. Very often is b_{lim} lower for minor feed motion. Typical operations, where are used to machine thin chip are more predisposed to chatter. On the other hand, milling process has the opposite behaviour, where the chatter is rising up due to higher value of feed motion. As is mentioned upper, at the beginning of the milling process has the width of chip value zero (up-milling), or the tooth of cutter leave the workpiece (down-milling) when the value of width of chip is zero. It could happen that the combination of thin chip/small feed motion is decreasing the stability of the process.

Influence of the stability by the cutting speed is connected with the damping process during machining. By the equation:

$$F_{dyn} = K_s \cdot b \cdot (Y_0 - Y) \tag{1.39}$$

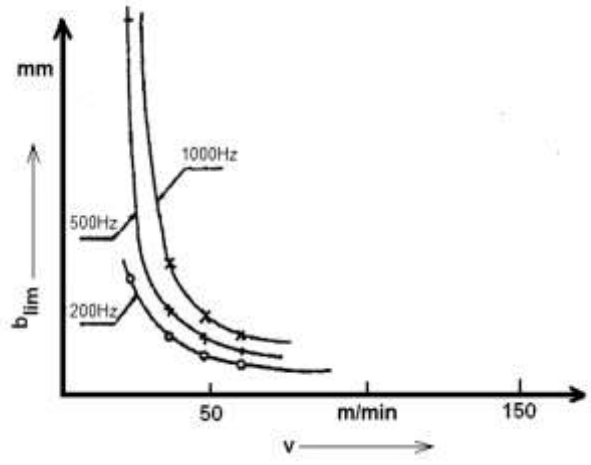

Figure 13: Stability influenced by the cutting speed [1]

is variable element of the cutting force proportional to variable width of the chip. There could be the mutual phase shift created by the generation of the cutting force. This process causes initial damping in the self-excited motion of the tool when the chip is creating. This type of damping is important for very low cutting speed, for example under 25m/min and especially under 10m/min. Cutting process during these conditions (low cutting speed) is more stable. Diagram in Figure 13 is typical for cutting processes of the carbon steel and it shows variability of the limit width of chip b_{lim} dependence on the function of cutting speed for the systems with variable natural frequencies: 200, 500 a 1000 Hz.

1.5 Analysing of the stability in chatter

The theory of chatter is based on a number of simplifications which, however, have been proven not to substantially alter the most important effects on the limit of stability as they are found experimentally.

These simplifications are shown below:

- the value of the variable component of the cutting force varies proportionally and instantaneously with the variation of chip thickness,
- the direction of the variable component of the cutting force is constant,
- the variable component of the cutting force depends only on vibration in the direction of normal to the cut,
- the frequency of the vibration and the mutual phase shift of undulations in subsequent overlapping cuts are not influenced by the relationship of wavelength to the length of cut; this assumption correspond to an infinite length for every cut or, practically, to planning [1],
- the vibratory system of the machine is linear, it means that the feedback of the system is directly proportion to the vibration; in practice the systems are not clearly linear, but for better description of sample systems (for modal analysis), the fittest linear approximation is considered[8].

The theory of chatter considers the linear vibration system, due to this consideration, function of feedback can be measured on the machine tools. Modal interpretation can be calculated due to mechanical difficultly. Linearity of the system established three major considerations:

1. homogeneity – determine the independence on the value of amplitude of excited frequency,
2. reciprocity – suppose the existence of symmetry and due to this, place of the excitation effects is changeable with place of the detection response, if the value transfer is same,
3. superposition – determines the independence of the order in composing of exciting effects [8].

1.5.1 Frequency theory

Figure 14 presents foundations for the condition of stability. The structure of a machine tool is described as a frame with the workpiece at one end and the tool at the opposite end.

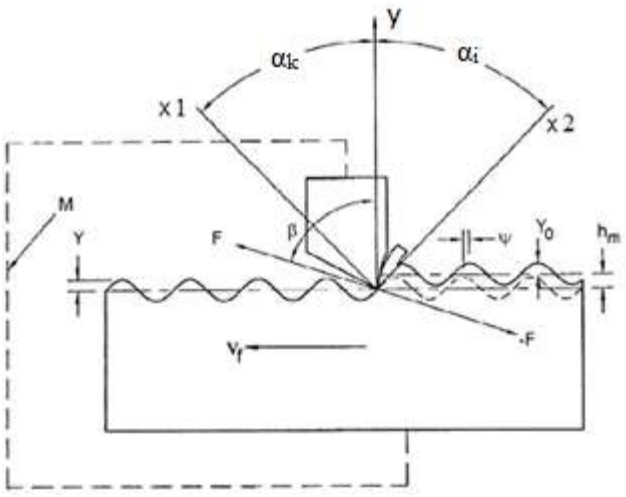

Figure 14: The regeneration diagram relating force, surface waviness and vibration [1]

To estimate the limit value of the chip width is possible to use the frequency theory. Figure 14 presents fundamentals of this theory. In the direction of the cutting speed v_f is the relative cutting motion between the tool and workpiece. The structure is a vibratory system that is characterized by the individual modes of vibration, each of which represents a freedom of the relative motion between the workpiece and tool and has a particular direction x1 and x2. The vibration component, which is normal to the cut surface, produces undulations with an amplitude $Y_0(t)$ in one cut, and in the subsequent cut this component has amplitude $Y(t)$. The direction of the cutting force is inclined by the angle β from y and by corresponding values of angle α_i. In subsequent cut the whole system is oscillating. Undulations and vibrations have an amplitude Y a Y_0 and between them is phase-shift ψ. The process of self-excitation is closed-loop one in which the vibration cause a force variation, and the variable force. Figure 15 also presents cutting force $F(t)$ inclined to normal y by the angle β [1][7].

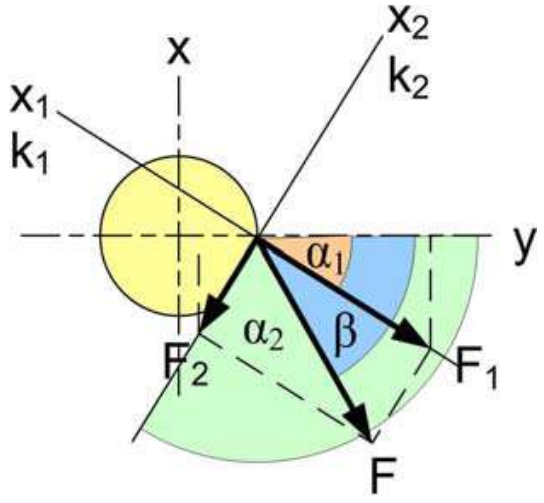

Figure 15: Directionality in frequency theory [7]

The force depends on vibrations in at least two subsequent passes:

$$F = R \cdot b \cdot (Y_0 - Y) \tag{1.40}$$

where (Y-Y_0) is equal h (chip thickness) and let's consider, that variables F, Y a Y_0 are not function of the time. The magnitude of coefficient R is dependence on workpiece material and this coefficient can be affected by the cutting conditions, geometry of tool, resp. tool wear. We consider, that coefficient R is equal to specific cutting resistance:

$$R = K_S \tag{1.41}$$

We also consider that coefficient R is real, it means that there is no phase shift between the cutting force F and chip thickness (Y-Y_0). The magnitude of the cutting force is not dependence to vibration frequency.

The deflection of the cutting tool is given:

$$Y = \Phi(f) \cdot F \tag{1.42}$$

Transfer function $\Phi(f)$ is complex receptance. Basically it is a ratio between complex amplitude in selected direction and excited force acted in different direction. Vibration element is analysed in direction of normal to the cut y which is acted by cutting force $F(t)$ inclined to normal by angle β. Transfer function is given by the equation:

$$\Phi = \frac{Y}{F} \tag{1.43}$$

Cutting force elements in directions *x1* and *x2* which act these forms are given by equations:

$$F_1 = F \cdot \cos(\alpha_1 - \beta) \tag{1.44}$$

$$F_2 = F \cdot \cos(\alpha_2 - \beta) \tag{1.45}$$

The deflections in relevant directions are computed by the equations:

$$X_1 = F_1 \cdot \Phi_1 \tag{1.46}$$

$$X_2 = F_2 \cdot \Phi_2 \tag{1.47}$$

The main purpose is in the direction of normal to the cut *y*. In this case the deflections X1 and X2 are inclined into this direction. The resulting deflection is given by the sum of the both of inclined deflections:

$$Y = X_1 \cdot \cos\alpha_1 + X_2 \cdot \cos\alpha_2 \tag{1.48}$$

after substituting:

$$Y = F \cdot [\Phi_1 \cdot \cos\alpha_1 \cdot \cos(\alpha_1 - \beta) + \Phi_2 \cdot \cos\alpha_2 \cdot \cos(\alpha_2 - \beta)] \tag{1.49}$$

where *u1* and *u2* are directional factors:

$$u_1 = \cos\alpha_1 \cdot \cos(\alpha_1 - \beta) \tag{1.50}$$

$$u_2 = \cos\alpha_2 \cdot \cos(\alpha_2 - \beta) \tag{1.51}$$

the final equation for the deflection of normal to the cut *y* is:

$$Y = F \cdot (\Phi_1 \cdot u_1 + \Phi_2 \cdot u_2) \tag{1.52}$$

The resulting complex transfer function between F and Y, which has various directions, is called transverse (oriented) receptance and it is a sum of the both forms of transfer functions:

$$\Phi = \frac{Y}{F} = \Phi_1 \cdot u_1 + \Phi_2 \cdot u_2 = \Phi_{01} + \Phi_{02} \tag{1.53}$$

To determine the condition for the limit of stability we combine equations (1.40) and (1.42) and we obtain:

$$Y = \Phi \cdot K_S \cdot b \cdot (Y_0 - Y) \tag{1.54}$$

$$\frac{Y_0}{Y} = \frac{1+\Phi \cdot K_S \cdot b}{\Phi \cdot K_S \cdot b} = \frac{\frac{1}{K_S \cdot b}+\Phi}{\Phi} \tag{1.55}$$

The major condition for the limit of stability of cutting process is given:

$$\frac{Y_0}{Y} = 1 \tag{1.56}$$

The limit of stability may be formulated so that vibrations do not decay nor increase from pass to pass. Combining equations (1.55) and (1.56) expresses the equality of the absolute values of two complex numbers. The function Φ is complex, while:

$$\left|\frac{1}{K_S \cdot b} + \Phi\right| = |\Phi| \text{ or } \left|\frac{1}{K_S \cdot b} + Re(f) + jIm(f)\right| = |Re(f) + jIm(f)| \tag{1.57}$$

The equality is evident. The + sign leads to $b = \infty$ (magnitude of width of chip is infinity). The – sign gives the resulting limit condition of the stability:

$$K_S \cdot b = \frac{-1}{2 \cdot Re(f)} \tag{1.58}$$

we can express the limit value of the chip width as equation:

$$b_{mez} = \frac{-1}{2 \cdot K_S \cdot Re(f)_{neg}} \tag{1.59}$$

The chip width *b* is a positive number, therefore equation (1.59) can be satisfied for the negative part of the function *Re(f)*. The smallest chip width at which chatter can occur for all of the values *b* that satisfy equation (1.59), there is a minimum one. [7] This is the actual critical limit of stability and it correspond to the largest negative value of Re*(f)* to the minimum Re$(f)_{min}$:

$$b_{crit} = \frac{-1}{2 \cdot K_S \cdot Re(f)_{neg,min}} \tag{1.60}$$

For $b > b_{lim}$ chatter will occur and grow. For chip widths $b < b_{lim}$ cutting is stable and there is no self-excited vibration. Equation (1.60) has practical significance. It offers a clearly different criterion for the dynamic properties of machine tool structures and it is used to analyse and design structures with maximum stability at minimum weight.

The minimum chip width represents a limit in a machining process. Since it is independent of the chatter frequency, there is only a fixed value determined by the materials and geometries of the cutter and workpiece [7].

1.5.2 Nyquist criterium

Another way of deriving the expression (1.59) is based on the classical approach of the control systems theory. Refer to the Figure 14 we can express this situation by the block diagram in Figure 16.

The variable force F_v excites the structure. Vibration, relative between workpiece and tool, is produced trough the corresponding transfer function Re(ω) of the structure. The waviness of the structure is produced by the difference between Y and Y_0 of the proceeding pass. From the waviness of the surface from which the cut is taken and which was delayed by τ (time between the two cutting phases) plus the feed per pass H_m is the average chip thickness H. The time delay for vector rotating with frequency ω result in phase shift $\varepsilon = \tau \cdot \omega$ and it is represented by factor $e^{-j \cdot \omega}$. The force F is produced by the $K_s b$, if the force F is compared with the mean force F_m ,leaves the variable force F_v that excites the structure.

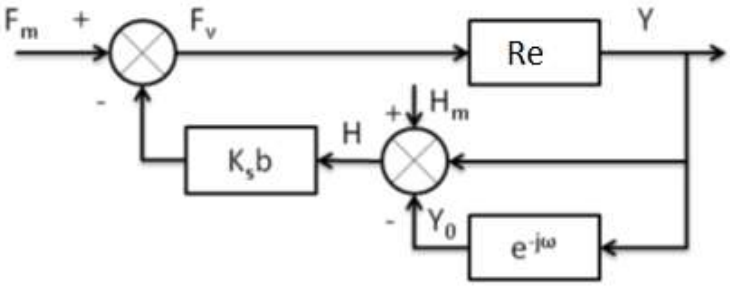

Figure 16: Block diagram of vibration in regenerative cutting [1]

Any vibration at the limit of stability would remain constant without decaying or increasing and the absolute values of amplitudes of vibrations in subsequent passes are equal ($|Y| = |Y_0|$). According to the Nyquist criterion, this will be obtained if the open-loop transfer function has the value -1:

$$K_s \cdot b \cdot Re(\omega) \cdot \left(1 - e^{-j \cdot \varepsilon}\right) = -1 \tag{1.61}$$

$$b_{lim} = \frac{-1}{K_S \cdot Re(1 - e^{-j \cdot \varepsilon})} \tag{1.62}$$

The value of the chip width *b* at the limit of stability is expressed by equation (1.62) and because of the coefficient *Ks* and the chip width *b* are obviously always real, the condition is satisfied only for following equation and the value of the chip width at the limit of stability will be:

$$Re\left(1 - e^{j\varepsilon}\right) = Re - Re \cdot e^{-j\cdot\varepsilon} \tag{1.63}$$

$$b_{lim} = \frac{-1}{2 \cdot K_s \cdot Re(G)} \tag{1.64}$$

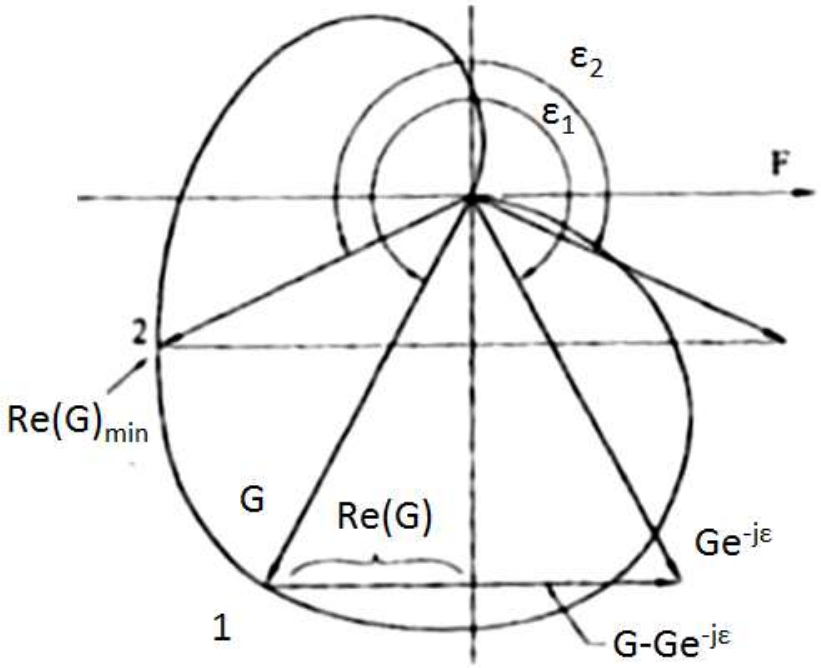

Figure 17: Nyquist diagram (amplitude-phase characteristic) [1]

Figure 17 depict the two vectors, the force *F* is taken as real and scaled to a unit value. The transfer function *Re* of the system is plotted in the complex plane, which represents a system with two degrees of freedom. The vector *G* drawn between the origin of coordinates and point 1 correspond to a particular frequency of the force *F*. The vector $Re \cdot e^{-j\varepsilon}$ has to be equal in magnitude, and the difference $Re - Re \cdot e^{-j\varepsilon}$ must be real, therefore, in the diagram it is parallel with the real axis. The vector Re drawn to point 1 corresponds to a particular value of the phase shift ε between undulations in subsequent cuts. There is a corresponding frequency of vibration that corresponds to point 1 on the transfer function. The smallest value of b_{lim} will correspond to the largest value of *Re(G)*, which give us the critical value of b_{lim} as expressed in (1.60) [1].

1.5.3 Stability evaluation in the time dimension

The system of differential equations which determined dynamical balances of forces in directions X_1 and X_2 is used to solve the simulation of the system by proceeding in small time steps d*t*. The count of the time steps is denoted *n*, which is also the subscript of selected variable at a given times. This simulation can involve nonlinearity during the

cutting process (due to vibration) [1]. The instantaneous chip thickness is usually taken as a difference of the tool positions in two subsequent passes:

$$h = h_{av} + y_{n-1} - y_n \tag{1.65}$$

h_{av} is average chip thickness, y_{n-1} is the amplitude of vibration in previous pass, and y_n is amplitude of vibration in actual pass. At any time t_n we may check which of the cuts preceding the present cut reached lowest in the workpiece material and denote such position. The instantaneous chip thickness is:

$$h = y_{min} - y_n \tag{1.66}$$

the cutting force at the instant t_n is proportional to chip thickness h and the chip width b:

$$F_n = K_s \cdot b \cdot h \tag{1.67}$$

cutting force cannot be negative number. If $F_n < 0$ then $F_n = 0$.

Cutting force is split into X1 and X2 directions:

$$F_1 = F_n \cdot \cos(\beta - \alpha_1) \tag{1.68}$$

$$F_2 = F_n \cdot \cos(\beta - \alpha_2) \tag{1.69}$$

the motion in these directions is described by:

$$m_j \ddot{x}_j + c_j \dot{x}_j + k_j x_j = F_j \;\; j = 1,2 \tag{1.70}$$

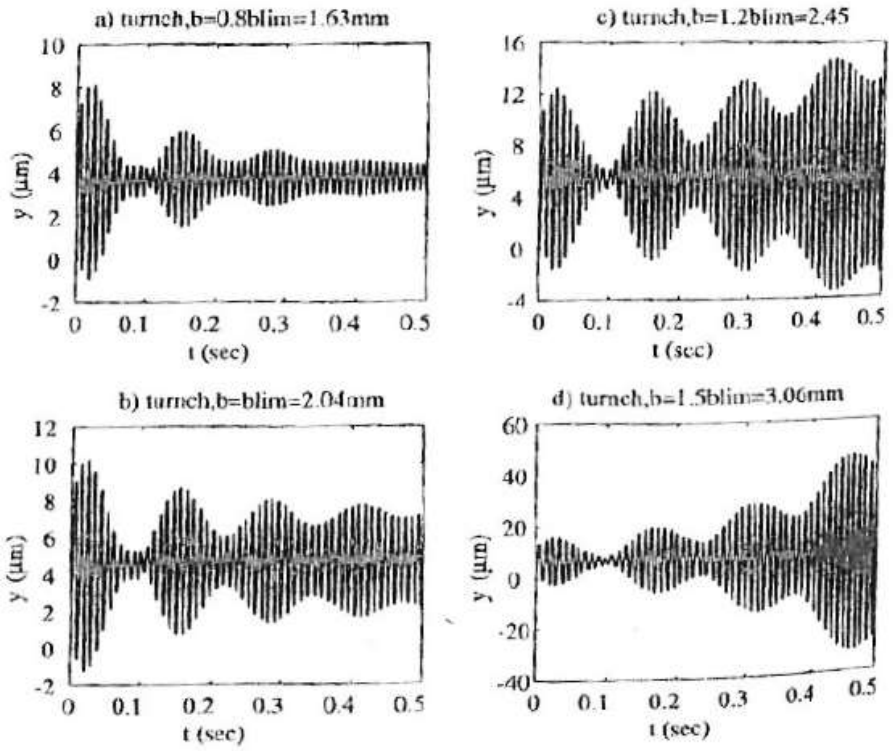

Figure 18: Simulated chatter: a), b) - stable, c), d) – unstable [1]

by the first integration of this equation we got an acceleration in the direction X1 in an actual time step. By the second integration we got a velocity and position in subsequent time step:

$$\ddot{x}_{1,n} = \frac{F_{1,n} - c_1 \dot{x}_{1,n} - k_1 x_1}{m_1} \tag{1.71}$$

$$\dot{x}_{1,n+1} = \dot{x}_{1,n} + \ddot{x}_{1,n} \cdot dt \tag{1.72}$$

$$x_{1,n+1} = x_{1,n} + \dot{x}_{1,n} \cdot dt \tag{1.73}$$

For X2 direction we do the same workflow and in following we express the deflection in the direction Y:

$$y_n = x_{1,n} \cdot \cos \alpha_1 + x_{2,n} \cdot \cos \alpha_2 \tag{1.74}$$

Figure 18 presents simulated chatter for different conditions of cutting process.

1.6 Stability Lobes

Lobe's diagram (see Figure 20) based on regenerative chatter theory is an effective tool to predict and control chatter (see Figure 19). Stability diagrams can be applied in machining processes to optimize the maximum depth of cut at the highest available spindle speed, thus improving the material removal rate and increasing productivity. A stability lobe diagram is formed by a series of intersected scallop-shaped borderlines of stability. The intersections of the lobes denote the deepest stable cuts at various ranges of spindle speed [1].

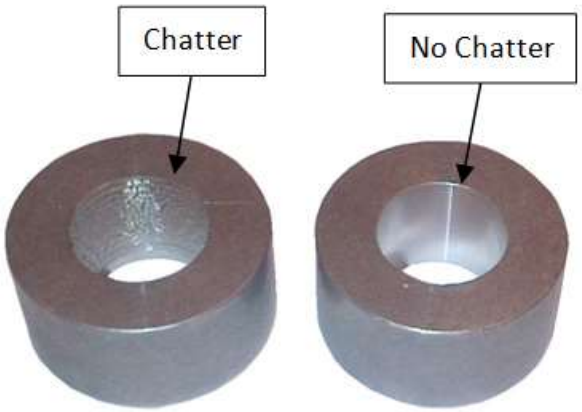

Figure 19: Example workpiece with and without chatter [24]

The governing equations of machine chattering can be derived from the general equation of vibration and the regenerative chatter equations. Substituting equation (1.40) into the general equation of vibration (1.21) we obtain the formula for chip width (1.38). When we solve equation (1.40) and (1.38) together, the chip width *b* is dependent on the frequency ω of the machine vibration or chatter through the frequency ratio $\frac{\omega}{\Omega}$.

Equation b_{min} can be also expressed as

$$b_{min} = \frac{2 \cdot k \cdot D \cdot (1+D)}{K_S} \tag{1.75}$$

As is mentioned above, roughness or waviness always exists on the machined surface of workpiece due to vibrations. According to regenerative chatter theory, chatter occurs whenever there is a shift of the phase shift angle ε between the current and previous surface waviness (1.34). Therefore, the ratio of chatter frequency ω to tooth-stroke frequency ω_t represents the number of surface waves between consecutive cutter teeth and can be written as an integer N_l. Phase shift angle ε between the current and previous surface waviness may be expressed as

$$\varepsilon = \pi + 2 \cdot \tan^{-1} \frac{Im(x)}{Re(x)} \tag{1.76}$$

where Re(x) and Im(x) are used from equation (1.33).

Substitute equation (1.38) and equation (1.76) and then into (1.34) we obtain the equation of regenerative chatter

$$\frac{\omega}{\omega_t} = n + \frac{1}{2} + \frac{1}{\pi} \tan^{-1} \frac{-2 \cdot D \cdot \frac{\omega}{\Omega}}{1 - \frac{\omega^2}{\Omega^2}} \tag{1.77}$$

This equation represents the relationships among the chatter frequency ω, the tooth frequency ω_t and the lobe number n. The spindle speed N can be related to the tooth frequency ω_t ($\omega_t = \frac{n_t \cdot N_l}{60}$, where n_t is the number of teeth on the cutter).

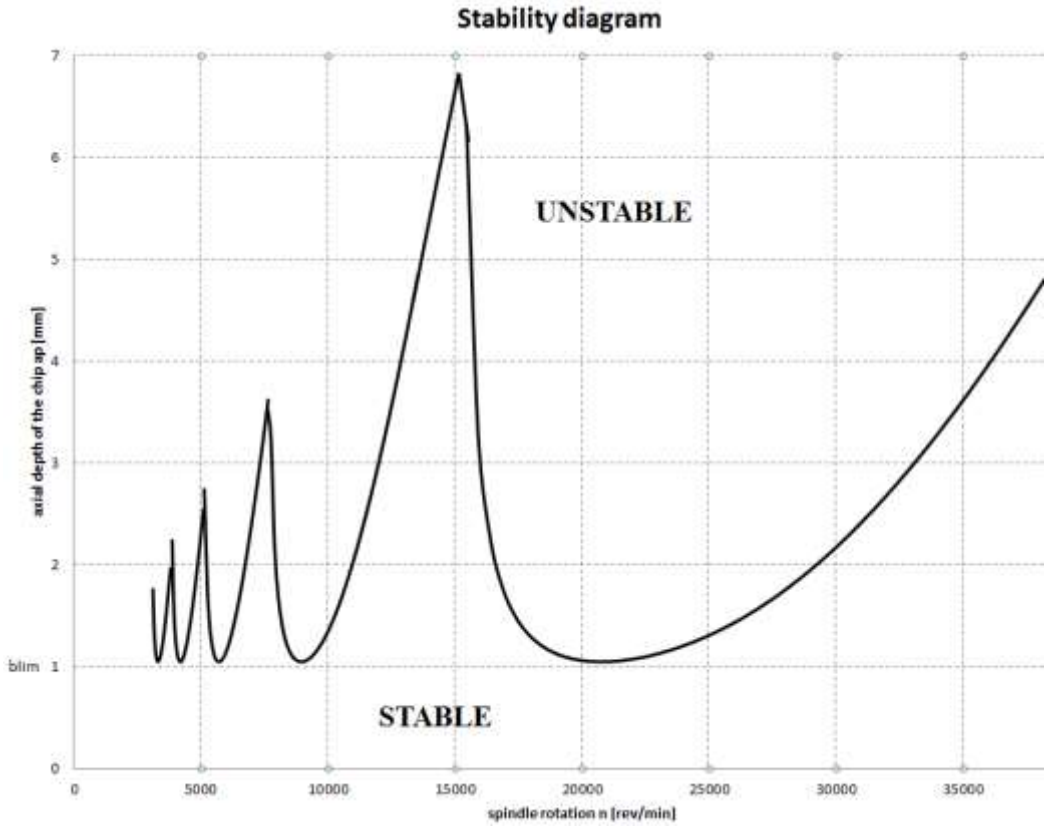

Figure 20: Lobes diagram (diagram of stability) with critical width of chip [7]

$$N = \frac{60 \cdot \omega_t \cdot f_n}{n_t} \tag{1.78}$$

From the equation (1.38) , (1.77) and (1.78) we can create a stability lobe diagram between the chip width b and spindle speed N [1].

The sections under the curve, where is the specifically magnitude of rotation for specifically magnitude width of chip, is process stable. The section above the curve is unstable and chatter will appear for this conditions. Due to the conditions, where the rotation of spindle is high, the stability is rising up, as we can see from the diagram [7].

1.7 Computing methods

1.7.1 Linear systems with discrete elements

The basic elements, like rigid points, rigid systems, intangible springs or dashpots create the computing models for linear discrete systems. These elements are called discrete elements or the elements with concentric parameters [9]. The computing model is create by the discretization of continuum Discretization model is not applicable for all alternatives, especially for difficult mechanical systems because of the difference from the real system [10].

a) One degree of freedom (1DOF)

Very often models with one degree of freedom are used for computation elementary systems with discrete elements. These models can be used for determine the dynamic properties of complex models, for instance computation of the lowest natural vibration frequencies [9].

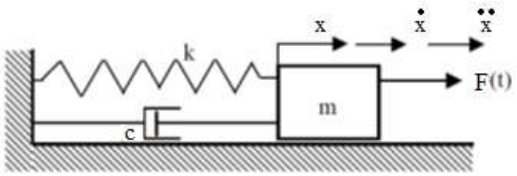

Figure 21: Dynamic model of vibration system with 1 DOF [10]

Dynamic model with 1DOF is show in Figure 21 which is acted by the force F(t). This force is reliant on time and its direction is identical with the direction of the velocity vector $\dot{x}$. The dynamic equation of motion is described by equation (1.21).

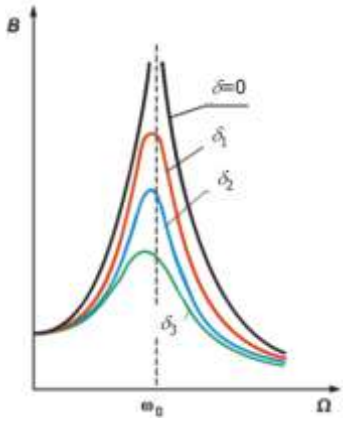

Figure 22: Amplitude-frequency characteristic [11]

Let's consider, that excitation effects on the acting system are harmonic functions of the time, for easier determination of dynamic parameters. In this case response to the excitation signal will have the character of harmonic oscillation [9].

Figure 22 presents amplitude-frequency characteristic with one degree of freedom for the damped and undamped vibrations. The natural undamped frequency of the system is bigger than natural damped frequency of the system. The amplitude of undamped deflection is rising to the theoretical infinity [11].

b) Multi degree of freedom (MDOF)

Models with one degree of freedom are mostly inadequate in the technical exercises. To compute frequencies for undamped or damped systems is necessary to use multi degree of freedom [9].

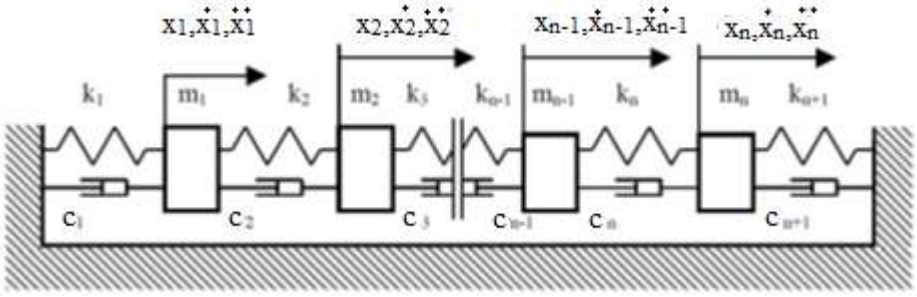

Figure 23: Linear discrete model with MDOF [9]

Systems with MDOF are solved by the systems of motion equations, where count of these equations is equal to degrees of freedom Figure 23 presents an example of discrete model with MDOF. The equation of motion in matrices' form can be expressed by:

$$\boldsymbol{M\ddot{q} + C\dot{q} + Kq = F}(t) \tag{1.79}$$

where ***M*** and ***K*** are matrices of the mass and stiffness and **C** is matrixes of damping, all of these are diagonal matrices. ***F(t)*** is vector of acting forces as a function of the time. Vectors $\boldsymbol{x, \dot{x}, \ddot{x}}$ are vectors of deflection, velocity and acceleration.

There is homogenous and particular solution of the second equation of the motion in equation (1.79). It also can be possible, that there is the system of the harmonic forced vibrations with multi degrees of freedom. In this case the particular solution for the acting force is differential equation $\boldsymbol{F}(t) = \boldsymbol{F_0} \cdot e^{i\omega t}$.

Let's consider the particular solution of the equation of the motion:

$$\boldsymbol{x_p} = \tilde{\boldsymbol{s}} \cdot e^{i\omega t} \tag{1.80}$$

where $\tilde{\boldsymbol{s}}$ is the complex vector of amplitudes.

Combining equation (1.80) and (1.79) and by the simple editing we obtain the response of complex vector:

$$\boldsymbol{x} = \sum_r \left[C_r \cdot e^{-\delta_r t} \cdot \sin(\Omega_r t + \varphi_r) \cdot \boldsymbol{v_r} + s_r \cdot \sin\left(\omega t + \varphi_{pr}\right)\right] \tag{1.81}$$

where $\boldsymbol{v_r}$ is eigenvector of natural undamped vibrations, s_r is the magnitude of amplitude response and its corresponding phase φ_{pr} $[rad]$ a C_r, φ_r are integration constant which we determine from the initial conditions [9].

1.7.2 Linear systems with continuum elements

Models with the discrete systems are used in limited cases, especially in the elementary models, which are similar to real object. The real mechanical parts have continuously or in pieces continuously distributed mass, we call them continuum elements [9]. In practice, there are differently difficult constructions which can be separated to elementary parts, in which we can analytically solve the vibrations. There are rods , membranes etc. with various initial conditions [10].

a) Analytical

The fundamental example of the continuum is the rod. The rod is an element where the length is considerably bigger then the diameter of the rod and there is just axial load. The rod assumptions are the basic condition for approximation of the rod [11]. The rigid body which is replaced by the rod must be axial symmetric and we don't consider deformation in transverse direction [9].

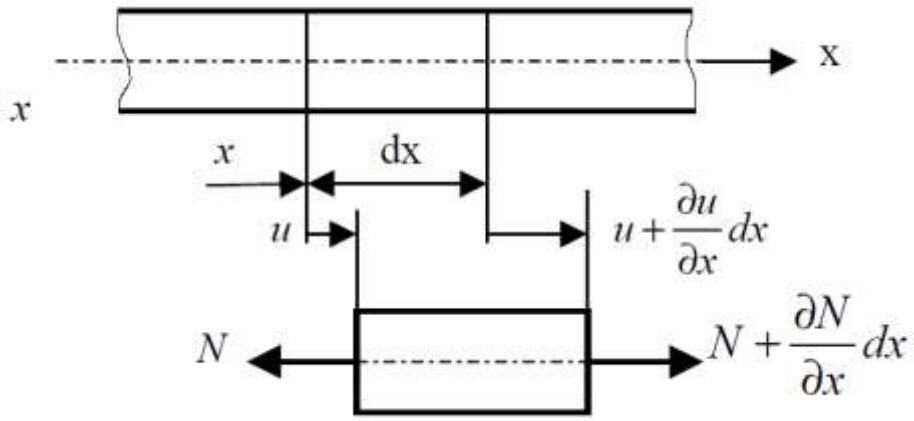

Figure 24: The rod vibration [9]

Figure 24presents the fundamental computing method, where the length of element is d*x* which demonstrate behaviour of the rod vibration. The motion equation is expressed by:

$$\frac{\partial^2 u(x,t)}{\partial t^2} = c^2 \frac{\partial^2 u(x,t)}{\partial x^2} \tag{1.82}$$

where $u(x,t)$ is displacement in x direction dependence on the time, c is phase velocity of the longitudinal wave of the rod [9].Velocity of the longitudinal displacement of the rod is:

$$c = \sqrt{\frac{E}{\rho}} \tag{1.83}$$

There are two parts of the displacement *u(x,t).* One of them is the function of displacement time and the second one is function of the time:

$$u(x,t) = U(x)T(t) \tag{1.84}$$

Computing equation (1.84) and (1.82) we obtain two harmonic functions:

$$T(t) = D_1 \cos \Omega_0 t + D_2 \sin \Omega_0 t \tag{1.85}$$

$$U(x) = C_1 \cos px + C_2 \sin px \tag{1.86}$$

where we mark:

$$p = \frac{\Omega}{c} = \Omega \sqrt{\frac{\rho}{E}} \tag{1.87}$$

and D1, D2, C1 a C2 are integration constants, which are identified by the initial conditions [9]. Natural frequency of undamped vibration is:

$$\Omega = p \sqrt{\frac{E}{\rho}} \tag{1.88}$$

b) Numerical solutions

To establish the frequency of the natural vibrations and to present the individual modes of vibrations we can use the **modal analysis**. This method can be used for the structures and liquids in case, that theirs mass and stiffness is constant. The matrix form of the equation of the motion by the finite element method for undamped system is:

$$\boldsymbol{M\ddot{q}} + \boldsymbol{Kq} = 0 \tag{1.89}$$

The structural matrix of the stiffness **K** can contain filled effect of pre-tension [12]. The solution obtained for the linear system with natural frequency:

$$q = \phi_i \cdot \cos \omega_i t \tag{1.90}$$

where $\boldsymbol{\phi_i}$ is natural vector represents *i*-shape of the natural frequency, ω_i is i-shape of angular frequency [11].

Combining equations (1.90) and (1.89) we obtain

$$(-\omega_i^2 \boldsymbol{M} + \boldsymbol{K})\phi_i = 0 \tag{1.91}$$

Equation (1.91) has two solutions, where one of them is $\phi_i = 0$, which is unless in this process and the second one is the problem of eigenvalue [12].

The condition for nonzero and nontrivial solution of equation (1.91) is that the determinant of the system is equal to zero. We called this “frequency determinant” [13].

$$|\boldsymbol{K} - \omega^2 \boldsymbol{M}| = 0 \tag{1.92}$$

The results of equation (1.92) are angular natural frequencies ω [$rad\ s^{-1}$], which are output and in following step transverse to natural frequencies f_i [*Hz*].

$$f_i = \frac{\omega_i}{2\pi} \tag{1.93}$$

Harmonic analysis by the final element method is used to compute the behaviour of vibrations and to find the response of the system to the acting harmonic signal. The equations of the motions dependence on the time for linear structures in the steady state are numerically solved in the tasks which are solved by the harmonic analysis. Solutions of these tasks are systems of differential equations which estimate the amplitude responses, phases and frequencies. Models in this analysis have constant or frequency dependent stiffness, damping and mass. All the loads and displacements are changed sinusoidally and theirs frequency is known and they don't have to be in phase [12]. Equation of the motion in final element method is:

$$\boldsymbol{M}\ddot{x} + \boldsymbol{C}\dot{x} + \boldsymbol{K}x = \boldsymbol{F} \tag{1.94}$$

where **F** is acting vector of the system, which can be expressed by

$$\boldsymbol{F} = \{F_{max}e^{i\Psi}\}e^{i\Omega t} \tag{1.95}$$

where F_{max} is an amplitude of the force and Ψ [rad] is phase shift of the force.

The phase shift of vibrations causes damping in the structure. The vector of displacements in the nodes can be expressed:

$$x = \{x_{max}e^{i\phi}\}e^{i\Omega t} \tag{1.96}$$

where x_{max} is the maximal deflection, ϕ is a phase shift, i is and imaginary unit of the complex number and Ω is an angular frequency [12].

Computing (1.95) and (1.96) and insert into (1.94) we obtain the final equation of the motion for numerical solution of harmonic analysis:

$$(\boldsymbol{K} - \Omega^2\boldsymbol{M} + i\Omega\boldsymbol{C})\{x_{max}e^{i\phi}\} = \{\boldsymbol{F}_{max}e^{i\Psi}\} \tag{1.97}$$

Equation of the motion (1.97) can be solved by two different ways:

1. **Full solution method**

Full solution method is complex method of harmonic response through the direct solution of the simultaneous equations of motion. Independence of this method on the previous results is the biggest advantage. It also can solve unsymmetrical matrices and it can use all the types of load (strain) for instance pressure, acceleration, load of individual nodes etc. [12].

2. **Mode superposition method**

Mode superposition method uses the linear combination of natural frequency and its shape to compute the harmonic response of the sinusoidal excitation function. For this type of analysis is necessary to perform the modal analysis in the double frequency range. The lower computing difficulty is advantage against the full solution method and this method can use modal damping dependence to the frequency. For mode superposition method, it is advantageous for you to select an existing modal analysis directly since calculating the eigenvectors is usually the most computationally expensive portion of the method. In this way, multiple harmonic analyses with different loading conditions could effectively reuse the eigenvectors.[12].

2 LITERATURE OVERVIEW

Chatter is a kind of self-excited vibration, which is often caused by a regenerative feedback occurring in the system. Accordingly, research on the origin of vibrations, whole process and validation of the results during milling processes has become extremely important. In following are several knowledges about this topic.

2.1 Milling articles

2.1.1 Stability prediction due to cutting force coefficients

Literature [14] present article about the evaluation of specific cutting coefficients in high speed milling due to frequency bandwidth of commercial force sensors and its variation with cutting velocity. Coefficients are identified at different spindle speeds thanks to an improved technique based on Kalman filter estimator. The obtained speed-varying force coefficients are used to improve the reliability of stability diagrams and the result are proved by experimental tests.

The aim of this study was to improve the reliability of chatter prediction implementing a speed-dependent stability lobe diagram starting from analytical prediction theory. Author proposed different method and the speed-dependent stability lobe diagram was calculated by set procedure. The experimental part was performed on CNC vertical machine with high speed spindle and material Aluminium 6092-T4 alloy was used.

In order to determine the average cutting force coefficients, cutting forces have been measured during slotting at different spindle speeds and for computing has been used linear regression. Also to ensure adequate accuracy of the cutting forces measured during the various cutting test a specific dynamic compensation techniques was applied. Predicted cutting force coefficients have been applied to stability lobe diagrams theory.

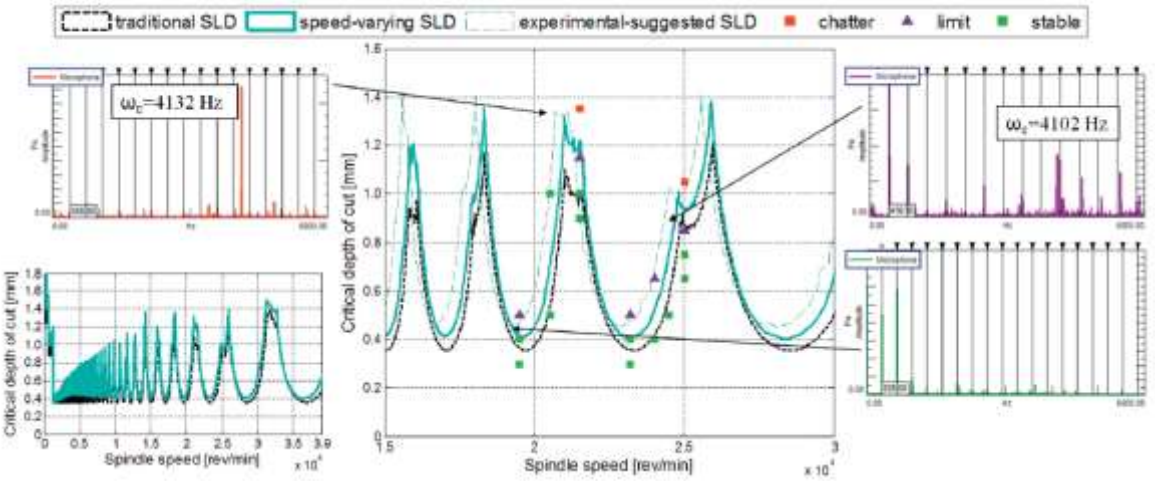

Figure 25: Stability diagrams for experimental validation [14]

Figure 25 presents the results. Resulting stability lobe diagram (blue line) is compared with the traditional theory (black line) built considering as coefficients obtained by low speed test. Chatter mark (red square) is indicated when chatter frequency is dominant on the spectrum. The chatter frequency in limit points marked by violet triangle is growing but it is no dominant, no chatter frequency is identified in the stable points marked by green square. Speed varying coefficients stability is more accurate than traditional

approach, anyway some discrepancies are shown. Experimental-suggested diagram is presented by dot line.

Conclusion of this work presents that increasing spindle speed an increase of damping should be expected and this should reflect in increase depth of cut. Experimental validation demonstrated the accuracy of the proposed approach, nevertheless more accurate identification could be obtained introducing speed varying frequency response functions, not considered in this work. More reliable stability limits could be predicted after experimental characterizaton of materials at different spindle speed. Cutting coefficients can be computed without comensating dynamometer dynamics in case of average cutting force method.

2.1.2 Back-propagation neutral network used for reliability of analysis

Neutral network is used to get a comprehensive analysis of the influences of random factors in milling. Literature [15] proposes a method for reliability of the regenerative chatter stability in milling and also establishes the dynamic model of milling regenerative chatter. Authors use full-discretization method to obtain a stability lobe diagram.

In this work, authors derive the transition matrix, where the chatter stability depends on the eigenvalues of this matrix. For the reliability analysis of the chatter stability author uses neutral network to approximate the functional relationship of the limit axial cutting depth. This neutral network method is based on following steps (see Figure 26):

1. Establishing a back-propagation neutral network
   1.1. Design of the input and the output layer
   1.2. Design of the hidden layer
   1.3. Data normalization
2. The Monte Carlo simulation method
3. Moment method

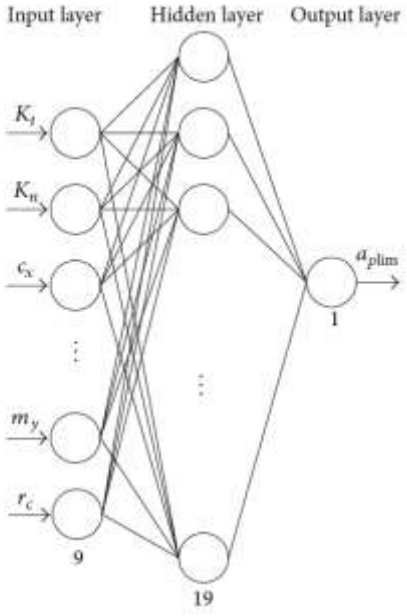

Figure 26: Topological structure of back-propagation neutral network model [15]

In following authors analysed the example utilizing a BP neutral network. The reliability of the stability of the milling process has been calculated for different spindle speeds using both the moment method and Monte Carlo simulations. The result is that this approach is more suitable for practical engineering applications than theoretical calculation based on fixed cutting parameters and it can be helpful for improving the machining accuracy and machining efficiency.

2.1.3 Prediction of milling chatter based on the information entropy and support vector machine

Literature [16] predict the milling chatter based on the information entropy. Support vector machine is proposed in this work. The permutation entropy and wavelet packet energy entropy of milling force signal can monitor the milling chatter symptom from the perspective of the time domain and frequency domain. In terms of decision-making support vector machine is a machine learning method based on statistical learning theory. This can solve the high dimensional patter identify issues which are nonlinear, local extremes and the small sample. Support vector machine is used as the classifier to predict milling chatter premonition.

Authors derive the equation for the layer of wavelet packet decomposition and also the function equation of classification feature based on support vector machine. The milling chatter prediction method (see Figure 27) based on information entropy and support vector machine is expressed by following processes:

1. de-noising of the milling force signal
2. calculation with the multi-scale permutation entropy
3. decomposing milling force signal and calculating the wavelet packet energy entropy
4. determine whether be in the milling state or not by the permutation entropy
5. test samples

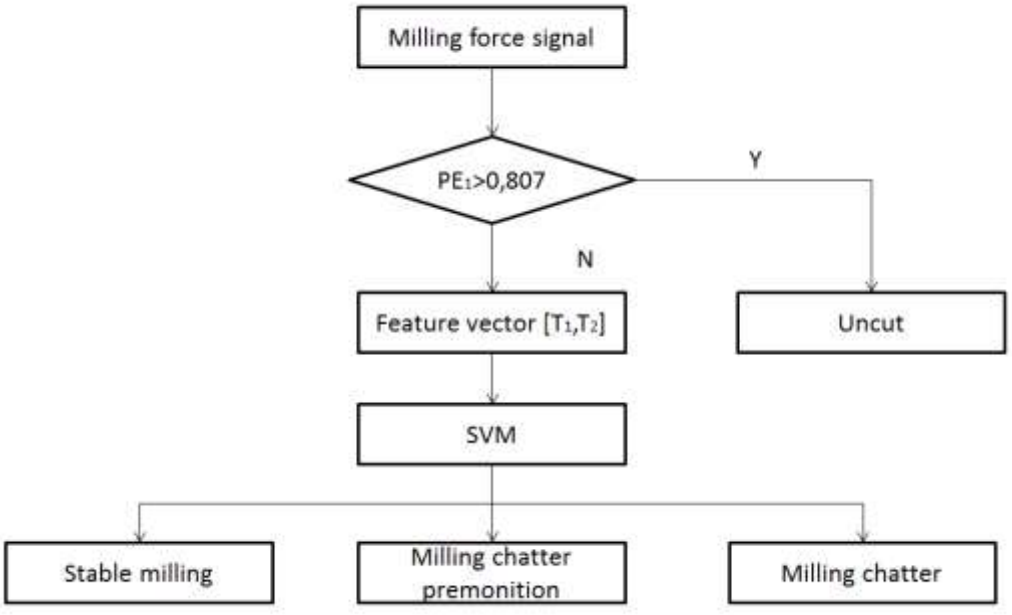

Figure 27: The milling chatter prediction model due to literature [16]

In following, the authors perform the experimental verification and analysis. 75 experiments have been performed, each of them in the different combinations of spindle speed, feed rate, radial and axial depth of cut etc. Authors calculated the 3-6 layers wavelet packet energy entropy. Experimental results show that the milling chatter prediction system can effectively identify the milling chatter premonition, because the accuracy was 95,8%.

This method is suitable for small sample classification recognition with high accuracy. It is in line with the needs of practical application and has engineering application value.

2.1.4 Simulation implementation and application research in regeneration type of chatter bases on Matlab

Literature [17] establishes regenerative type stability domain simulation flow chart of high speed milling and through the Matlab simulation algorithm for the analysis. The authors discuss the dynamic model of milling force in high speed milling and the chatter stability domain algorithm.

In order to verify the validity and accuracy of chatter stability domain simulation algorithm, experimental verification has been performed, see Figure 28. Validation experiment were performed in 6 selected points from the diagram (■ said the stable cutting zones, ● said flutter) Together with Table 1, where the processing parameters are used in the experiment, the results are presented.

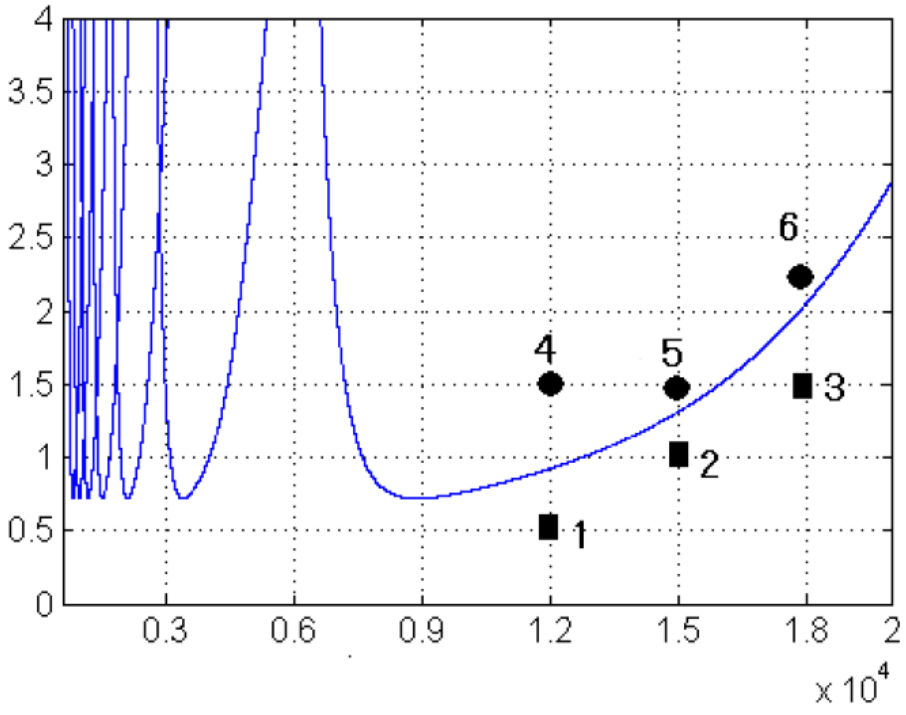

Figure 28: The simulation results due to literature [17]

Authors provided theoretical basis on the theories and algorithms of milling parameters. The simulation algorithm is proved to be efficient and accurate by cutting experiment and in plant practical application reflect its practical value.

Table 1: The flutter stability domain verification due to literature [17]

Number	1	4	2	5	3	6
Spindle speed (r/min)	12 000	12 000	15 000	15 000	18 000	18 000
The critical cut depth (mm)	0.5	1.5	1.0	1.5	1.5	2.2
Workpiece surface topography						
Conclusion	Stable	Flutter	Stable	Flutter	Stable	Flutter

2.1.5 Milling process performed by industrial robots

In literature [18] authors discuss a method to predict the static displacement as well as low frequency oscillation of the tool tip by coupling a robot model with a milling process model. Authors also performed experimental studies of the milling operation and differences between the milling operation on a standard three axis milling machine and the industrial robot. Two experimental tests are analysed on two different machine types using full slotting. In order to model the displacement of the tool centre point trajectory, a dynamic model of the robot and cutting force model are performed in MATLAB software.

In the experimental part of this work the displacements of the tool centre point y, z and the process forces F_y and F_z are measured, evaluated and compared. Authors summarize that the z displacement is influenced by the integrated gravity compensation of the robot which causes a high damping on the mechanical structure and the force signal in z direction shows strong distortions. They assign z-direction as a major disadvantage in milling with industrial robots. On the other hand the static forces during the milling operation of the industrial robot and at standard machine tool have nearly equal force level.

This work also presents simulation of the dynamics of the mechanical robot structure which is built in Matlab/ Sim mechanics. Experimentally measured vectors of joint angles are used as the input of the robot model and to calculate tool centre point trajectory. Measured trajectory has been compared with calculated trajectory. Figure 29 shows the model of the robot used for simulating dynamics of the structure.

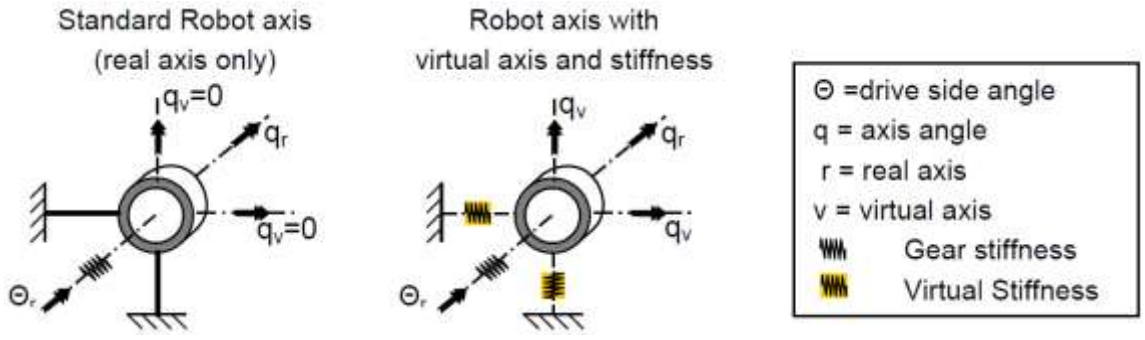

Figure 29: Modelling of the robot axis due to literature [18]

2.2 Review of chatter in the contemporary literature

Literature [19] reviews fundamental modeling of chatter vibrations in grinding processes. Authors also present avoidance of chatter vibrations in industry. The fundamentals of orthogonal chatter stability law and lobes are reviewed for single point machining where the process is one dimensional and time invariant. Various stability models are compared

against experimentally validated time domain simulation model results. The dynamic time domain model transverse and plunge grinding operations is presented also with experimental results. In this work is presented a series of research topics.

Authors in the literature [20] explain the origin of chatter that is particularly due to regenerative effects during inner and outer diameter as well as surface grinding. Influence on surface quality is discussed; the possibilities related to process monitoring for the detection of chatter during grinding is also presented. Special attention is paid to the suppression of chatter by employing passive or active damping methods.

Numerical prediction of tool wear in metal cutting operations is presented in the literature [21]. An analytical model, which is able to take into account the diffusive wear mechanism, is implemented through a specific subroutine and an advanced approach to model heat transfer phenomena at the tool-chip interface has been included in the numerical simulation. The 3D finite element method results have been compared with experimental data obtained by experiment and good agreement has been found out.

Literature [23] discuss increasing demands on function and performance which call for burr-free workpiece edges after machining (see Figure 30). Understanding and control of burr classifications along with the corresponding measurement technologies, butt formation mechanism in machining are described. Authors present two possible ways to deal with burrs, which is deburring and burr control. For both an insight into current research result are presented in this work. There is also number of case studies on burr formation control and deburring along with their economic implications.

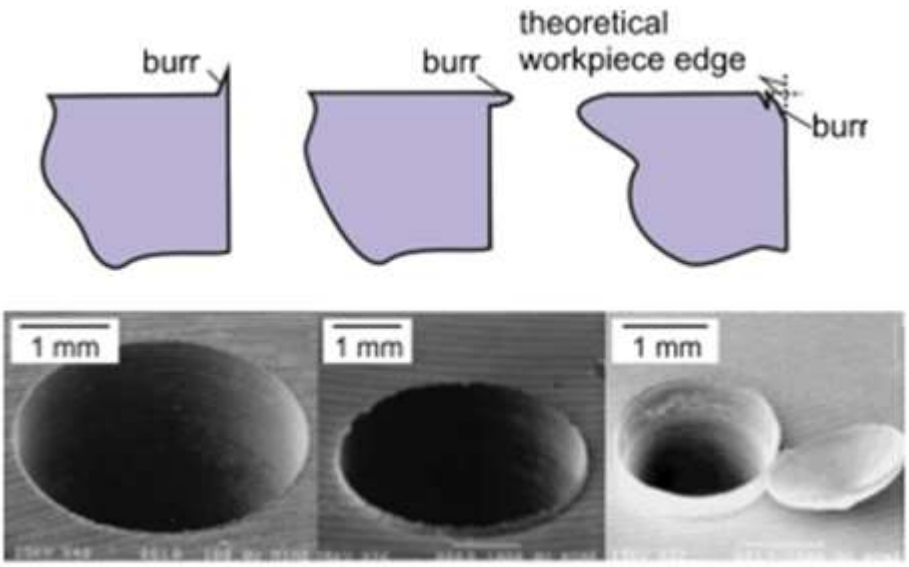

Figure 30: Possible burr types [23]

3 GEOMETRY MODEL OF THE MILLING MACHINE AND FINAL ELEMENT MESH

In order to perform the analysis on milling machine, I used 3 axis "hobby" milling machine, which was the theme of bachelor thesis of Martin Knížek [25]. This machine has been made and nowadays is used for machining (see Figure 31 a)). It was necessary to edit and update the model for following analysis. The final model, which is used in this work and corresponds to real model, is shown in Figure 31 b).

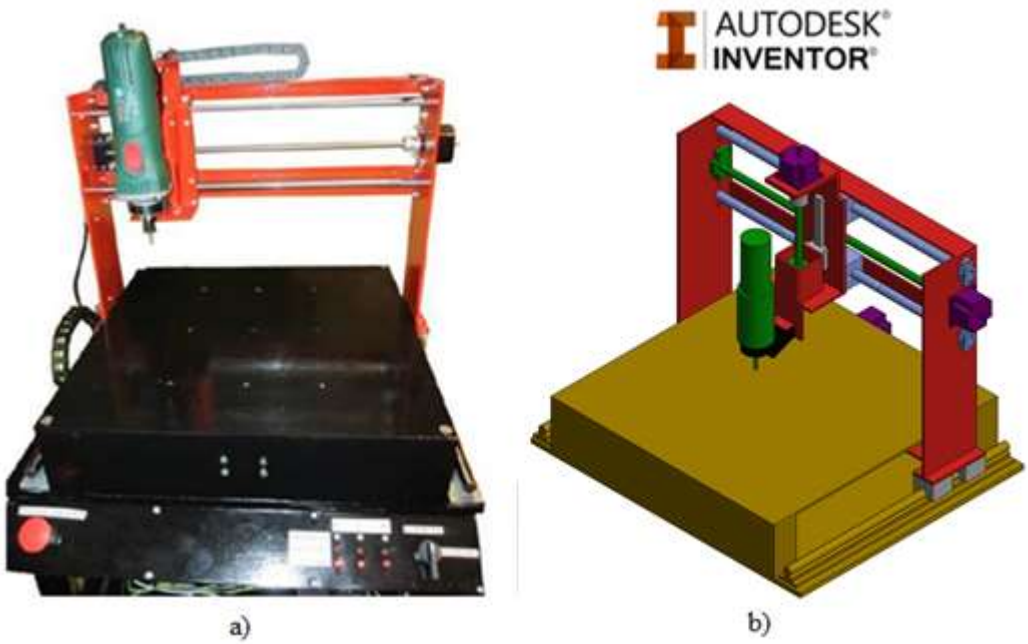

Figure 31: 3 axis milling machine a) real product b) model in Autodesk Inventor

3.1 Geometry of the model

Model in Figure 31 b) represents real assembly of analysing milling machine. All the parts are made from the steel, properties of this material presents Table 2. In order to reduce difficulty of the model for computing and analysing, some parts have been simplified and connection parts (as a bolts and nuts) have been suppressed. Properties of the simplified parts, as a weight and moment of inertia have been kept due to get as much precision results as possible.

Table 2: Steel properties

Material properties of steel			
Signification	Modulus of elasticity E [MPa]	Poisson's ratio μ [-]	Density ρ [$kg \cdot m^{-3}$]
EN 1.0038	200 000	0.3	7 850

Figure 32 represents the real assembly with general description of all the parts. There are two linear guideways connected on the mill base, which ensure the motion of the column base in y-direction. The column saddle move in x-direction and hold the head-

stock. Head-stock move in z-direction and it is connected to head-holder, which holds the spindle. Spindle is the straight grinder *DWT GS06-27V* with 600*W* power. Motions are ensured by the assembly of the stepper motor *Nema 23* which are connected by the clutches to trapezoidal screws. Smooth movements are ensured by the feed rods. Workspace of the milling machine is 380x350x90 *mm* [25].

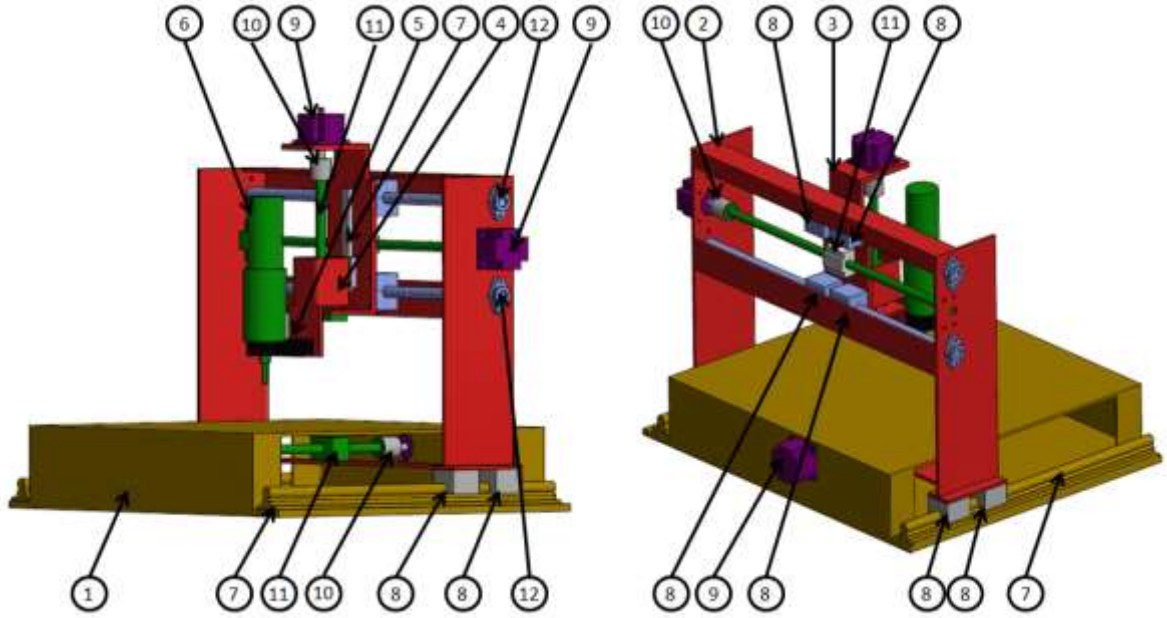

Figure 32: General description of the model

All the general parts are also presented in the Table 3.

Table 3: Parts of the milling machine

Item no.	Description	QTY	Item no.	Description	QTY
1	Mill base	1	7	Rails	3
2	Column base	1	8	Linear carriage	8
3	Column saddle	1	9	Motor	3
4	Head-stock	1	10	Clutch	3
5	Head-holder	1	11	Trapeziodal screw	3
6	Spindle	1	12	Feed rod	2

3.2 Analysis properties

To analyse the vibration and following behaviour of the construction is necessary to determine the natural frequencies and theirs shapes. Due to this analysis, dimension of the construction can be modified in order to reach better condition for milling process. The results of this analysis give us information, if shapes of vibration are close to natural frequencies of construction.

Determination of the frequency range is the first step for experiment. The frequency range has been chosen for modal analysis for first one hundred natural frequencies. Software ANSYS Workbench 16.0 has been used to perform the analysis.

3.2.1 Meshing method

The Hex Dominant method has been used to create the mesh of elements for the model. Generated mesh is created by the hexagonal elements and parts. To determine the element size of the mesh for the model, bending waves has been considered. As opposed to oscillation in the longitudinal and transverse direction, bending wavelength is dependent to frequency. The construction of the milling machine is mostly created by the parts, which we can consider as plates respectively rods. Theory is used that the bending waves has been detective for this type of parts, which is created by oscillation in the longitudinal and traverse direction [26].

To calculate the speed of the bending waves has been used for the column base. This part has been chosen as part with lowest bending rigidity. There should be probably the biggest deformation in the construction. Maximal frequency f_{max} has been chosen for 4 000 *Hz*. The speed of the bending waves can be calculated from the general equation:

$$c_B = \sqrt{2\pi f_{max}} \cdot \sqrt[4]{\frac{E \cdot I_M}{m'}} \tag{3.1}$$

where E is modulus of elasticity of the material, m' [*kg/m*] is the unit weight of the considered part and I_M [m^4] moment of inertia for cross-section is calculated by equation:

$$I_M = R_M^2 \cdot S \tag{3.2}$$

where R_M^2 [m] is radius of gyration for cross-section S [m^2]. R_M^2 has been calculated as:

$$R_M^2 = \frac{h^2}{48} \tag{3.3}$$

where h is thickness of the frame. The thickness of the column base part is 5*mm* and this part is made from the steel EN 1.0038. If all the parameters are inserted in the equation (3.1) the speed of the bending waves is equal:

$$c_B = \sqrt{2\pi f_{max}} \cdot \sqrt[4]{\frac{E \cdot I_M}{m'}} = \sqrt{2\pi \cdot 4000} \cdot \sqrt[4]{\frac{2 \cdot 10^{11} \cdot 4.1 \cdot 10^{-11}}{2.466}} = 213.96[m \cdot s^{-1}] \tag{3.4}$$

Equation (3.1) is derived for the oscillation of the rod. It is necessary to considered with influence of contraction of the plate. To calculate the speed of plate waves c'_B is the result from equation (3.4) edited in following:

$$c'_B = c_B \cdot \frac{1}{\sqrt{1-\mu^2}} = 2 \cdot \frac{1}{\sqrt{1-0.3^2}} \cong 219.06\ [m \cdot s^{-1}] \tag{3.5}$$

where μ is Poisson's ratio of the material.

It has been set that the minimal number of element is six and the element size of the mesh is equal:

$$l_{max} = \frac{\lambda_B}{6} = \frac{\frac{c'_B}{f_{max}}}{6} = \frac{\frac{219.06}{4000}}{6} = 9.1 \cdot 10^{-3}[m] \tag{3.6}$$

The global element size of the mesh, which is connected with the column base, has been chosen 0.009 *m*. No problems did occur during the meshing operation. In this case the whole mesh is created by computed element size.

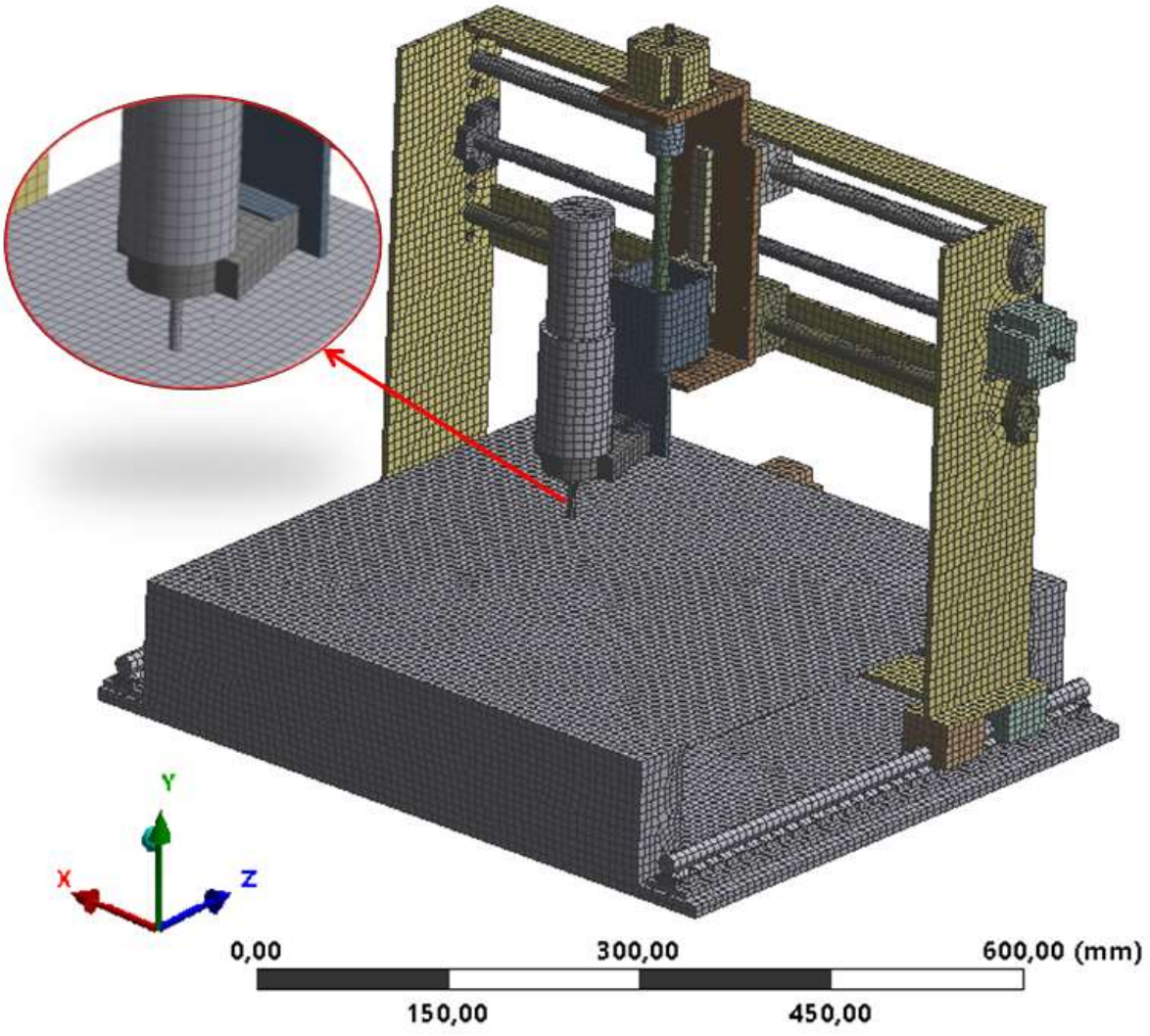

Figure 33: Generated mesh in the ANSYS software

Density test of generated mesh has been performed. Condition for correctly computed element size from equation (3.6) is generally set that the precentral difference between computed natural frequencies is lower than 10%. Table 4 present slected element size and corresponding calculations. For element sizes 8, 6 and 4 *mm* are obvious, that diferencies of computed natural frequencies are very close to element size 9 *mm*.

Table 4: Density test of the generated mesh

Element size	**12 mm**		**10 mm**		**9 mm**	**8 mm**		**6 mm**		**4 mm**	
# of nodes	160 241		206 804		296 414	296 797		528 182		891 943	
# of elements	45 367		57 576		80 179	80 398		135 383		252 274	
Elapsed time [*s*]	421		655		1 418	1 523		2 791		5 237	
Mode	**Freq. [*Hz*]**	**%**	**Freq. [*Hz*]**	**%**	**Freq. [*Hz*]**	**Freq. [*Hz*]**	**%**	**Freq. [*Hz*]**	**%**	**Freq. [*Hz*]**	**%**
1	24.21	1.310	23.83	0.280	23.90	23.81	0.360	23.72	0.749	23.83	0.276
2	32.10	1.884	29.87	5.193	31.51	29.34	6.878	29.55	6.211	29.91	5.078
3	57.28	1.512	50.34	10.794	56.43	51.91	8.003	51.43	8.864	57.08	1.154
4	74.15	1.316	70.68	3.423	73.18	69.97	4.384	68.81	5.977	69.37	5.209
5	76.75	1.917	74.26	1.391	75.30	73.62	2.242	74.11	1.585	76.92	2.145
6	90.99	13.370	80.37	0.145	80.26	80.06	0.245	79.90	0.446	80.02	0.296
7	105.15	1.014	92.75	10.898	104.09	103.87	0.214	101.85	2.161	99.98	3.953
8	105.49	0.470	104.69	0.291	105.00	104.49	0.482	104.33	0.634	104.62	0.358
9	140.62	0.234	140.33	0.439	140.95	139.73	0.865	139.73	0.865	139.94	0.716
10	165.20	1.549	161.75	0.572	162.68	163.16	0.295	161.37	0.805	162.51	0.105
11	217.46	11.777	172.66	11.251	194.55	189.89	2.395	190.74	1.958	190.88	1.886
12	212.14	1.342	209.05	0.134	209.33	208.39	0.449	206.40	1.400	206.86	1.180
13	222.02	0.040	221.58	0.238	222.11	220.46	0.743	219.71	1.080	221.86	0.112
14	227.98	2.395	223.62	0.437	222.65	220.99	0.744	220.89	0.789	222.04	0.272
15	268.54	0.830	259.30	2.639	266.33	269.75	1.285	263.93	0.901	264.04	0.859
16	269.73	1.140	266.93	0.090	266.69	264.97	0.645	263.89	1.050	265.99	0.262
17	279.33	0.524	267.36	3.784	277.87	276.19	0.606	279.69	0.654	278.94	0.384
18	294.69	2.919	277.46	3.098	286.33	286.57	0.083	289.18	0.995	285.28	0.367
19	338.14	4.200	326.78	0.700	324.51	321.98	0.779	322.92	0.490	320.11	1.356
20	346.03	1.392	342.26	0.287	341.28	340.86	0.123	339.15	0.624	342.01	0.214
.											
.											
.											
98	1560.6	0.873	1560.8	0.860	1574.34	1550.6	1.508	1560.8	0.855	1549.1	1.603
99	1595.6	0.540	1583.5	0.222	1587.02	1568.0	1.199	1555.5	1.983	1563.2	1.501
100	1610.9	1.182	1585.7	0.401	1592.09	1576.2	0.998	1567.6	1.538	1562.4	1.866

3.2.2 Boundary conditions and contacts

The bottom of the milling base has been chosen as a fixed support of the milling machine (see Figure 34). This is a real support how the machine is connected nowadays.

The model contains all the general contacts which are not complicated to realize. There are 33 bonded - active contact regions. Some examples of the contact regions are presented in Figure 35. The first contacts from the left side present connection between the motor and clutch. In the middle is connection between column base and the linear carriage.

On the right side is connection between the linear carriage and the linear rail. For the completeness and reliability of the results, the analysis was performed for the whole construction.

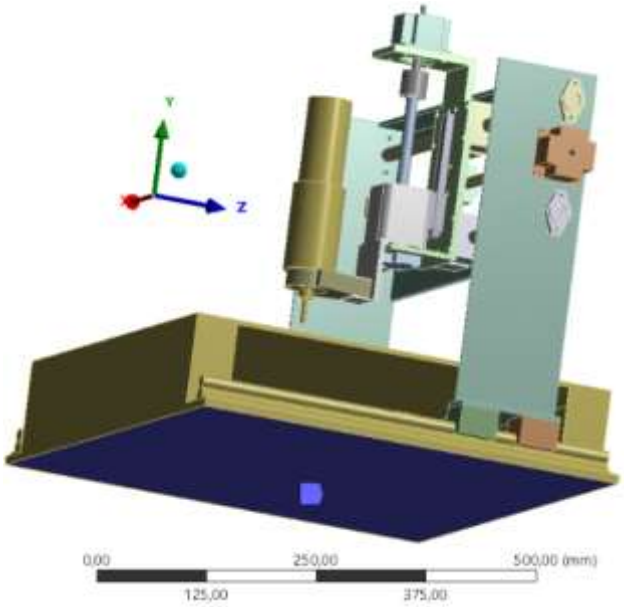

Figure 34: Boundary conditions for the analyses

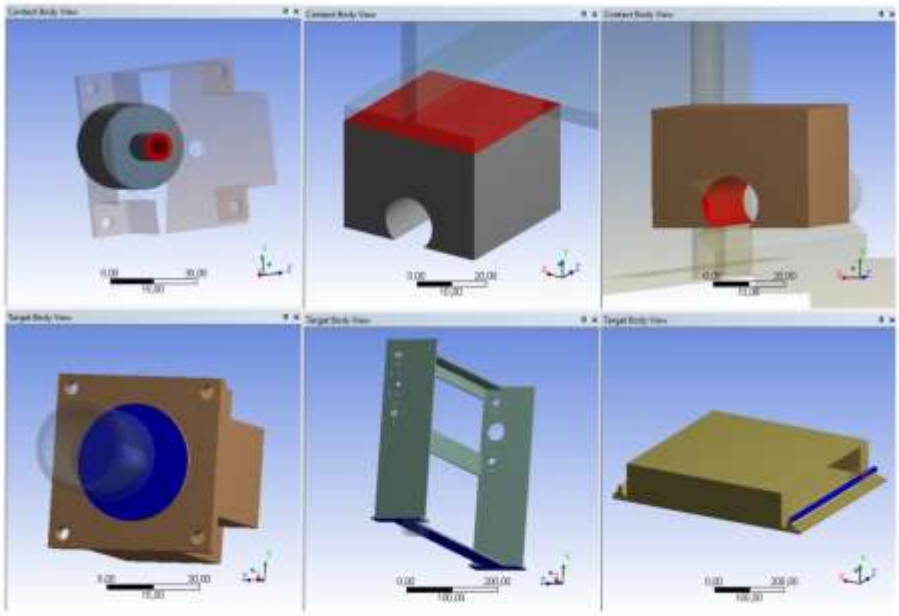

Figure 35: Contact regions in the model

4 ANALYSES AND RESULTS

As it mentioned above, modal analysis of the model should be performed at the beginning. This type of analyse represents system A in the scheme (see Figure 36). In this system A has been also generated mesh (Chapter 3.2.1). System B represents harmonic response of the model, which was analysed by mode superposition method. This type of method is usually used to save analysing time. On the other hand, computed results are not as precious as in full method. Because of the model has been simplified and computing time of harmonic response has not been too long, results of mode superposition method never been used. Systems C, D and E represent harmonic response of the model solved by the full method in corresponding directions X,Y and Z.

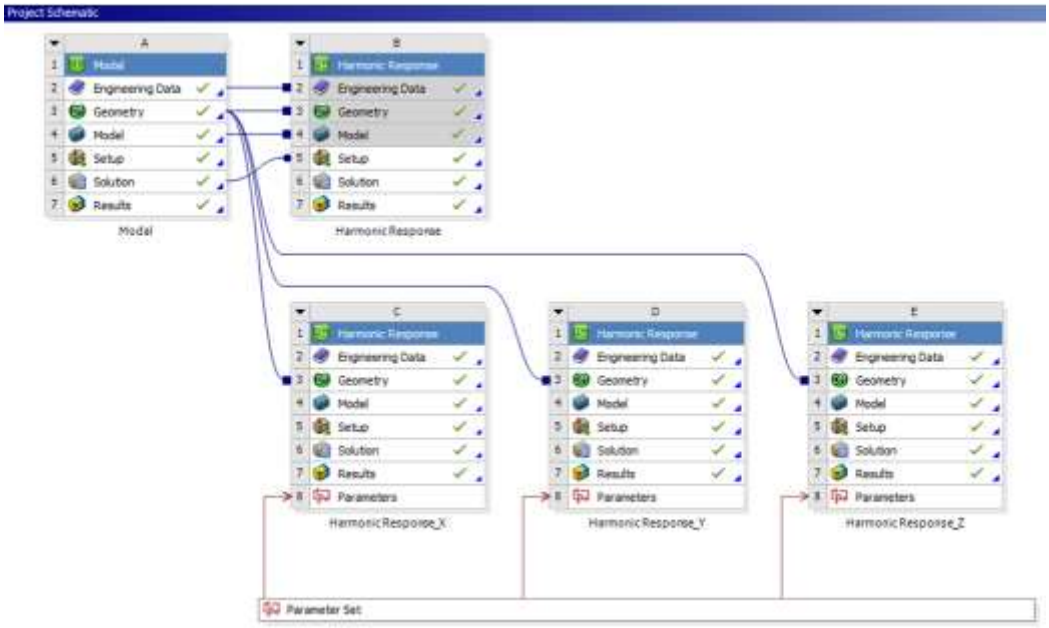

Figure 36: Scheme of the project

4.1 Modal analyses

A modal analysis determines the vibration characteristics (natural frequencies and corresponding mode shapes) of a structure or a machine component. It can serve as a starting point for other types of analyses by detecting unconstrained bodies in a contact analysis or by indicating the necessary time-step size for a transient analysis, for example. In addition, the modal-analysis results may be used in a downstream dynamic simulation employing mode-superposition methods, such as a harmonic response analysis, a random vibration analysis, or a spectrum analysis. The natural frequencies and mode shapes are important parameters in the design of a structure for dynamic loading conditions.

Computing of the modal analysis took 1 418 seconds for element size 9 *mm* on the workstation HP ProBook 640 G2 with 8th core processor Intel(R) Core (TM) i5-6200U CPU with frequency 2.30 *GHz* and with physical memory 8*GB* RAM. For instance, computation time for element size 4 *mm* took 5 237 seconds.

Solution of the modal analysis is derived for the first 100 natural frequencies. The first computed mode has frequency 23.89 *Hz* and the last 100th mode has the frequency 1592.08 *Hz*.

Figure 37 presents the first four natural frequencies and theirs corresponding shapes. The bending and torsion vibrations or theirs combination cause that the whole construction move and rotate.

The first mode (in the upper left-hand corner in Figure 37) shows displacement of the column base in x-direction by the frequency 23.89 *Hz*. The second mode (in the upper right-hand corner in Figure 37) by the frequency 31.51 *Hz* and the third mode (in the lower left-hand corner in Figure 37) by the frequency 56.42 *Hz* show the rotation of the spindle and spindle holder around the *x* axis. The fourth mode (in the lower right-hand corner in Figure 37) shows the rotation and displacement around *x*-axis of the assembly of spindle holder. Each picture presents undeformed and deformed model of the milling machine.

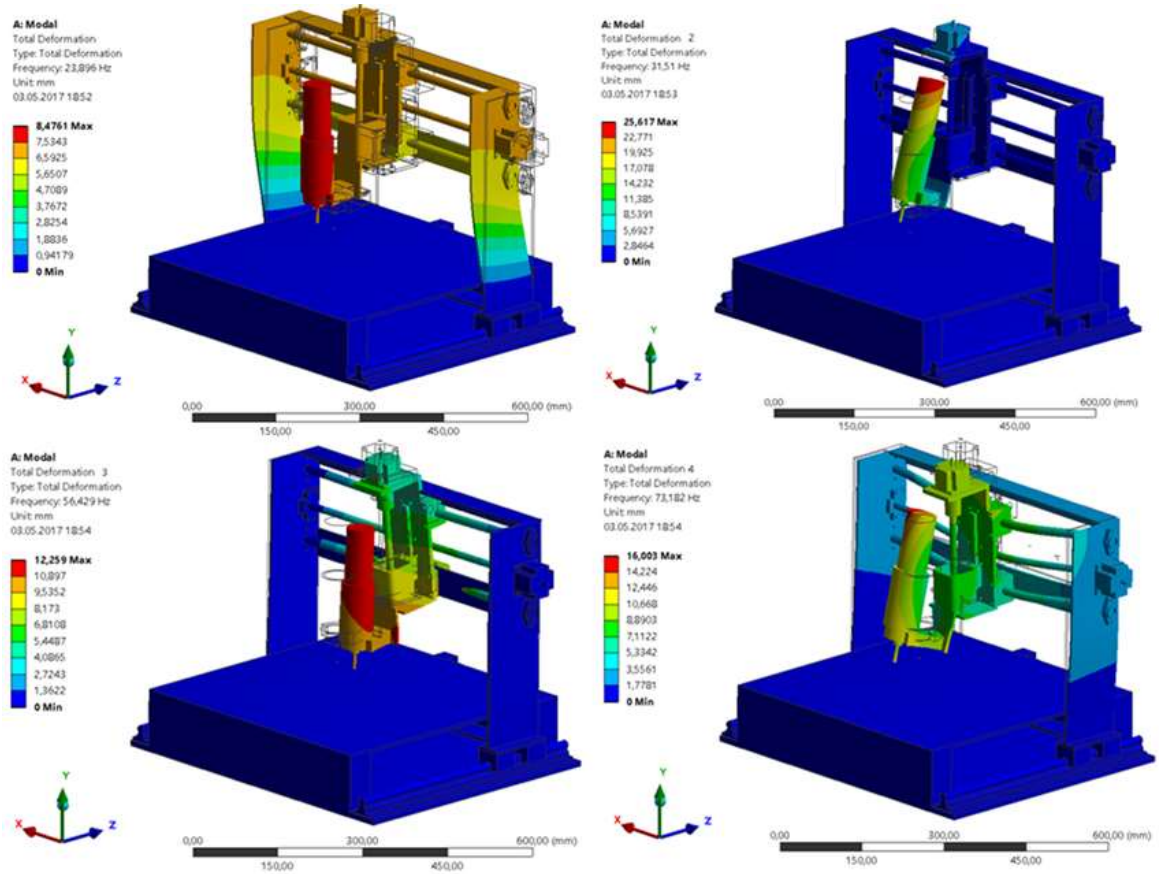

Figure 37: The first four natural vibration shapes in the row: mode 1, mode 2, mode 3 and mode 4

Following tables (Table 5, Table 6 and Table 7) present evaluated results of the natural frequencies by modal analysis. Those tables are sorted by the by the highest participant factor value (absolute value, because there can occur the negative values) in each direction *x*, *y* and *z*.

The most significant modes, which have the highest impact to behaviouh of the construction are shown in Figure 37. Other modes, pictures (Figure 38, Figure 39 and Figure 40) bellow each table, show chosen natural frequency from corresponding table. Corresponding picture is marked by the orange colour in each table.

Table 5: Natural frequencies of the model sorted by the participation factor in X-axis

MODE	FREQUENCY [Hz]	PERIOD	PARTIC. FACTOR	RATIO	EFFECTIVE MASS	CUMULATIVE MASS FRACTION	RATIO EFF. MASS TO TOTAL MASS
1	23.8960	0.418E-01	0.14575	1	0.212E-01	0.873494	0.297340
95	1515.19	0.659E-03	0.019402	0.133126	0.376E-03	0.975690	0.526E-02
99	1587.02	0.630E-03	-0.016532	0.113432	0.273E-03	1.00000	0.382E-02
96	1535.73	0.651E-03	0.015237	0.104544	0.232E-03	0.985237	0.324E-02
26	433.528	0.230E-02	0.015200	0.104293	0.231E-03	0.894403	0.323E-02
27	442.045	0.226E-02	0.013180	0.090433	0.173E-03	0.901547	0.240E-02
69	1084.58	0.922E-03	0.011752	0.080631	0.138E-03	0.936087	0.193E-02
30	456.649	0.218E-02	0.011177	0.076691	0.124E-03	0.907396	0.174E-02
33	543.262	0.184E-02	-0.010563	0.072475	0.111E-03	0.912236	0.156E-02
68	1076.14	0.929E-03	0.010397	0.071340	0.108E-03	0.930408	0.151E-02
.							
.							
.							
SUM					0.243E-01		0.340403

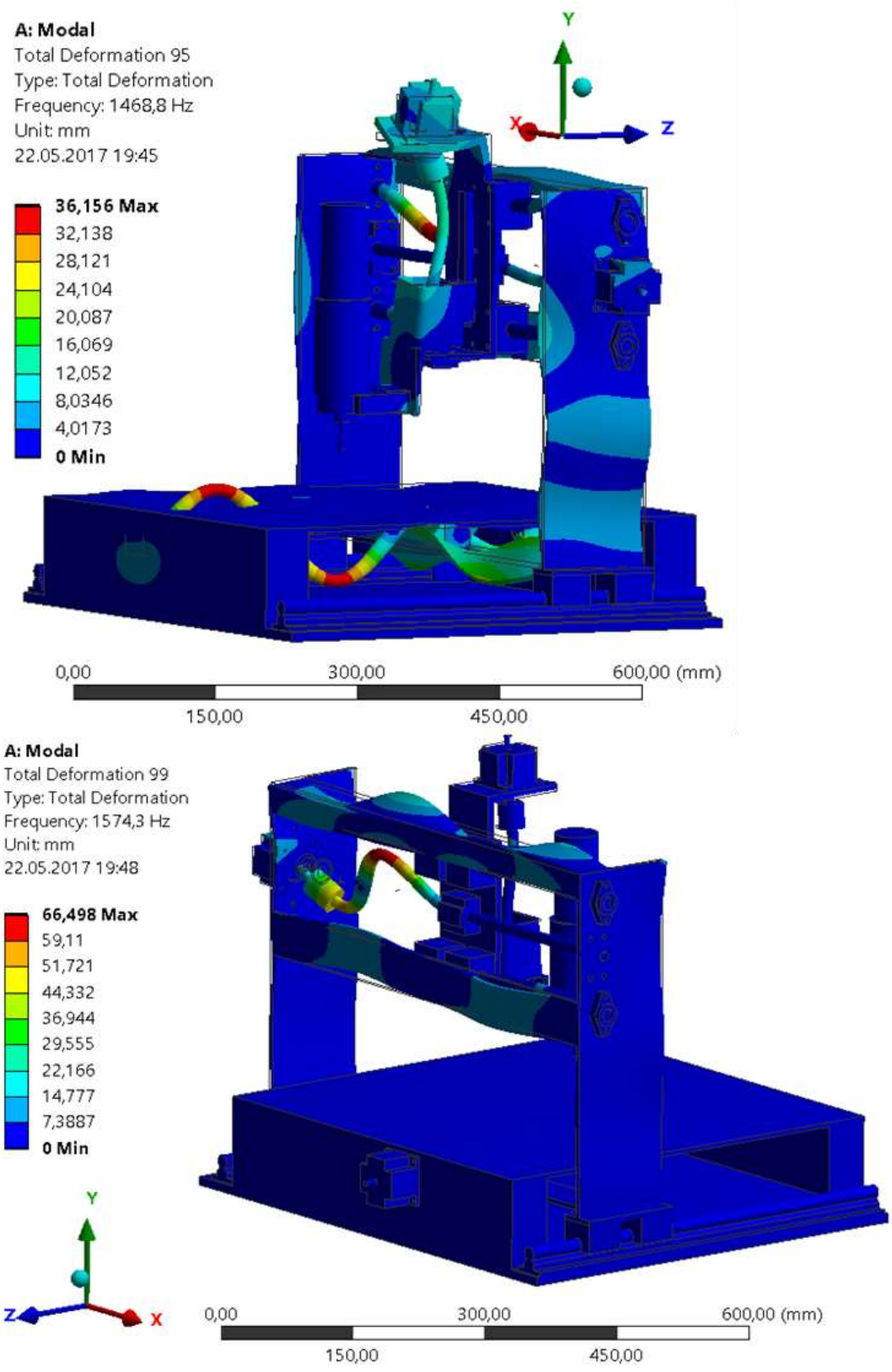

Figure 38: Natural shapes of vibrations - Mode 95 on the top and mode 99 bellow

Table 6: Natural frequencies of the model sorted by the participation factor in Y-axis

MODE	FREQUENCY [Hz]	PERIOD	PARTIC. FACTOR	RATIO	EFFECTIVE MASS	CUMULATIVE MASS FRACTION	RATIO EFF. MASS TO TOTAL MASS
8	104.996	0.952E-02	0.083839	1.000000	0.702E-02	0.745954	0.983E-01
2	31.5102	0.317E-01	0.059663	0.711631	0.355E-02	0.126975	0.498E-01
4	73.1819	0.136E-01	-0.054833	0.654030	0.301E-02	0.328761	0.420E-01
7	104.095	0.960E-02	-0.052902	0.630990	0.279E-02	0.495340	0.391E-01
3	56.4288	0.177E-01	-0.051506	0.614340	0.265E-02	0.221560	0.371E-01
5	75.3043	0.132E-01	0.042094	0.502078	0.177E-02	0.391937	0.248E-01
14	222.647	0.449E-02	0.029773	0.355125	0.886E-03	0.831880	0.124E-01
34	550.320	0.181E-02	-0.028911	0.344840	0.835E-03	0.906102	0.117E-01
35	550.689	0.182E-02	-0.020746	0.247445	0.430E-03	0.921447	0.602E-02
85	1338.74	0.746E-03	0.020044	0.239080	0.401E-03	0.979046	0.562E-02
.							
.							
.							
SUM					0.280E-01		0.392605

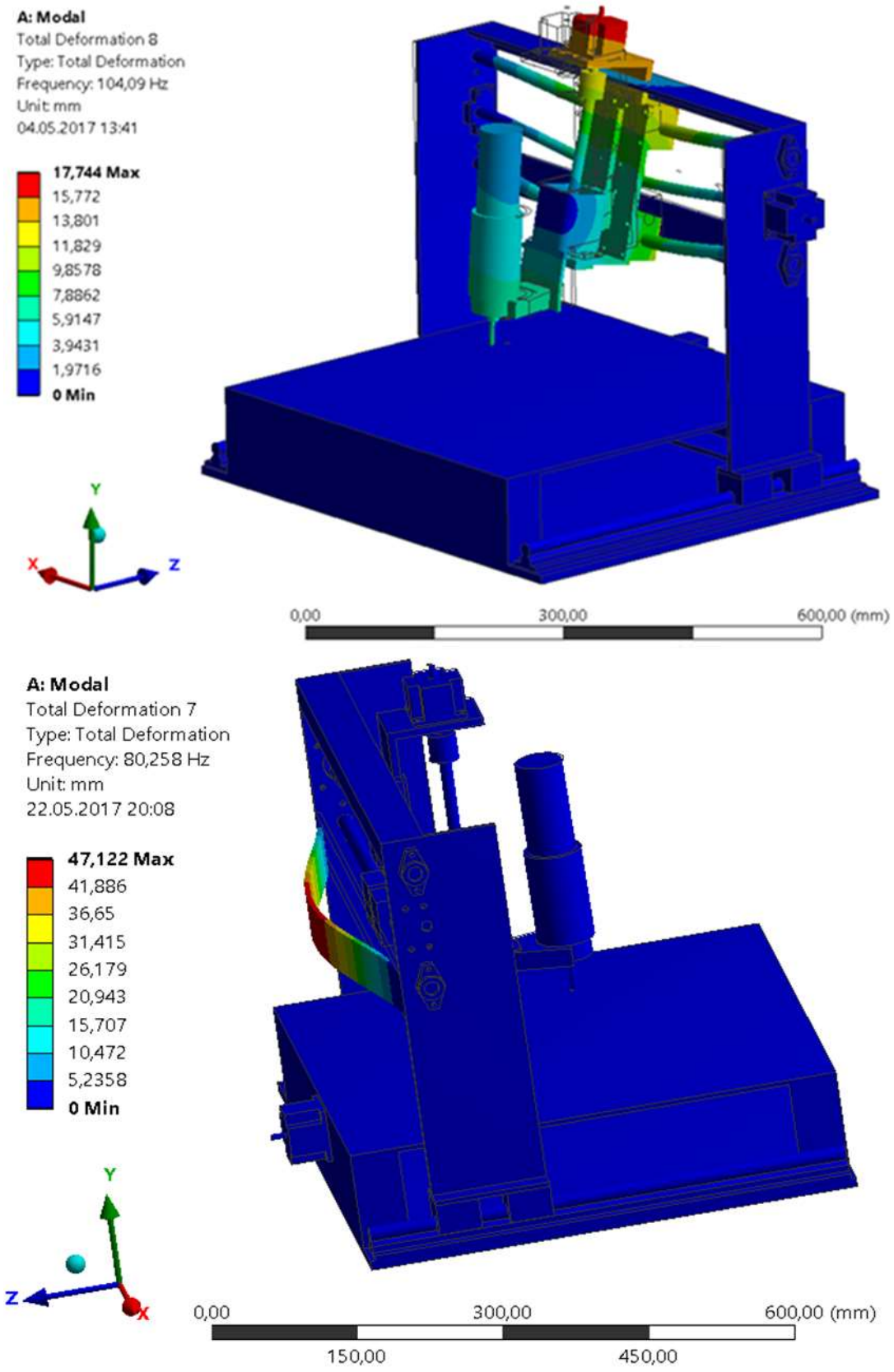

Figure 39: Natural shapes of vibrations - Mode 8 on the top and mode 7 bellow

Table 7: Natural frequencies of the model sorted by the participation factor in Z-axis

MODE	FREQUENCY [Hz]	PERIOD	PARTIC. FACTOR	RATIO	EFFECTIVE MASS	CUMULATIVE MASS FRACTION	RATIO EFF. MASS TO TOTAL MASS
3	56.4288	0.177E-01	0.10055	1	0.101E-03	0.300265	0.141522
35	550.689	0.181E-02	0.099391	0.988481	0.987E-02	0.966587	0.138281
34	550.320	0.181E-02	-0.065376	0.650191	0.427E-02	0.696931	0.598E-01
16	266.689	0.374E-02	0.053213	0.529222	0.283E-02	0.525083	0.396E-01
5	75.3043	0.132E-01	0.046121	0.458693	0.212E-02	0.410046	0.297E-01
4	73.1819	0.136E-01	-0.043527	0.432889	0.189E-02	0.351981	0.265E-01
2	31.5102	0.317E-01	0.029825	0.296618	0.889E-03	0.242879	0.121E-01
31	474.871	0.210E-02	-0.025091	0.249543	0.629E-03	0.573025	0.881E-02
14	222.647	0.449E-02	0.024677	0.245422	0.608E-03	0.446270	0.852E-02
29	452.966	0.220E-02	0.021274	0.211582	0.452E-03	0.555825	0.633E-02
.							
.							
.							
SUM					0.366E-01		0.512805

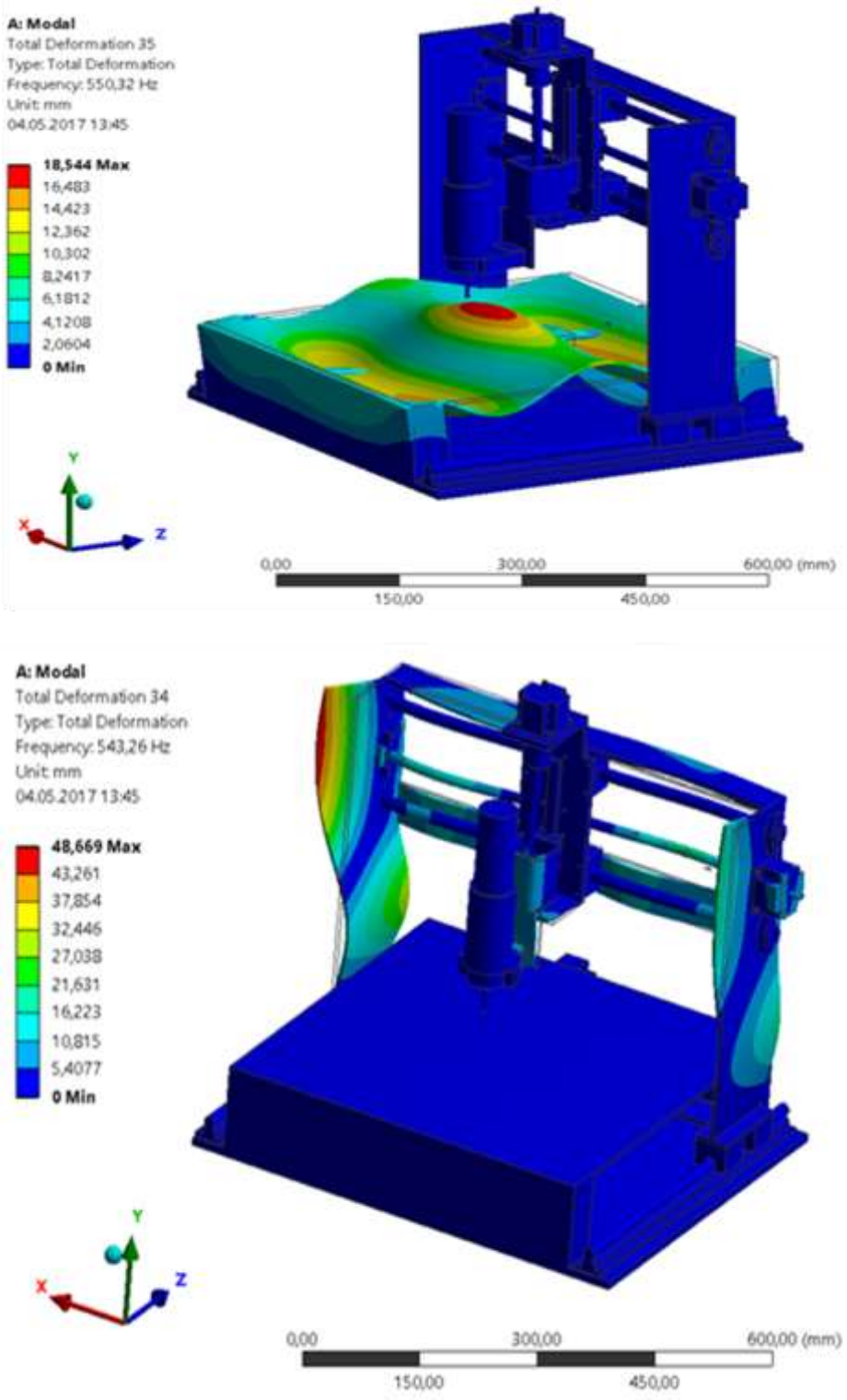

Figure 40: Natural shapes of vibrations - Mode 35 on the top and mode 34 bellow

Petontial resonanse can occur in any cases. It is usualuly if the frequency from acting force is close to natural frequency. Software ANSYS can calculate values of equivalent strain ε (Von-mises). This function can find places with the highest deformation. These modes can be edited and corresponding natural frequency can be

shifted by the geometry edition. Figure 41 shows equivalent strain for natural frequencies of mode 1 (23.89 *Hz*) and mode 2 (31.51 *Hz*).

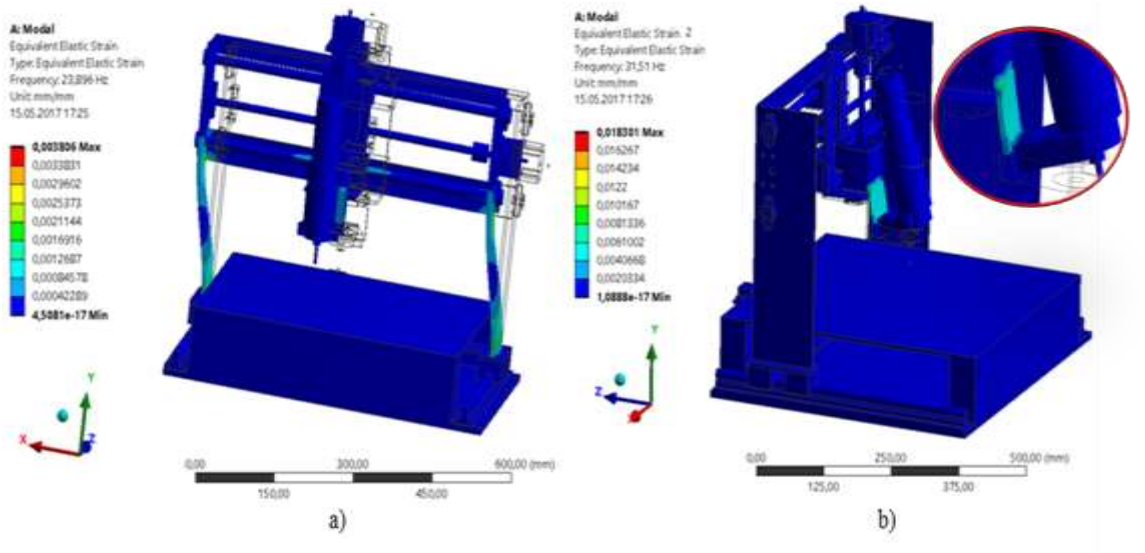

Figure 41: Equivalent strain (Von-mises) for: a) Mode 1 and b) Mode 2

4.2 Harmonic response

In a structural system, any sustained cyclic load will produce a sustained cyclic or harmonic response. Harmonic analysis results are used to determine the steady-state response of a linear structure to loads that vary sinusoidally (harmonically) with time, thus enabling to verify whether or not your designs will successfully overcome resonance, fatigue, and other harmful effects of forced vibrations. This analysis technique calculates only the steady-state, forced vibrations of a structure. The transient vibrations, which occur at the beginning of the excitation, are not accounted for in a harmonic analysis.

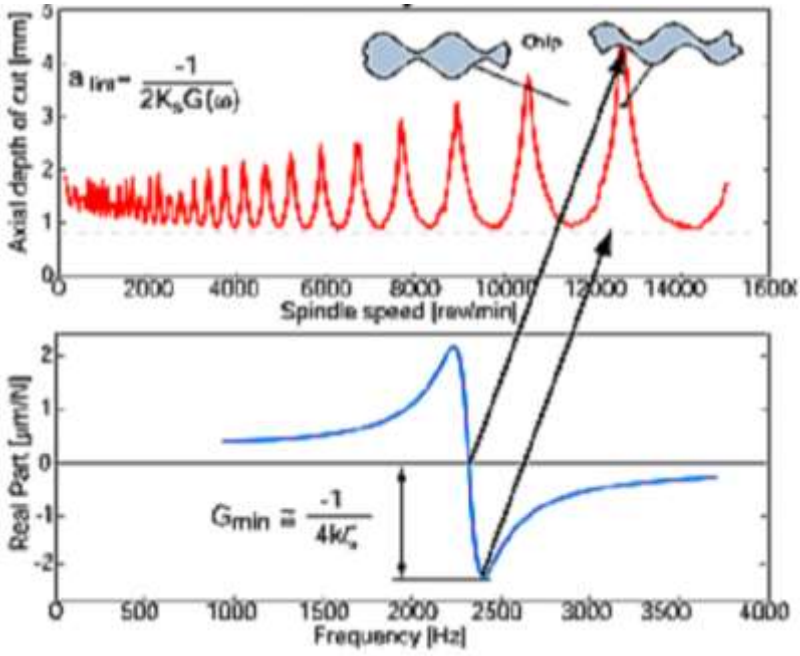

Figure 42: Stability lobe diagram (on the top) and corresponding parts in real part of transfer function (bottom) [27]

In this analysis all loads as well as the structure's response vary sinusoidally at the same frequency. A typical harmonic analysis will calculate the response of the structure to cyclic loads over a frequency range (a sine sweep) and obtain a graph of some response quantity (usually displacements) versus frequency. Peak responses are then identified from graphs of response vs. frequency.

Figure 42 presents two graphs, one on the top represents the stability lobe diagram (same type as Figure 20). Graph below represents the real part of the transfer function (same type as Figure 6 a)). There are also arrows in Figure 42, which help us to realize, which significant parts of the real part of transfer function correspond to part of stability lobe diagram. Due to this aspect, maximum negative value of real part transfer function values is chosen for following calculations.

Harmonic response has been solved in directions X, Y and Z (see Figure 43). Generated mesh and fixed support has been used same as in modal analysis. An acting force 100 *N* has been set in each direction and full method has been used. Frequency range and all the corresponding calculations have been performed. This step in this work was very time-consuming. In the first time, big range has been set. Thank to this, the biggest peak value has been found. In following, frequency range has been reduced with better frequency resolution. The final step was to establish range to get sufficient frequency resolution for creating stability lobe diagrams.

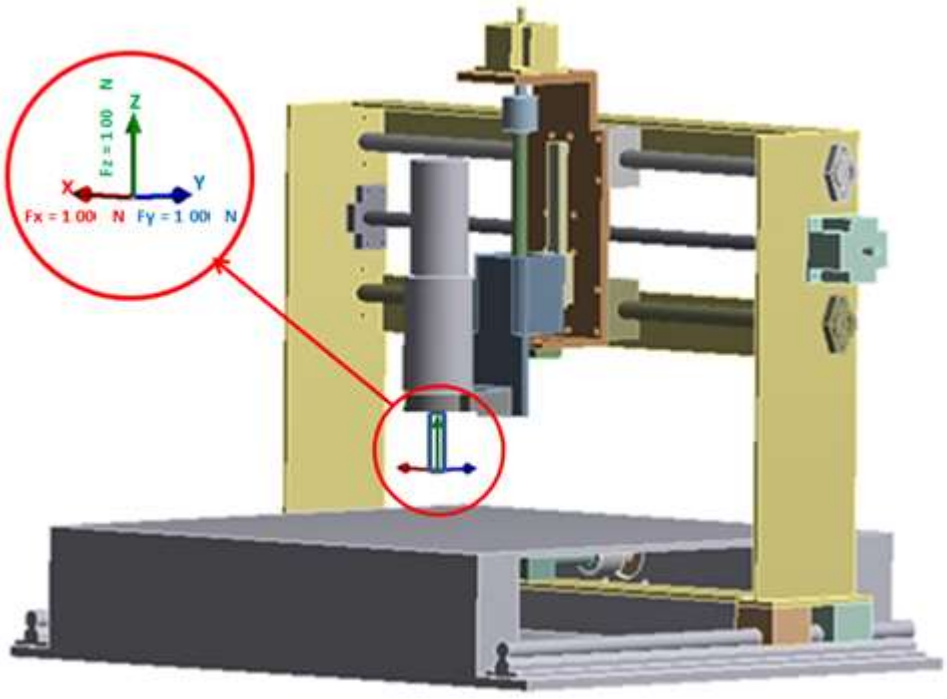

Figure 43: Simulated acting cutting forces (red – x, blue – y and green z- direction)

Microsoft Excel has been used to calculate and plot stability lobe diagrams for all the directions. Values of the real part of transfer function have been inserted in the equation (1.38) to calculate chip width. Corresponding frequencies to real part of the transfer function has been inserted into equation (1.77) and spindle speed has been computed by equation (1.78). Material properties for structural steel are the same as in Table 2. Because of the damping in joints between individual parts, damping constant ratio

is set to 0.05 value due to literature [29]. Cutting force coefficient of machined workpiece has been chosen for alluminium 6082-T4 alloy, where Ks=800 *MPa* [14]. Number of teeth is equal 1.

4.2.1 Stability lobe in X-direction

Figure 44 represents final result of harmonic response in X-direction. There is real part of transfer function on the top. In the middle is imaginary part of transfer function and on the bottom is amplitude response. All these results are investigated in frequency range 0 – 400 *Hz*.

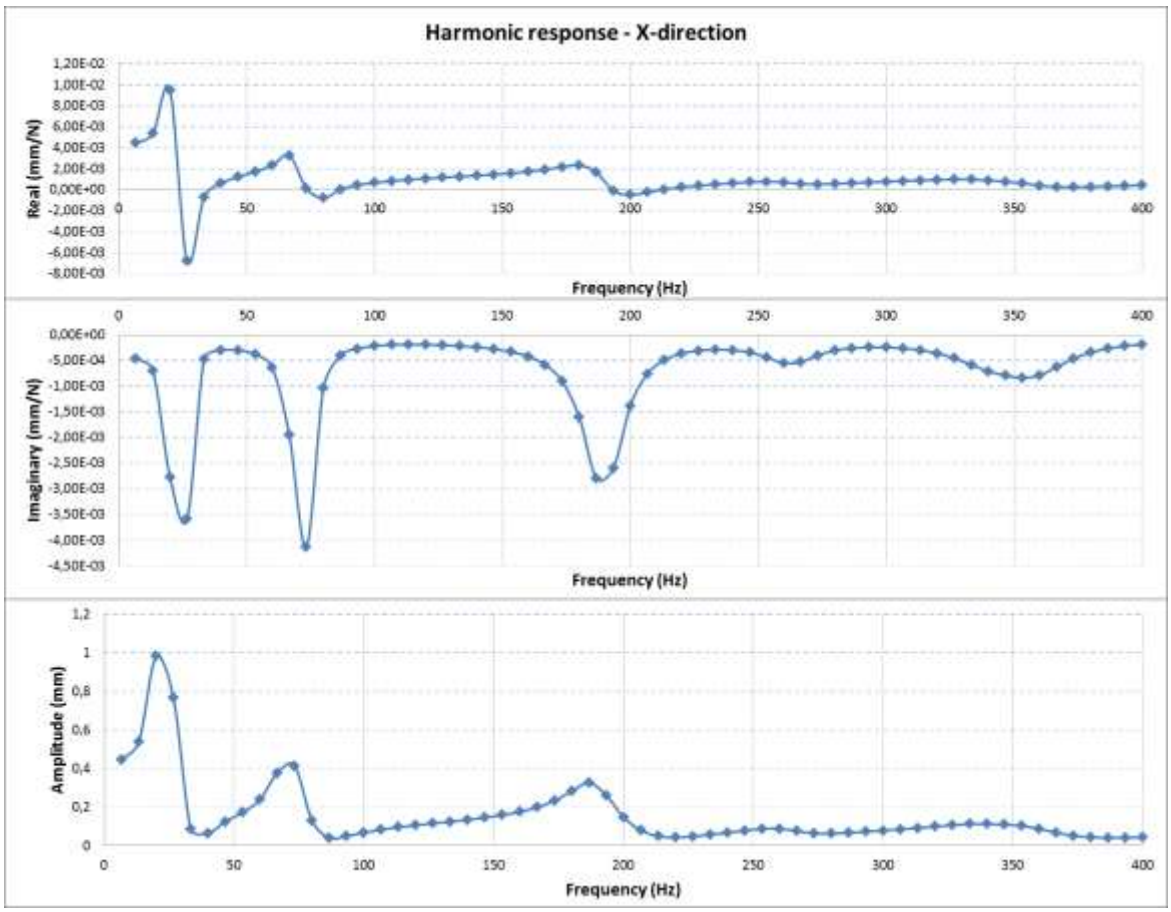

Figure 44: Harmonic response in X direction

Figure 45 presents harmonic analyse of real part of transfer function in X direction. The first range has been set from 0 to 400 *Hz* and 60 interval has been used. The second response has been investigated in range 13 - 40 *Hz* and 80 solution intervals have been used. The last range minimum has been set from 22 *Hz* and range maximum to 27 *Hz*. Final step solved 100 intervals and minimum value is for 25 *Hz* and corresponding value of real part of transfer function is -0.01078 *mm/N*. Reducing frequency range in order to get sufficient frequency resolution for creating stability lobe diagrams cause, that computed real parts are more precious.

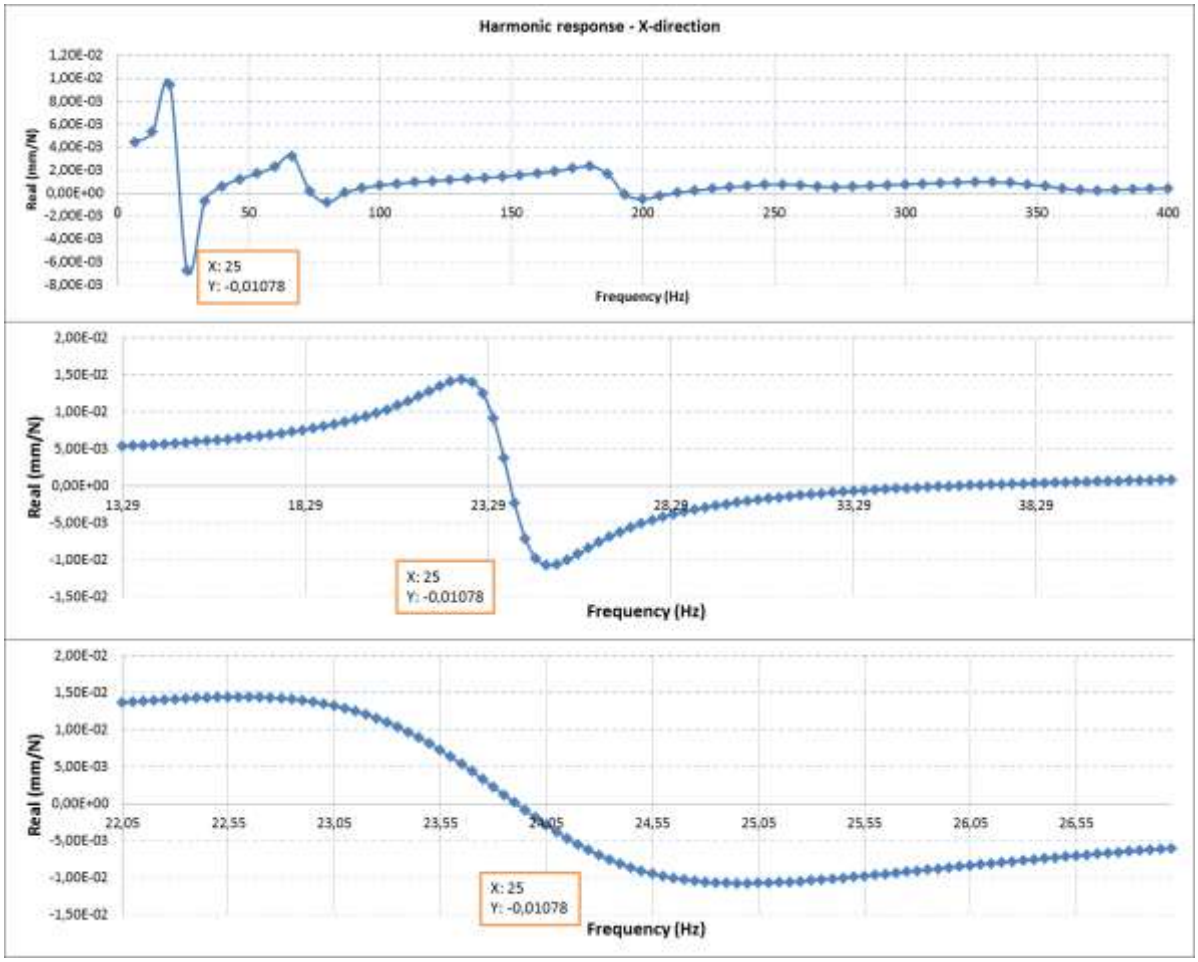

Figure 45: Real part of transfer function in X- direction

Figure 46 represent stability lobe diagram in X direction. The critical chip width has been calculated 0.057 *mm*. The highest spindle speed corresponds to the critical chip width is 2 028 *rev/min*.

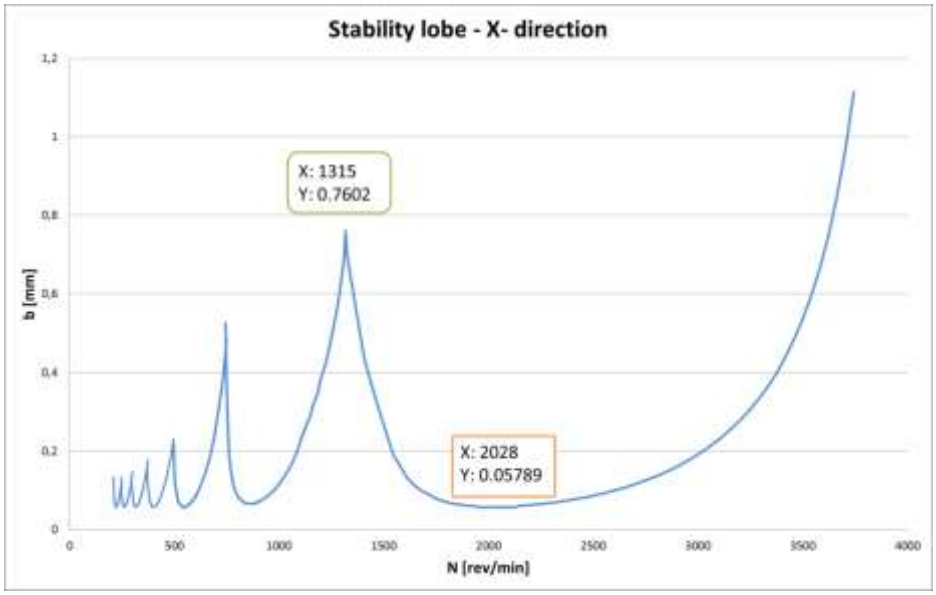

Figure 46: Stability lobe diagram X- direction

On the other hand, cutting process should be stable for spindle speed 1 315 *rev/min* for corresponding chip width 0.76 *mm* as can be seen in Figure 46. These cutting conditions in X – direction are influenced by the flexible construction of machine. Figure 47 a) presents total deformation in frequency peak (25 *Hz*) and Figure 47 b) represent the most deformed part, which is column base. Editing of column base should improve cutting conditions in X direction.

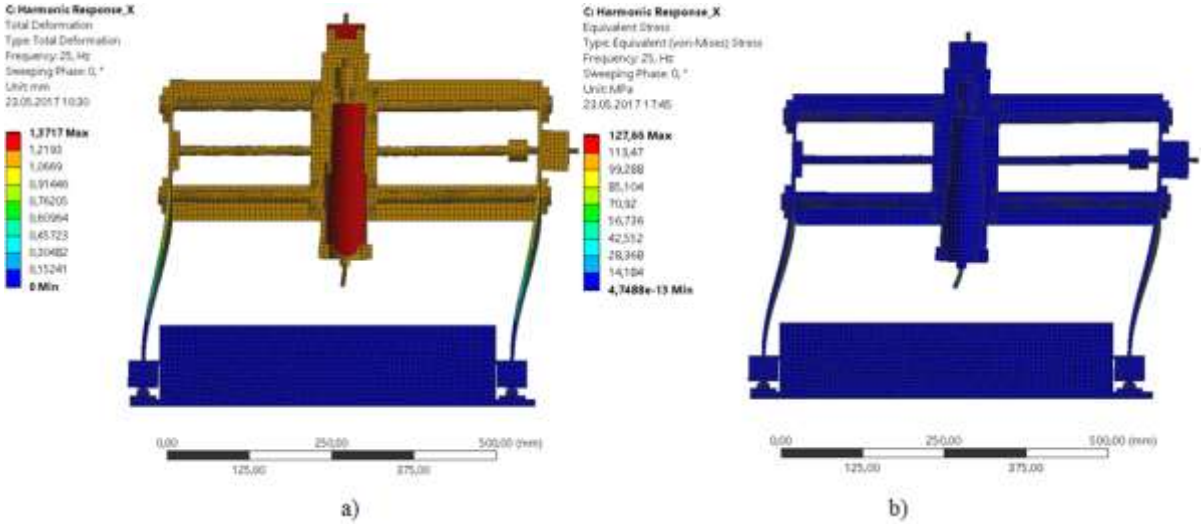

Figure 47: a) Total deformation for frequency 25 *Hz* (corresponding to maximum negative value of real part of the transfer function in X - direction), b) Corresponding equivalent stress (von Mises) – maximum value 127 *MPa*

Figure 48 represents Total deformation for frequency 20 Hz which corresps to the second highest peak (see Figure 44) in harmonic response. This value refers to 20 *Hz*. Figure 48 b) represents the most deformed part in X direction, which is column base.

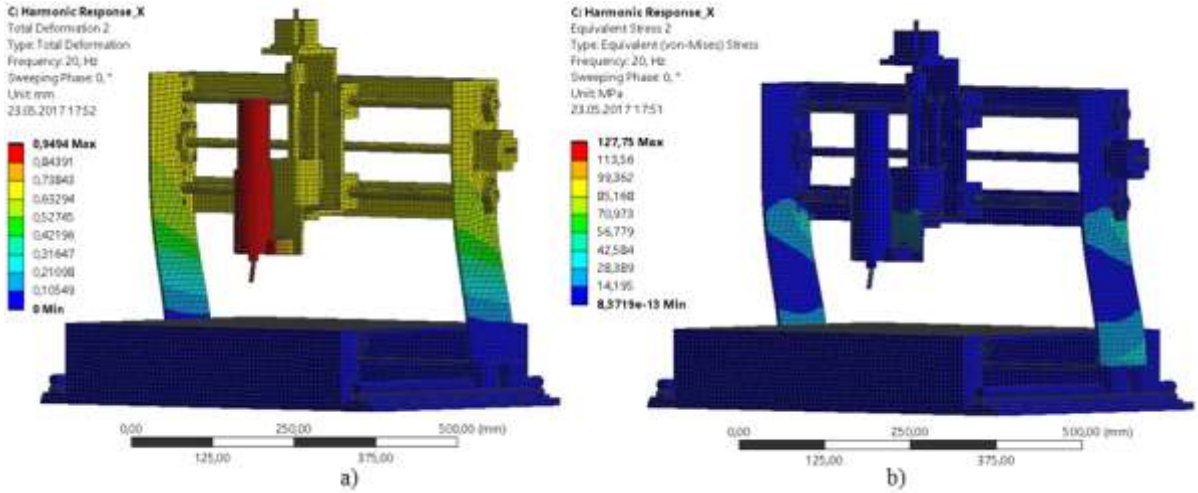

Figure 48: a) Total deformation for frequency 20 *Hz* (corresponding to the second peak in amplitude graph in X - direction), b) Corresponding equivalent stress (von Mises) – maximum value 127 *MPa*

4.2.2 Stability lobe in Y-direction

Figure 49 presents harmonic analyse of real part of transfer function in Y direction. The first range has been set from 0 to 400 *Hz* and 60 interval has been used. The second

response has been investigated in range 20 - 46 *Hz* and 80 solution intervals have been used. The last range minimum has been set from 31 *Hz* and range maximum to 50 *Hz*. Final step solved 100 intervals and minimum value is for 33.35 *Hz* and corresponding value of real part of transfer function is -0.01446 *mm/N*. Reducing frequency range in order to get sufficient frequency resolution for creating stability lobe diagrams cause, that computed real parts are more precious.

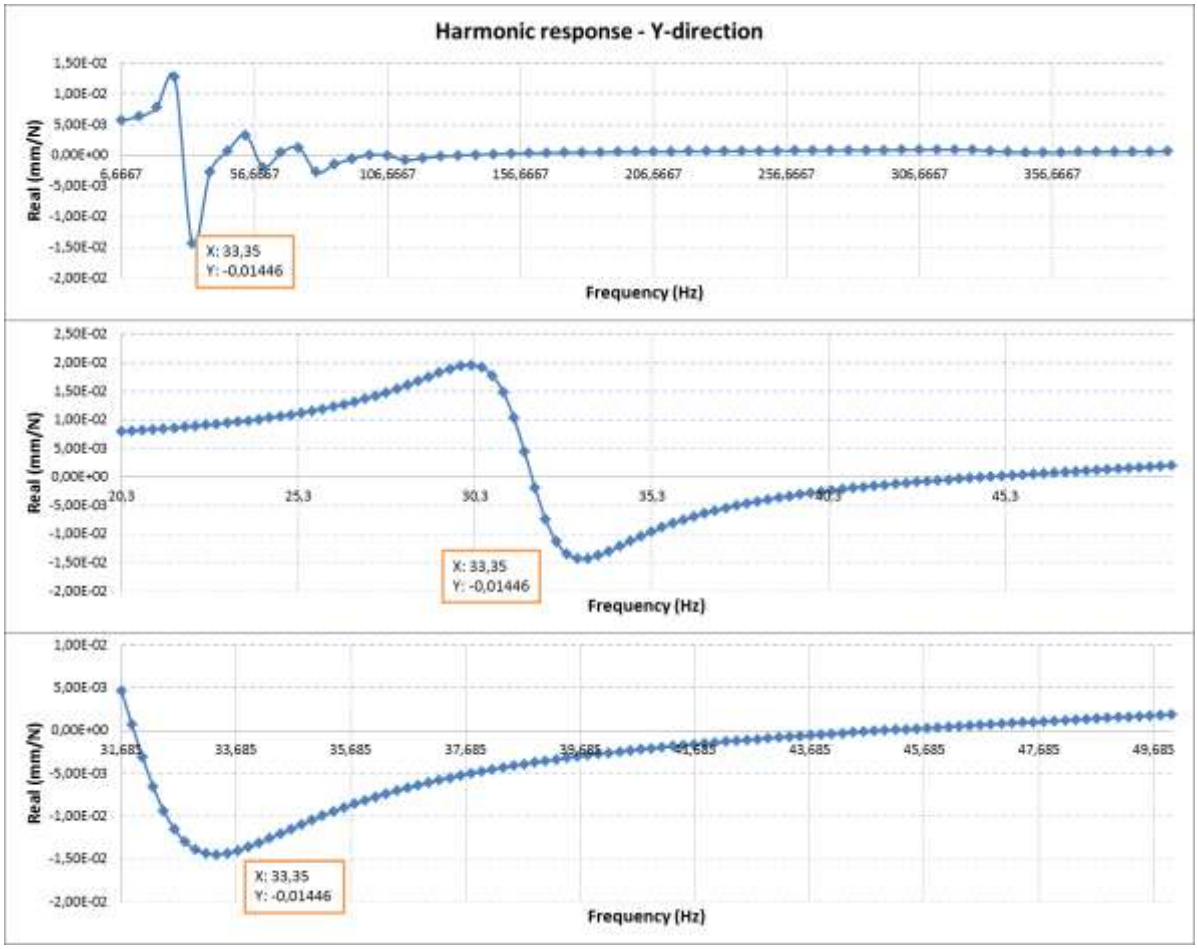

Figure 49: Real part of transfer function in Y- direction

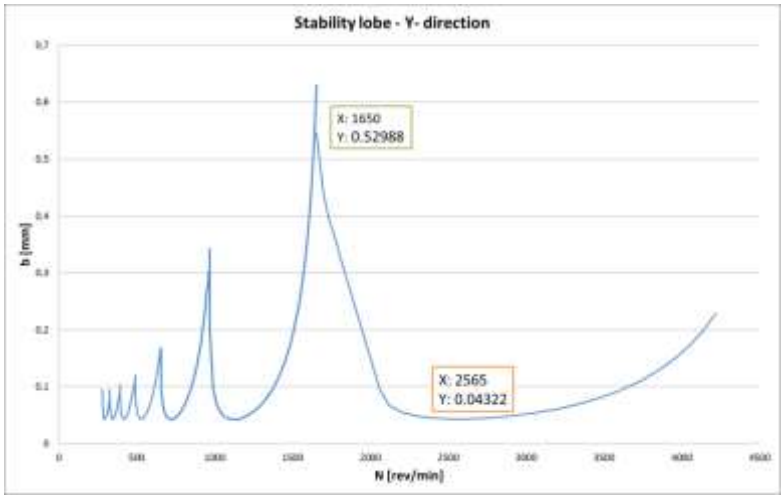

Figure 50: Stability lobe diagram Y- direction

Figure 50 represent stability lobe diagram in Y direction. The critical chip width has been calculated 0.043 *mm*. The highest spindle speed corresponds to the critical chip width is 2 565 *rev/min*.

On the other hand, cutting process should be stable for spindle speed 1 650 *rev/min* for corresponding chip width 0.53 *mm* as can be seen in Figure 50. These cutting conditions in Y – direction are influenced by the flexible construction of machine. Figure 51 a) presents total deformation in frequency peak (33.35 *Hz*) and equivalent stress Figure 51 b) represent the most deformed part, which is head-stock. Editing of head-stock should improve cutting conditions in Y direction.

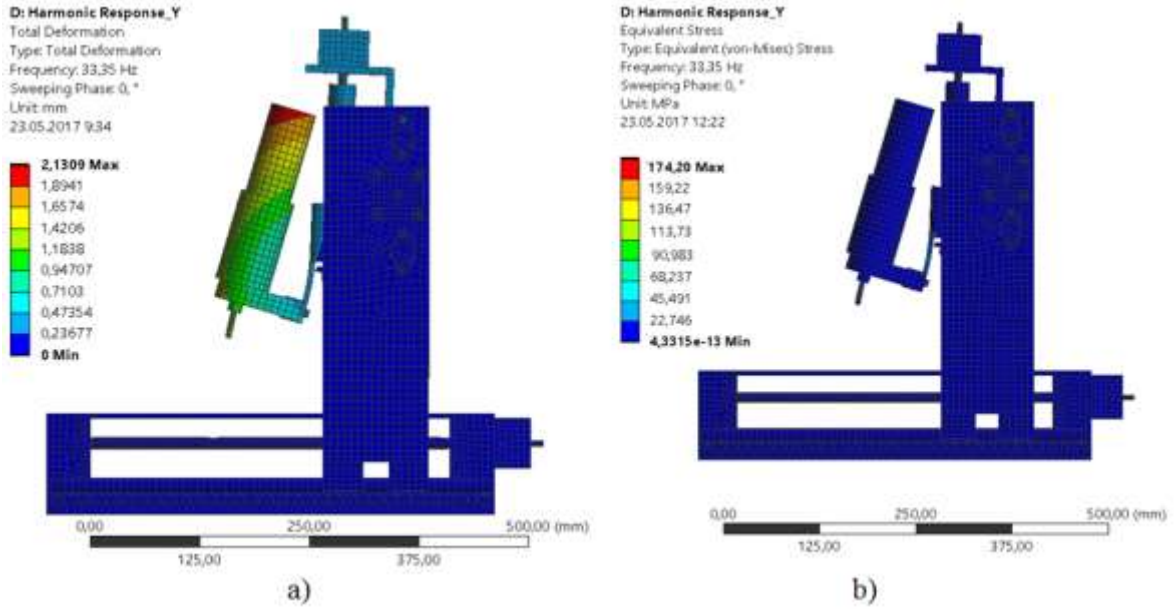

Figure 51: a) Total deformation for frequency 33.35 *Hz* (corresponding to maximum negative value of real part of the transfer function in Y- direction), b) Corresponding equivalent stress (von Mises) – maximum value 174 *MPa*

4.2.3 Stability lobe in Z-direction

Figure 52 presents harmonic analyse of real part of transfer function in Z direction. The first range has been set from 0 to 400 *Hz* and 60 interval has been used. The second response has been investigated in range 20 - 50 *Hz* and 80 solution intervals have been used. The last range minimum has been set from 28 *Hz* and range maximum to 37 *Hz*. Final step solved 100 intervals and minimum value is for 31.15 *Hz* and corresponding value of real part of transfer function is -0.01889 *mm/N*. Reducing frequency range in order to get sufficient frequency resolution for creating stability lobe diagrams cause, that computed real parts are more precious.

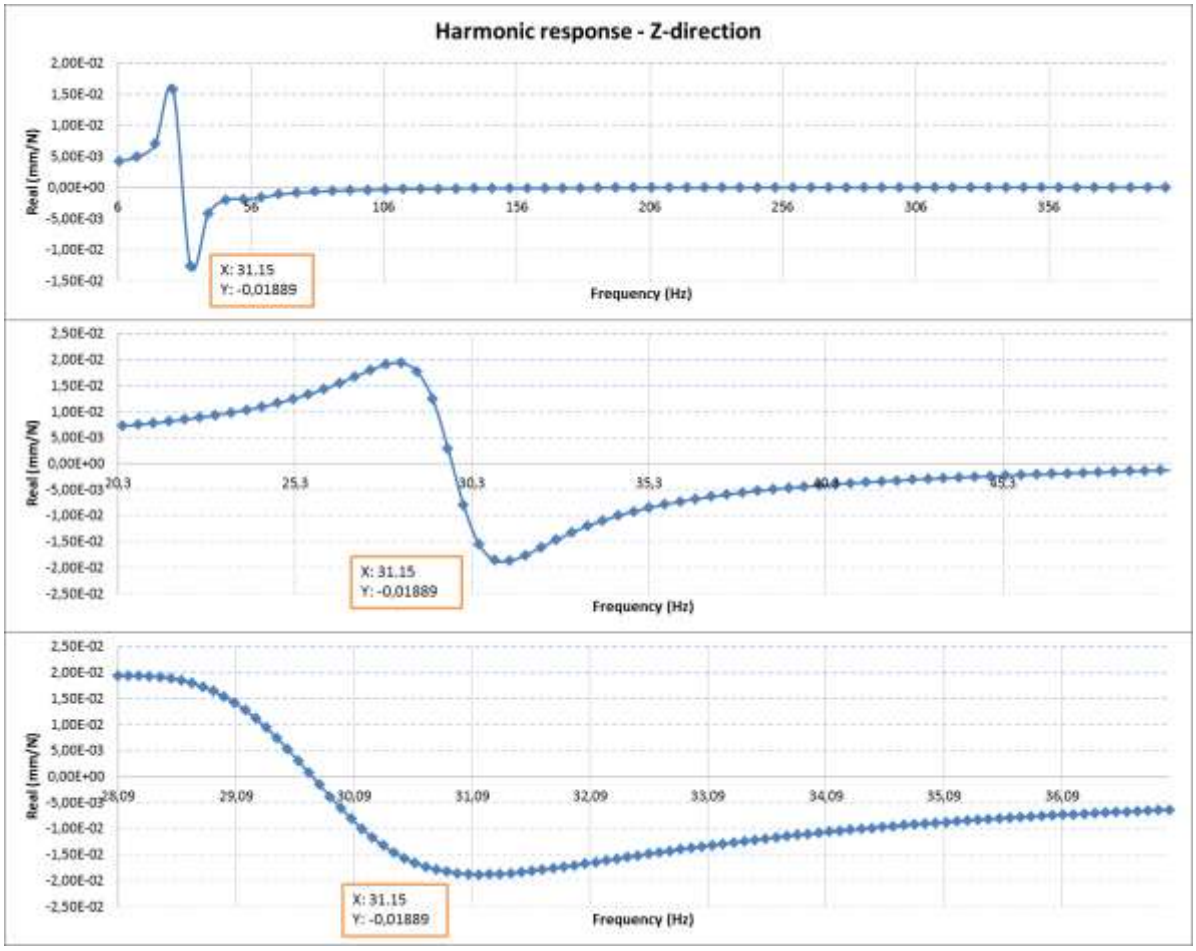

Figure 52: Real part of transfer function in Z- direction

Figure 53 represent stability lobe diagram in Z direction. The critical chip width has been calculated 0.033 *mm*. The highest spindle speed corresponds to the critical chip width is 2 692 *rev/min*.

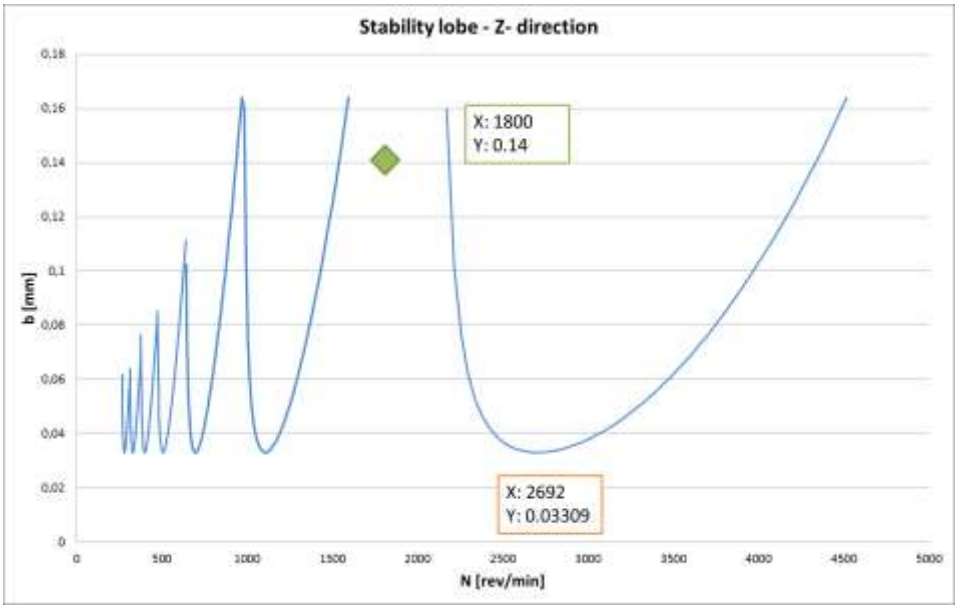

Figure 53: Stability lobe diagram Z- direction

On the other hand, cutting process should be stable in case that spindle speed is 1 800 *rev/min* for corresponding chip width 0.14 *mm* as can be seen in Figure 53. These cutting conditions in Z – direction are influenced by the flexible construction of machine. Figure 54 a) presents total deformation in frequency peak (31.15 *Hz*) and Figure 54 b) represent the most deformed part, which is head-stock. Editing of head-stock should improve cutting conditions in Z direction.

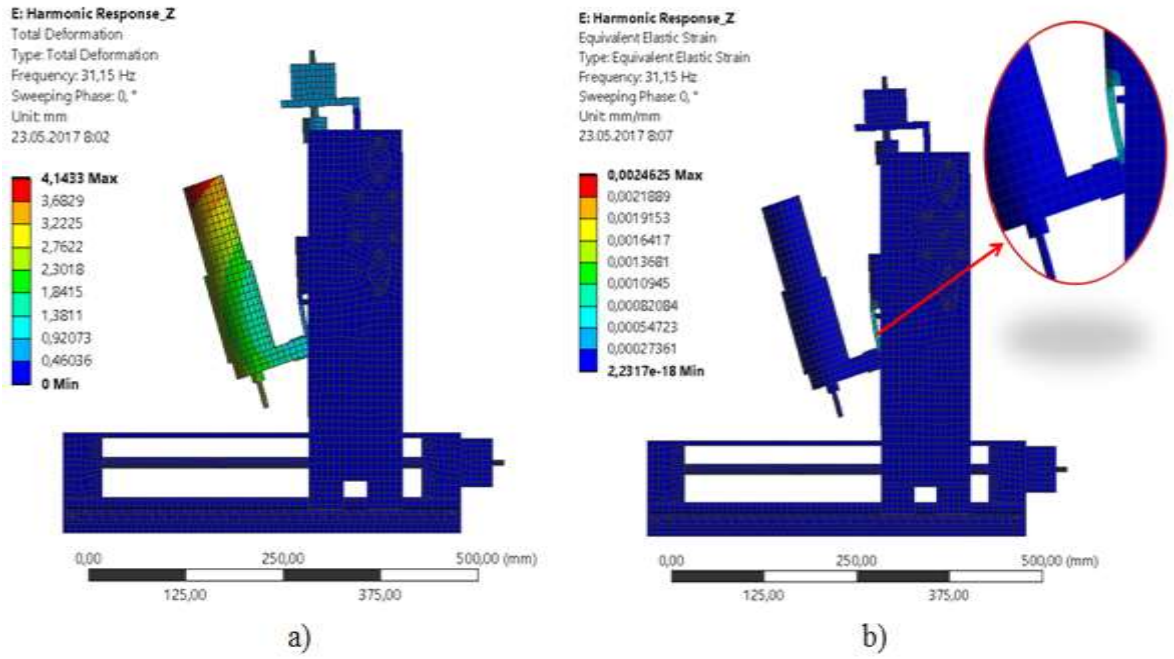

Figure 54: a) Total deformation for frequency 31.15 *Hz* (corresponding to maximum negative value of real part of the transfer function in z - direction), b) Corresponding equivalent elastic strain

5 SPECIFIC PARTS FOR ANALYZING

5.1 Material improvement

In order to improve cutting conditions for milling in Y direction, high density polyethylene has been used for the most deformed part - head-stock (see Figure 55). Polyethylene has different material properties than structural steel, which represents Table 8.

Table 8: Polyethylene properties

Material properties of polyethylene				
Signification	Modulus of elasticity E [*MPa*]	Poisson's ratio μ [-]	Damping constant ratio b_r [-]	Density ρ [$kg \cdot m^{-3}$]
HDPE	1 100	0.42	0.03	970

Viscoelastic properties of conventionally processed high density polyethylene material depend on temperature and frequency [28]. Due to this statement damped constant for polyethylene has been chosen 0.03.

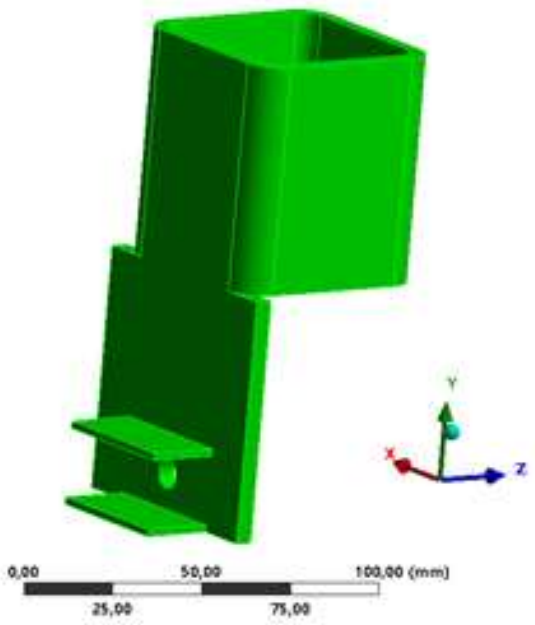

Figure 55: Head stock - material edited part – polypropylene

Figure 56 presents harmonic analyse of real part of transfer function in Y direction for edited material of head-stock. Investigated range (from 2 to 7 *Hz)* has been reduced from previous harmonic analysis and 60 intervals has been used. Minimum value is for 2.6 *Hz* and corresponding value of real part of transfer function is -4.2788 *mm/N*. This value has big magnitude and computed critical chip width corresponds to -1.92647E-06 *mm*.

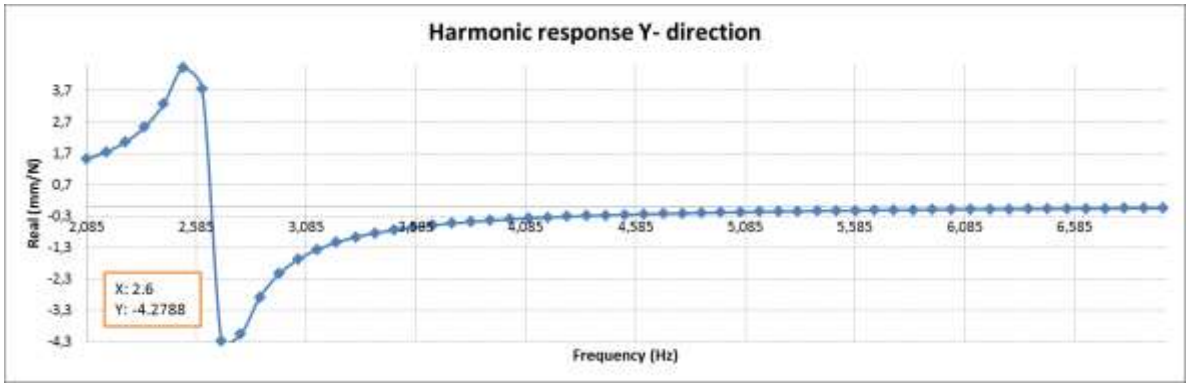

Figure 56: Real part of transfer function in Y- direction due to material change

Change in material is not correct way to improve machining conditions. Critical chip width is pretty low. The most significant difference is in modulus of elasticity, which is 1 100 *MPa* and for steel is 200 000 *MPa*. Figure 57 presents total deformation of the milling machine. Head stock could bend and stability and rigidity of the construction getting lower.

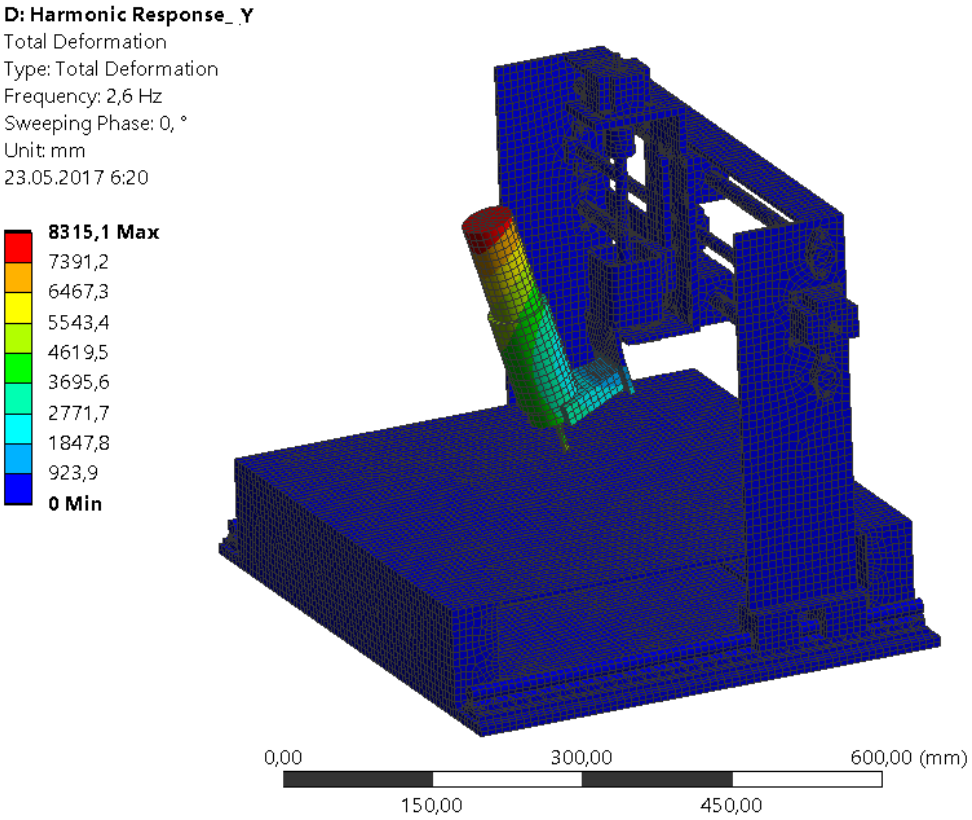

Figure 57: Total deformation - deformed head-stock

5.2 Model improvement

Editing construction is the second way how to try improve machining conditions. Figure 41 presents that head stock and column base are the most flexible part of the machine. In order to get rigider construction, these two parts has been improved (see Figure 58).

Table 9: Natural frequencies of edited and non-edited construction

Mode	Natural frequency [*Hz*]	
	Non-edited	Edited
1	23.90	35.083
2	31.51	39.144
3	56.43	60.339
4	73.18	76.726
5	75.30	79.916
6	80.26	81.088
7	104.09	89.864
8	105.00	93.633
9	140.95	104.56
10	162.68	109.73
.		
.		
.		
95	1515.19	1248.3
96	1535.73	1261.4
97	1553.36	1275.2
98	1574.34	1277.9
99	1587.02	1303.8
100	1592.09	1332.6

For edited construction modal analyses has been performed. Table 9 shows comparison of natural frequencies for non-edited and edited construction. It is clear that natural frequencies are different. This is the first significant change.

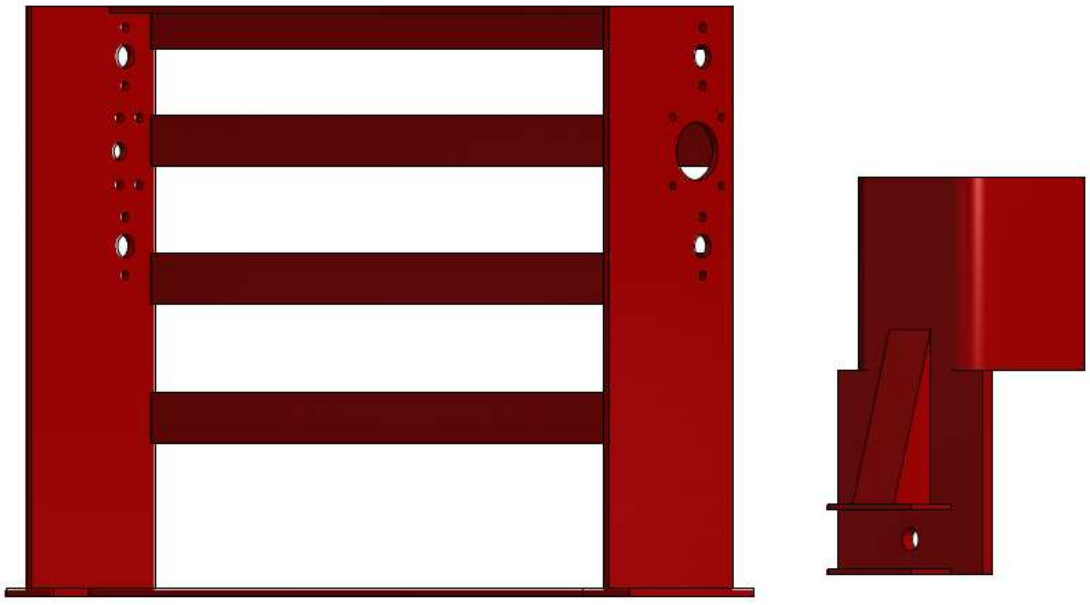

Figure 58: Edited construction - parts column base on the left, head stock on the right

Figure 59 presents harmonic analyse of real part of transfer function in X direction for edited construction. Minimum value is for 31.15 *Hz* and corresponding value of real part of transfer function is -0.01889 *mm/N*.

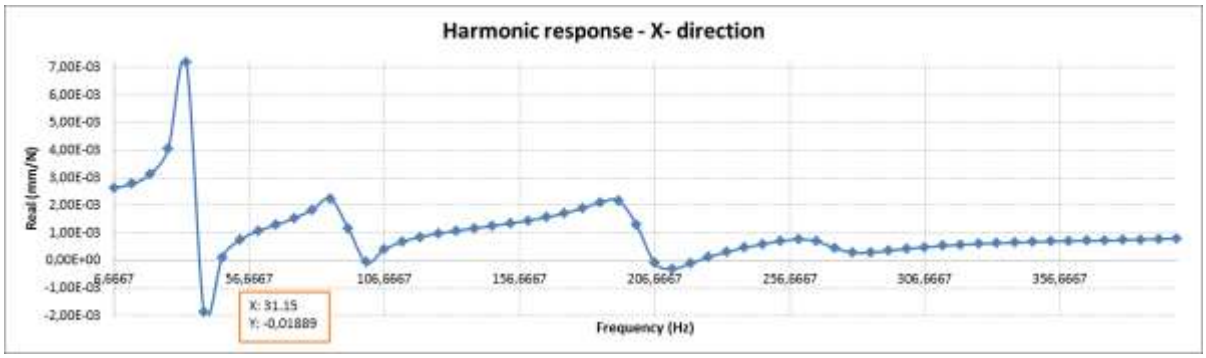

Figure 59: Real part of transfer function in X- direction due to construction change

Figure 60 represent stability lobe diagram in X direction for edited construction. The critical chip width has been calculated 0.1515 *mm*. The highest spindle speed corresponds to the critical chip width is 2 925 *rev/min*.

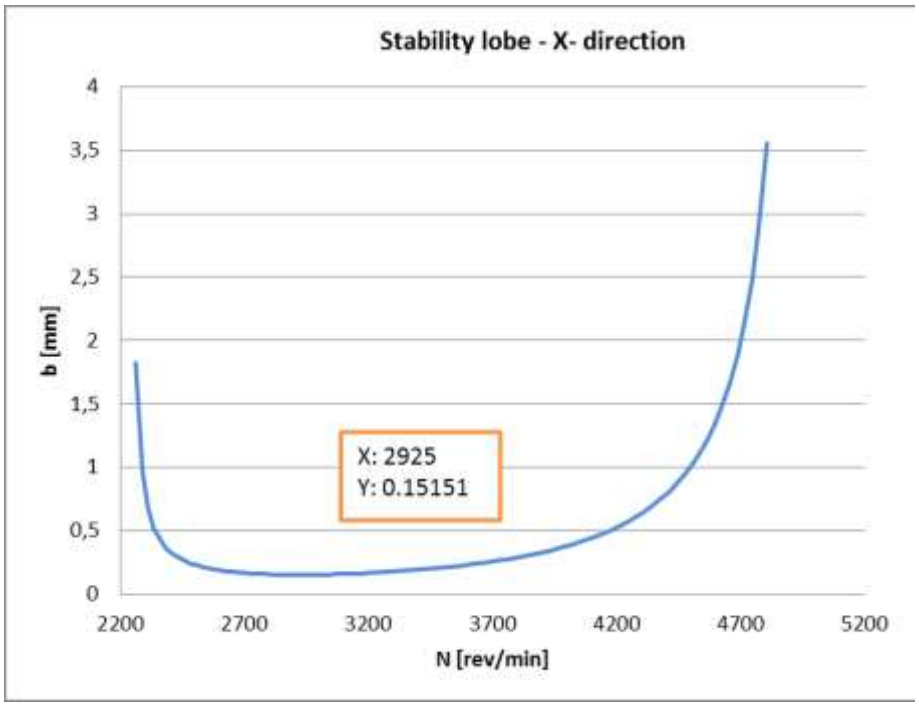

Figure 60: Stability lobe diagram X- direction due to construction change

Figure 61 presents harmonic analyse of real part of transfer function in Y direction for edited construction. Minimum value is for 41.25 *Hz* and corresponding value of real part of transfer function is -0.0915 *mm/N*.

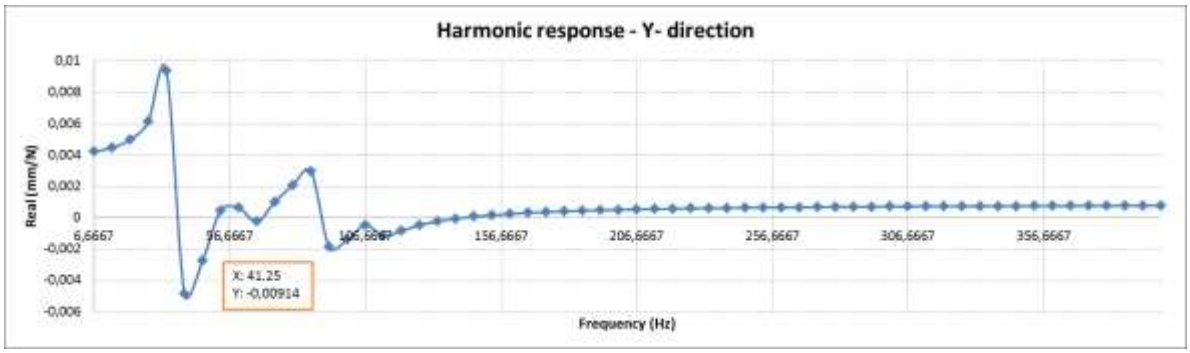

Figure 61: Real part of transfer function in Y- direction due to construction change

Figure 62 represent stability lobe diagram in Y direction for edited construction. The critical chip width has been calculated 0.0683 *mm*. The highest spindle speed corresponds to the critical chip width is 4 169 *rev/min*.

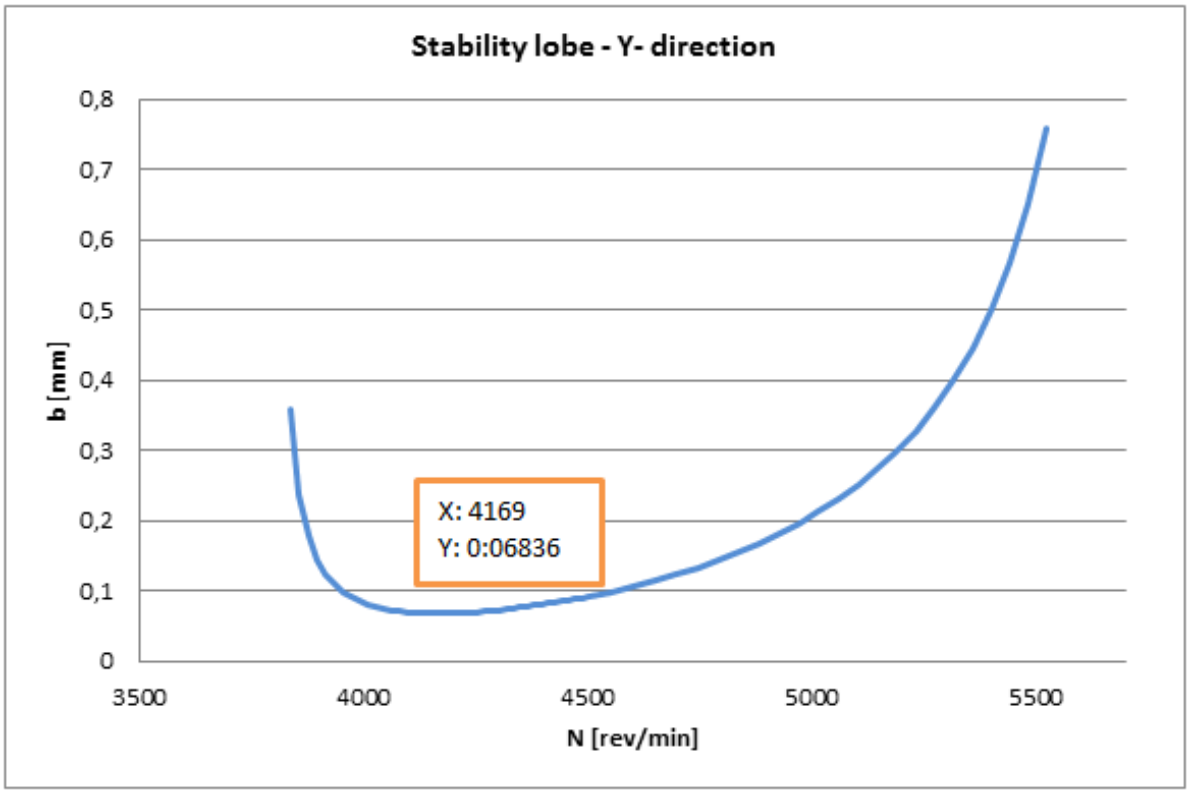

Figure 62: Stability lobe diagram Y- direction due to construction change

Table 10 presents comparsion of harmonic results and critical chip width due to edited and non edited construction. Critical chip width has raise from 0.05789 *mm* to 0.1515 *mm* in X direction. Coressponding spindle speed has raise from 2 028 *rev/min* to 2925 *rev/min*. Critical chip width has raise from 0.04322 *mm* to 0.0683 *mm* in Y direction. Coressponding spindle speed has raise from 2 565 *rev/min* to 4 169 *rev/min*.

Table 10: Comparison of harmonic results and critical chip width due to edited and non-edited

Direction X							
Non-edited construction				Edited construction			
Frequency [*Hz*]	Real [*mm/N*]	b [*mm*]	N [*rev/min*]	Frequency [*Hz*]	Real [*mm/N*]	b [*mm*]	N [*rev/min*]
25	-0.01078	0.05789	2028	31.15	-0.01889	0.1515	2925
Direction Y							
Non-edited construction				Edited construction			
Frequency [*Hz*]	Real [*mm/N*]	b [*mm*]	N [*rev/min*]	Frequency [*Hz*]	Real [*mm/N*]	b [*mm*]	N [*rev/min*]
33.35	-0.01446	0.04322	2565	41.25	-0:00915	0.0683	4169

CONLUSION

The aim of this master thesis was analysis of cutting process and creating stability lobe diagrams for milling machine CNC LH_2015 thanks to finite element method. All the fundamentals and necessary equations and symbols related to chatter were explained in theoretical part. Base on frequency theory, equation of critical chip width was derived. Necessary equations for creating stability lobe diagram were described too. Brief literature overview was discussed in the second chapter. For instance, experimental studies of the milling operation and differences between the milling operation on a standard three axis milling machine and the industrial robot. There are also mentioned problematics of cutting force coefficients etc.

The most significant task was a creation of deterministic geometric model as precise as possible in order to represent the real milling machine. It was important to achieve dynamic properties of the geometrical model. At the beginning, geometric model was created in software Autodesk Inventor. Computing model and generated mesh was created in software Ansys Workbench using a finite element method. Element size was tested due to modal analyses results. All the contacts between individual parts were modelled as bonded contact.

Computing part was divided into two sections. The first section dealt with determination of natural frequencies and corresponding shapes. Creation of stability diagrams was the second one. Determining first one hundred natural frequencies was a result of first part of modal analysis. The lowest natural frequency was equal to 23.89 Hz and the highest natural frequency was equal to 1 592.08 Hz. Mostly all the calculated natural frequencies were connected with column base and head stock vibrations. It was necessary to perform harmonic analysis in order to reach harmonic response of the machine. This was a crucial part of data to obtain in order to create stability diagrams. Acting force was applied in three orthogonal directions (horizontal, vertical, longitudinal). Based on harmonic analysis results stability lobe diagrams were created for given directions.

Extrapolated stability lobe diagrams have shown that current construction wasn’t rigid enough. Resulting critical chip width was in range of tenths of millimetres. Yet values from peaks of diagrams suggest that we might work in range of millimetres. Computed results shown nearly the same values in X a Y directions, however result in Z directions referred to a very high flexibility of construction in this direction.

Based on results of modal analysis there were proposed two different approaches to improve cutting conditions. The first approach was about material change of headstock. The material modified was polyethylene. This change was insufficient due to the fact that results of re-calculated critical chip width was lower than for original material. It was due to lower modulus of elasticity for polyethylene. Editing and reinforcement of construction of column base and head stock was the second approach. Evaluation of re-calculated critical chip width found out that conditions of cutting process have improved the most when adjusting parameters in X direction. The critical chip widt have increased three fold.

In case of extending this master thesis, as the main topic I would suggest experimental evaluation of results by measuring vibrations on real milling machine. This would first required measuring of input parameters such as damping, material parameters, etc. Due to relatively small chip width values obtained, I would first suggest to reinforce construction or use more appropriate materials.

REFERENCES

1. TLUSTY, Jiri. *Manufacturing processes and equipment*. Upper Saddle River, NJ: Prentice-Hall, c2000. ISBN 02-014-9865-0.
2. A. YOUSSEF, H.; EL-HOFY, H. Machining technology: machine tools and operations [online]. New York : CRC Press, 2008 [cit. 2016-12-22]. Dostupné z WWW: <http://books.google.cz/books
3. KOCMAN, K.; PROKOP, J. *Technologie obrábění. druhé*. Vysoké učení technické: AKADEMICKÉ NAKLADATELSTVÍ CERM, s.r.o. Brno, 2005. 270 s.
4. TLUSTÝ, J; KROENIGSBERGER, F. *Specifications and Tests of Machine Tools*. Manchester : UMIST, April, 1970.
5. MAREK Jiří, *Konstrukce CNC obráběcích strojů.* Brno, MM publishing, 2010. 420 s. ISBN 9788025479803
6. Alexander Janáč, Zdenko Lipa, Jozes Peterka. *Teória obrábania*. Bratislava: Vydavateľstvo STU Bratislava, 2006. 199 s. ISBN 80-227-2347-9
7. Ing. Fojtů Petr, *Problematika samobuzeného kmitání* [online]. [cit. 2016-12-22]. Dostupné z <stc.fs.cvut.cz/History/2009/Papers/pdf/FojtuPetr-304483.pdf>
8. TOBIAS, S.A. *Machine Tool Vibrations*. London : Blackie & Son, 1965. 24s.
9. SLAVÍK, Jaroslav. Počítačové metody mechaniky I. Brno: Akademické nakladatelství CERM, 2003. ISBN 80-214-2311-0
10. SLAVÍK, Jaromír, Vladimír STEJSKAL a Vladimír ZEMAN. *Základy dynamiky strojů: měření a hodnocení.* Vyd. 1. Praha: České vysoké učení technické, 1997. ISBN 80-010-1622-6.
11. NOVOTNÝ, Pavel. *Přednášky z předmětu: Vibrace a Hluk*. Brno: Vysoké učení technické v Brně, Fakulta strojního inženýrství, 2015.
12. ANSYS. Theory reference: Analysis Procedures. Pennsylvania 2012.
13. MALENOVSKÝ Eduard: Studijní opora z předmětu: Počítačové metody mechaniky v dynamice [online], 12.2.2007 [cit. 2016-12-23]. Dostupné z: < http://www.umt-old.fme.vutbr.cz/~pkrejci/opory/pmm_dyn/index.html>.
14. GROSSI, N., L. SALLESE, A. SCIPPA and G. CAMPATELLI. Chatter Stability Prediction in Milling Using Speed-varying Cutting Force Coefficients. *Procedia CIRP* [online]. 2014, **14**, 170-175 [cit. 2017-03-16]. DOI: 10.1016/j.procir.2014.03.019. ISSN 22128271. Dostupné z: http://linkinghub.elsevier.com/retrieve/pii/S2212827114001620
15. HU, Sen, Xianzhen HUANG, Yimin ZHANG and LV. *International Journal of Aerospace Engineering* [online]. 2016, **2016** [cit. 2017-03-19]. DOI: 10.1155/2016/5259821. ISSN 1687-5966. Dostupné z: https://www.hindawi.com/journals/ijae/2016/5259821/
16. CHEN, Bing, Jie YANG, Ju ZHAO and Jingbo REN. Milling Chatter Prediction Based on the Information Entropy and Support Vector Machine. *Proceedings of the 2015 International Industrial Informatics and Computer Engineering Conference* [online]. Paris, France: Atlantis Press, 2015, , - [cit. 2017-03-21]. DOI: 10.2991/iiicec-15.2015.86. ISBN 978-94-62520-54-7. Dostupné z: http://www.atlantis-press.com/php/paper-details.php?id=16972
17. YUAN, Lingling, Wentao MEI and Yongfeng ZHENG. Simulation Implementation and Application Research of High Speed Milling Regeneration Type Chatter Based on

MATLAB. *Proceedings of the 2015 International Industrial Informatics and Computer Engineering Conference* [online]. Paris, France: Atlantis Press, 2015, , - [cit. 2017-03-21]. DOI: 10.2991/iiicec-15.2015.72. ISBN 978-94-62520-54-7. Dostupné z: http://www.atlantis-press.com/php/paper-details.php?id=16958

18. ABELE, E. and J. BAUER. *Prediction of the Tool Displacement by Coupled Models of the Compliant Industrial Robot and the Milling Process* [online]. [cit. 2017-03-27]. Dostupné z: http://citeseerx.ist.psu.edu/viewdoc/summary?doi=10.1.1.172.3250
19. ALTINTAS, Y. and M. WECK. Chatter Stability of Metal Cutting and Grinding. *CIRP Annals - Manufacturing Technology* [online]. 2004, **53**(2), 619-642 [cit. 2017-03-29]. DOI: 10.1016/S0007-8506(07)60032-8. ISSN 00078506. Dostupné z: http://linkinghub.elsevier.com/retrieve/pii/S0007850607600328
20. INASAKI, I., B. KARPUSCHEWSKI and H.-S. LEE. Grinding Chatter – Origin and Supperssion. *Annals of the CIRP, vol. 50, no. 2* [online]. [cit 2017-03-28]. Dostupné z: http://www.sciencedirect.com/science/article/pii/S0007850607629928
21. ATTANASIO, A., E. CERETTI, S. RIZZUTI, D. UMBRELLO a F. MICARI. 3D finite element analysis of tool wear in machining. *CIRP Annals - Manufacturing Technology* [online]. 2008, **57**(1), 61-64 [cit. 2017-03-30]. DOI: 10.1016/j.cirp.2008.03.123. ISSN 00078506. Dostupné z: http://linkinghub.elsevier.com/retrieve/pii/S0007850608000930
22. Studijní texty Obráběcí stroje. [online]. [cit. 2017-05-01]. Dostupné z: http: //www.kvs.tul.cz/download/vyrobni_stroje/obrabeci.pdf
23. *Burrs - Analysis, Control and Removal* [online]. Berlin, Heidelberg: Springer Berlin Heidelberg, 2010 [cit. 2017-04-12]. ISBN 978-3-642-00567-1.
24. *Suppression of Chatter in High-Speed Machining* [online]. [cit. 2017-04-14]. Dostupné z: http://academic.csuohio.edu/romadyc/research/projects/suppression-chatter-high-speed-machining.html
25. KNÍŽEK, Martin. *MODELÁŘSKÁ CNC FRÉZKA*. Pardubice, 2015. Bakalářská práce. Univerzita Pardubice Fakulta elektrotechniky a informatiky. Vedoucí práce Ing. Libor Havlíček, Ph.D.
26. NOVÝ, Richard. *Hluk a chvění.* Vyd. 3. V Praze: České vysoké učení technické, 400 s. ISBN 978-80-01-04347-9.
27. Ing. Švancara Pave Ph.D. *Chatter Samobuzené kmitání při obrábění: Možnosti modelování.* Přednáška, VUT Brno 2015
28. Lyon, R. H., DeJong, R.G, Theory and Application of Statistical EnergyAnalysis, *Butterwortth-Heinemann, Boston, 1995*
29. V. Adams and A. Askenazi, *Building Better Products with Finite Element Analysis*, On Word Press, Santa Fe, N.M., 1999.

SYMBOLS AND SHORTCUTS

Shortcur/Symbol	Unit	Description
A	mm	amplitude
a_p	mm	axial depth of chip
b_{cum}	mm	cumulative chip width
b_{lim}	mm	limit chip width
b_r	-	damped constant
c	N/m	damping coefficient
CNC	-	Computer Numeric Control
e	-	Euler number
E	MPa	Modulus of elasticity
F	N	Power
f	Hz	frequency
f_n	Hz	natural frequency
F_{dyn}	N	dynamic power
F_p	N	Spring force
F_t	N	Friction force
G	Pa	shear modulus
h	mm	chip width
k	kg/s	spring stiffness
Ks	-	Specific cutting resistance
m	kg	mass
N	rev/min	spindle speed
T	s	time
v_c	m/min	cutting speed
v_f	m/min	feed
x	mm	deflection
x_0	mm	initial deflection
$\dot{x}$	m/s	velocity
$\ddot{x}$	m/s^2	acceleration
δ	rad/s	decay coefficient

ω	Hz	frequency
μ	-	Poisson number

FIGURE LIST

TABLE LIST

ATTACHMENT LIST